LARS Information Note 090776

Analytical and Experimental Design and Analysis of an Optimal Processor for Image Registration

by Martin Svedlow,
C.D. McGillem, &
P.E. Anuta

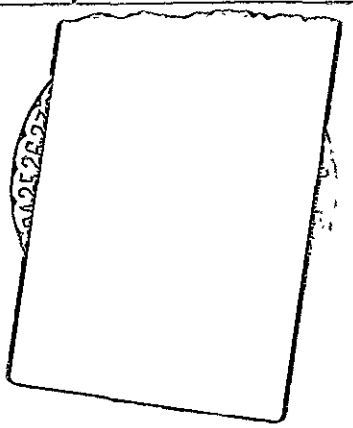

The Laboratory for Applications of Remote Sensing
Purdue University West Lafayette, Indiana

1976

LARS Information Note 090776

ANALYTICAL AND EXPERIMENTAL DESIGN AND ANALYSIS OF AN OPTIMAL PROCESSOR FOR IMAGE REGISTRATION

Martin Svedlow
C.D. McGillem
P.E. Anuta

Published by the

Laboratory for Applications of Remote Sensing (LARS)

Purdue University
Lafayette, Indiana 47907

This work was sponsored by the National Aeronautics and Space Administration (NASA) under contract NAS9-14016.

TABLE OF CONTENTS

LIST OF TABLES

LIST OF FIGURES

ABSTRACT

Svedlow, Martin, Ph.D., Purdue University, August 1976, Analytical and Experimental Design and Analysis of an Optimal Processor for Image Registration. Major Professor: Clare D. McGillem.

The registration of temporally differing images is defined in a way that allows its analysis via parameter estimation theory. Assuming spatial congruence between the images, one image is defined as the signal and the second image is assumed to be the signal plus additive noise, where the noise is comprised of the temporal changes and any additional noise introduced by the sensor system. The parameters to be estimated are the relative translations between the images.

With this formulation, a quantitative measure of the performance of the registration processor is defined which leads to the derivation of an optimum processor that yields the best possible performance in terms of the criteria chosen. The performance measure used is the variance of the registration error, where the error is the spatial difference between the registration position indicated by the processor in the presence of noise and the true overlay location. With this performance criterion the optimum processor is that which minimizes the variance of the registration error. Derivation of the processor which satisfies this criterion shows it to be the matched filter, which also maximizes the output signal-to-noise ratio. Substitution of this processor into the general expression for the variance of the registration error yields a compact

expression in terms of the effective bandwidth and signal-to-noise ratio.

Given the matched filter processor, two methods of implementation are shown. In the first approach the second image (signal plus noise) is passed through a single filter where the position at which the output is a maximum is taken as the indicated registration position. For the second technique of implementing the matched filter both of the images are passed through a prewhitening filter and the resulting outputs are crosscorrelated, where the prewhitening filter is designed so as to prewhiten the input noise (temporal changes). Again the indicated registration position is the location of the maximum of the output. This second method is the one that finds itself applicable to image registration algorithms that have been implemented by other investigators in the form of utilizing a preprocessing operation on the images prior to overlaying them.

Actual determination of the matched filter processor to be used in a particular situation requires a model of the autocorrelation function of the noise (temporal changes). For application of this type of registration processor to LANDSAT I satellite imagery an estimation procedure for determining a model of the autocorrelation function is carried out. It is found that for the imagery examined, the autocorrelation function of the temporal changes is of an exponential form. Utilizing this parametric form for the autocorrelation function an example is presented in which the matched filter is evaluated. It is found that with the prewhitening followed by crosscorrelation approach to implementation of the matched filter, that the preprocessing or prewhitening filter applied to both images is a derivative type operator. This result indicates that a derivative type preprocessor should be applied to both images prior to overlaying them.

One of the basic assumptions made in the derivation of the optimum processor is that the images be spatially congruent. However, this is not necessarily true when given two sets of actual imagery due to unavoidable perturbations in the scanner viewing platform orientation. An analysis is presented in which the loss in the output signal-to-noise ratio due to the violation of the spatial congruency assumption is shown. The results show that in the presence of relative spatial distortions which are increasing in image size, such as a linear scale change, that there is an optimum integration area size for the cross correlation stage of the processor which yields a maximum output signal-to-noise ratio. Determination of this optimum integration area size is a straightforward procedure which is shown in a series of examples illustrating several types of relative spatial distortions. In two of the examples, models of the distortions observed between temporally differing LANDSAT I images were used. In this way it is shown how the optimum integration area size for the registration of images in practice may be found in a straightforward manner.

Finally, an experimental comparison of the techniques used in several registration algorithms proposed or implemented by other investigators is presented. This study provides both an objective comparison of the different algorithms plus a corroboration of the analytical results derived in the earlier sections. It is found that preprocessing the images via a gradient type operator, which is a derivative type operation, improved the overall performance of the registration processor. This agrees with the preprocessing stage of the optimum filter derived in the application of the matched filter to the registration of images where the preprocessing filter is found to be a derivative type operator.

CHAPTER 1

INTRODUCTION

1.1. General Discussion

Image registration is a topic that has become important with the advent of satellite borne sensors capable of producing large quantities of multitemporal imagery. Analysis of the differences between images taken at different times requires that the images be matched spatially so that it can be determined how the corresponding data points change with time. This spatial alignment or overlaying of images is what is meant by image registration.

One of the primary objectives for overlaying temporally differing images is to provide the capability of utilizing the time dependent characteristics of a scene for its analysis. For example, imagery of agricultural areas are subject to change from one season to the next due to the growing cycle of the crops. If the classification of different crop species is the purpose of a project and the crop types of concern are indistinguishable spectrally at a particular time, then their growing cycles might provide the necessary information for separating one from the other.

Various investigations have been carried out attempting to determine what type of additional information is obtainable from the use of the time as well as spectral dimensions of the imagery. Several studies involve use of imagery taken by the multispectral scanner aboard the LANDSAT I satellite which orbits at an altitude of approximately 600

miles. The multispectral scanner operates in four spectral bands (0.5 - 0.6 μm, 0.6 - 0.7 μm, 0.7 - 0.8 μm, and 0.8 - 1.1 μm) and has a resolution of approximately 50 meters along the scan sweep by 80 meters along the satellite's path.

Utilizing LANDSAT I imagery, Anuta and Bauer [5] have performed an investigation of the use of multitemporal data for the recognition of different crop cover types and agricultural and urban feature change detection. With access to multitemporal imagery over the same area it was found that classification performance for different crop species could be improved during certain growing seasons. This study also showed that the automatic identification of urban change was promising but required further investigation. Another study also concerned with the problem of automatic crop identification is discussed in references [10] and [19]. Part of this investigation involved the effect of the use of multitemporal data as opposed to a single time data set on the performance of correctly recognizing particular crop types.

Design of a processor to carry out the overlay of images requires a certain amount of information about the spatial relationships of the imagery to be registered. If the images are spatially congruent, then the processor need only find the relative translation between the images. For images that differ not only by translation, but which are also distorted spatially relative to each other, the processor must be capable of determining the spatial distortions as well as the translation.

These are the classes of imagery addressed in this study, with the primary emphasis on spatially congruent images. The processor under investigation is that designed to find the relative translation between the images, assuming that no relative spatial distortions exist. Such

an analysis is directly applicable to a particular class of imagery which is currently available in large volume. The multispectral scanner data acquired by the LANDSAT I satellite has the property that the relative distortions between multipass imagery over the same area are minimal, which may be attributed to the stability of the viewing platform. Thus, as a first approximation, for small enough subimages the assumption of spatial congruence is reasonable.

Figures 1-1 through 1-4 contain examples of several sets of multitemporal imagery taken by the LANDSAT I multispectral scanner. Each of the figures displayed is from the 0.6 - 0.7 μm spectral band. Figure 1-1 shows two images over Tippecanoe County, Indiana which were taken in September and November of 1972. A scene from Hill County, Montana for two times during the spring and summer seasons is pictured in Figure 1-2. Figure 1-3 illustrates an example of a year's span over western Kansas where the data was taken in July of 1973 and 1974. And two temporally differing data sets over Missouri are shown in Figure 1-4. Note that although each of the scenes are recognizable from one time to the next, temporal changes are evident. Also observe that the spatial scale of both images in each time pair appears to be the same with little relative distortion. This supports the spatial congruence assumption for small subimages.

The assumption of spatial congruence for small subimages underlies several registration algorithms that have been proposed and implemented [1, 3, 8, 9, 11, 30]. This approach allows the overlay of a sample of corresponding subimages from each image assuming no relative spatial distortions exist for the small subimages. In the absence of spatial distortions each of the subimage registrations can be accomplished by a

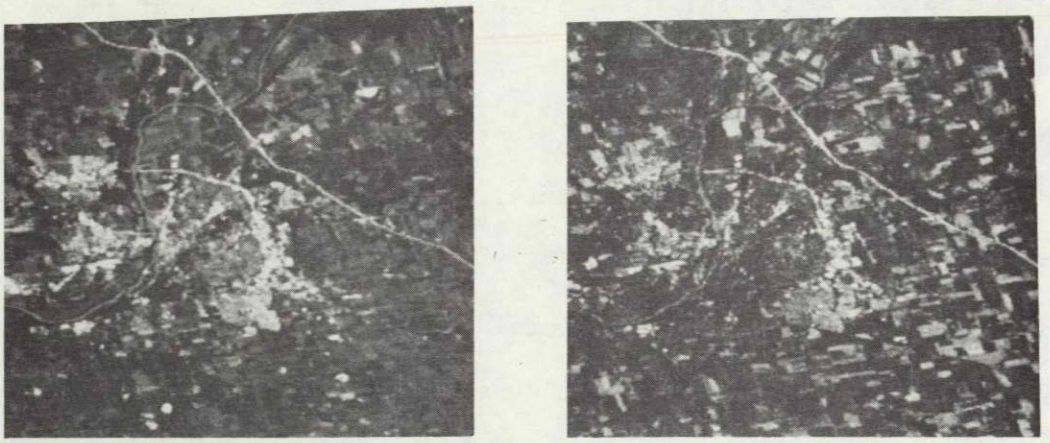

	9/30/72		11/29/72
LARS Run #	Spectral Band	Lines	Columns
72053603	0.6 - 0.7 μm	(500,750)	(575,825)

Figure 1-1. LANDSAT I imagery over Tippecanoe County, Indiana.

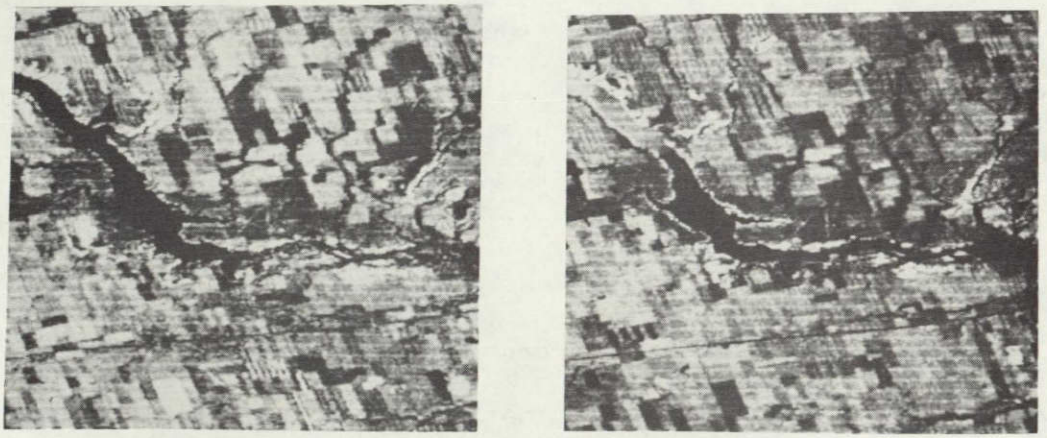

	5/5/73		7/16/73
LARS Run #	Spectral Band	Lines	Columns
73124700	0.6 - 0.7 μm	(110,360)	(110,360)

Figure 1-2. LANDSAT I imagery over Hill County, Montana.

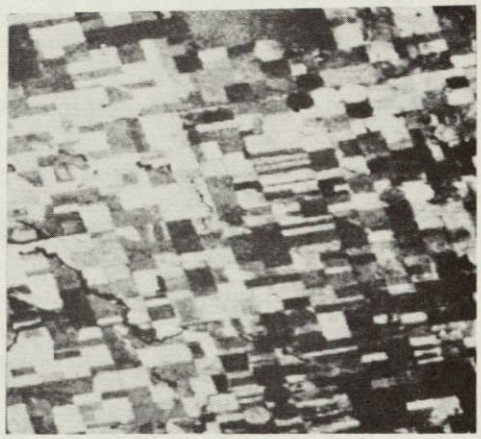

	7/6/73		7/1/74	
LARS Run #	Date Data Taken	Spectral Band	Lines	Columns
73046000	7/6/73	0.6 - 0.7 μm	(175,425)	(275,525)
74024200	7/1/74	0.6 - 0.7 μm	(275,525)	(175,425)

Figure 1-3. LANDSAT I imagery over Kansas.

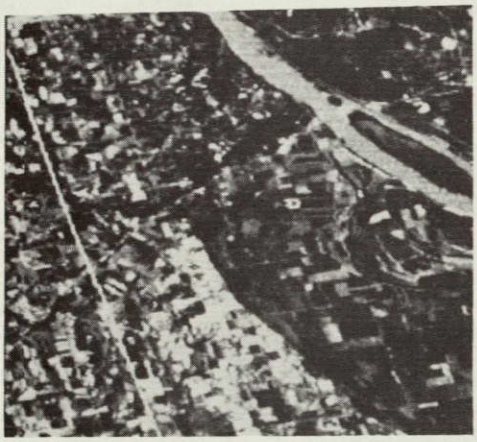

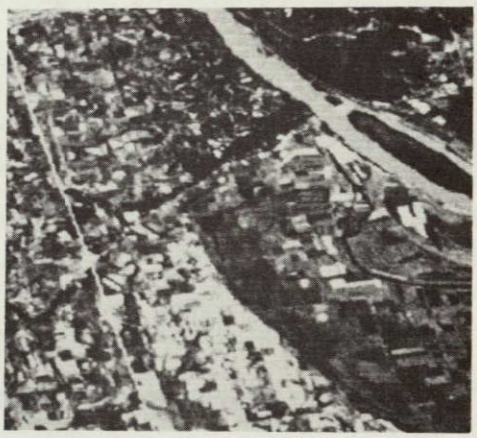

	8/26/73		10/1/72
LARS Run #	Spectral Band	Lines	Columns
72033804	0.6 - 0.7 μm	(375,625)	(475,725)

Figure 1-4. LANDSAT I imagery over Missouri.

relative translation. However, since the original images may be spatially distorted, all of these relative translations of the subimages may not be the same, so that the registration of the total image (full frame) cannot be accomplished by a simple translation. Therefore, given the translations for each of the corresponding subimages, a spatial warping or coordinage transformation is applied to one of the images so as to align all of the subimages simultaneously.

Once the relative spatial characteristics of the temporally differing images have been established, (which in this case is the spatial congruency of small subimages), a determination must be made of the remaining parameters required to achieve registration. For example, since registration is, by definition, a spatial matching, it requires a quantitative measure of the similarity between two images so that a determination can be made as to whether the match has been achieved or not. Thus, one requirement that must be met is that an appropriate similarity measure be chosen. A second parameter that must be considered is the temporal change that has occurred, since it is this change that contributes largely to the uncertainty in the registration of the images. Although the change at a particular data sample is unpredictable, a model of the overall characteristics and the spatial correlation of the temporal changes will increase the information available for the processor to use.

Another consideration that should be taken into account is the performance of the registration processor. Ultimately, the optimum processor is that which yields the best performance. This necessitates the development of a quantitative measure of the performance so that the optimum can be defined in terms of this measure. One example of such a criterion is the variance of the registration error, where the error is

the spatial difference between the true registration location and the position indicated by the processor. This error arises due to random differences in the images resulting from temporal changes that have occurred. In this case, the optimum processor is that which minimizes the variance.

The presence of the need to develop a processor capable of registering imagery has provided the impetus for research in the attempt to find a solution to this problem. The following section briefly outlines some of the previous developments and analyses that have been carried out.

1.2. Previous Investigations

With the availability of large volumes of multitemporal images acquired by the LANDSAT I multispectral scanner several image registration algorithms have been proposed and implemented. As mentioned in the preceeding section, the minimal relative spatial distortion between multitemporal imagery gathered by LANDSAT I has made feasible the design of processors based on the assumption that small subimages are spatially congruent. With this assumption a sampling of subimages from each of the images to be overlayed may be registered and the corresponding relative translation recorded for each subimage. Since the entire images may not be spatially congruent, all of the translations need not be the same, so that a spatial warping of one of the images is required to simultaneously align all of the subimages. Therefore, this minimal relative spatial distortion allows the registration process to be broken down into two stages. The first is that in which the spatially congruent subimages are registered and the second is that in which the spatial warping is carried out.

First consider those algorithms concerned only with images that are not relatively distorted spatially. Although all of these methods are similar in the fact that each performs a search for a given subimage in a larger background image containing the temporal changes, the actual procedure for carrying out this overlay and criteria for determining when the registration is achieved are different. The LARS registration system [1, 5] uses the correlation coefficient as the similarity measure (Table 6-1), where a maximum of its magnitude indicates the overlay location. A complete search is made over all possible registration locations, computing a value for the correlation coefficient at each translation.

A second algorithm which comes under the heading of sequential similarity detection algorithms (SSDA's) [8, 9], uses a different similarity measure at only a sample of points for each translation. The similarity measure used is the sum of the absolute values of the differences between the corresponding subimage data samples at each translation (Table 6-1). With this measure a minimum value indicates registration.

Another algorithm employing a similarity measure like the correlation coefficient plus saving computational time in a manner similar to the SSDA's, performs a preprocessing step prior to overlaying the imagery [30]. Instead of using the original imagery for registration, a gradient type operation is applied to each of the images first: then they are thresholded to produce binary images (images having values of only zero or one). Finally, these binary images are used to estimate the correct registration position.

Once a set of subimages has been registered a spatial warping of one of the images may be performed to match all of these subimages at the

same time. The algorithms developed to handle this part of the processor differ primarily in the amount of spatial warping necessary to adequately model the relative spatial distortions. The system at LARS [1 ,5] is set up to handle a second order two-dimensional polynomial transformation over an entire image. This may be refined by using a biquadratic warping over smaller subimages and then fitting the subimages back together [46], which in effect accommodates a higher order spatial warping. A further extension is made by an algorithm designed to accommodate spatial distortions on a line by line basis [12, 20, 22, 25, 26, 33, 42].

A second area of study has concerned analyses of the different aspects of the image registration problem as opposed to the development of specific algorithms for registering images. One series of investigations involves the distinguishability of the output of the processor at the correct registration location compared with the output at all surrounding locations [6 ,16, 32]. With the basic design criterion that the processor yield a maximum output at the correct registration position, a processor has been designed to maximize the ratio of the output at the correct registration position to the variance of the output at all surrounding positions. In this manner, the output at the correct registration position is made more easily distinguishable from that at the surrounding locations.

Another study examines the pull-in range of a processor, where the processor is simply a product correlator [13,14]. This analysis concerns the ability to determine the correct direction of movement in the search for the registration location, so that it is not necessary to search all prospective registration positions.

With regard to the situation in which the images to be registered are spatially distorted relative to one another, several studies have been made to determine ways of estimating this distortion. One approach uses the properties of the Fourier transforms of the images [16,17], and a second utilizes a least squares estimation procedure [45].

1.3. Outline of Investigation

The development of a registration processor is begun by first defining the image and temporal change properties in such a way as to form a foundation from which a solution may be approached in an organized fashion. For purposes of the present study one of the images to be registered is considered as the signal, while the second image is assumed to contain all of the temporal changes and is defined as the signal plus additive noise, where the temporal changes are modeled as additive noise. In this fashion the registration of the images may be approached as a parameter estimation problem in the presence of noise. The parameters to be estimated are the relative translations between the images. The noise is the temporal change and any measurement noise that may be present in the system.

Given this definition of how the images and temporal changes are to be treated, it is possible to determine a quantitative measure of the processor performance. This is done in Chapter 2 where an expression for the variance of the registration error is derived. The error is the difference between the correct registration position, and that position indicated by the processor which is operating in the presence of temporal changes. Alternatively, a second criterion which may be used to evaluate the processor is the output signal-to-noise ratio of the processor at the correct registration location.

Either of these quantitative criteria now may be utilized to define an optimum processor. For example, when considering the output signal-to-noise ratio, the optimum processor is that which maximizes it at the registration position. Alternatively, an optimum processor can be defined as the one that minimizes the variance of the registration error. Both of these considerations are explored and related in Chapters 2, 3 and Appendix A. In Chapter 2, where an expression for the registration error variance is derived, it is found that use of a filter which maximizes the output signal-to-noise ratio, the matched filter (2-36), leads to a compact expression for the variance. While in Appendix A it is shown that given the general expression for the registration error variance, the processor which minimizes this variance is the same as the one which maximizes the output signal-to-noise ratio. Therefore, the definition of optimum in terms of registration error variance minimization is equivalent to defining optimum in terms of output signal-to-noise maximization since both yield the same processor, which is the matched filter.

Using these results, Chapter 3 presents the method by which the matched filter may be found and implemented. An example is given illustrating this. The particular example chosen is designed to conform with experimental observations of autocorrelation function estimates for the temporal changes found between LANDSAT I images described in Chapter 5, which indicate that the autocorrelation function of the temporal changes is of an exponentially decaying form. This functional form for the autocorrelation function is the model chosen for the example. Thus, the example in Chapter 3 derives an optimum processor applicable to the registration of images in practice.

In Chapter 4 the effect of relative spatial distortions on the performance of a processor designed to operate on spatially congruent imagery is discussed. This degradation of performance is found in terms of the loss in signal-to-noise ratio as a result of the spatial distortions, where the relationship between performance and signal-to-noise ratio is given in Chapter 2 in terms of the variance of the registration error. One of the purposes of this section is to determine the optimum size of the images to be registered. For spatially congruent imagery it is readily shown that the largest possible image should be used for registration. However, this is not necessarily true when relative spatial distortions exist, since the spatial distortions cannot be removed by translation only. For the situation in which the distortions are increasing with image size (as for a constant scale factor change) it is shown that there is a particular image size which yields a maximum output signal-to-noise ratio. Determination of the optimum area size is a straightforward procedure which may be accomplished directly by evaluation of an integral expression. This is illustrated in section 4.5 where the expression for the output signal-to-noise ratio is evaluated by a numerical integration method for several different types of spatial distortions. Two general linear spatial distortions are presented as well as two examples using models of the spatial distortions observed for temporally differing LANDSAT I images. In these last two examples a straightforward method of applying the analytical results to practical image registration is illustrated.

In Chapter 5 the experimental analyses are begun. This chapter concerns the experimental estimation of the temporal change properties which are pertinent to the development of an optimum processor for

practical image registration. The derivation of an optimum processor presented in Chapter 2 is formulated via two approaches both of which require knowledge about certain properties of the temporal changes. The first method of solution necessitates the assumption that the probability density function of the temporal changes is Gaussian. Further examination of this formulation also shows that a model of the autocorrelation function of the temporal changes is required. This latter requirement is inherent in the Gaussian density function assumption. The second method of solution requires knowledge of only the temporal change autocorrelation function. Therefore, the two properties of concern are the probability density function and autocorrelation function of the temporal changes. The purpose of this chapter is to provide a model of these properties for LANDSAT I imagery so that an optimum registration processor may be designed for the overlaying of LANDSAT I images in practice. An experimental procedure is carried out for estimation of a general model for both of these properties. The first part of the study concerns the probability density function and the second part is concentrated on the autocorrelation function estimate. The general model observed for the autocorrelation function indicates that it is of an exponential form. This observation conforms with both the analyses in Chapters 2, 3, and Appendix A, and their application to the results of the experimental investigation carried out in Chapter 6.

Chapter 6 presents an experimental comparison of several different types of registration algorithms that have been proposed and implemented by other investigators [1, 3, 8, 9, 11, 30]. The impetus for such an investigation lies in the fact that each of these algorithms had been developed and tested independently of one another, thus leaving the

potential user at a loss to objectively compare their performance. This study is directed towards the relative evaluation of the techniques utilized in these registration algorithms for accomplishing the overlay of images. The techniques of concern are the similarity measure, the criterion used to measure the spatial matching between the images and and therefore indicate the registration location, and the effect of different preprocessing techniques on the registration performance. In this analysis it is found that the results support the combined analytical findings of Chapters 2, 3, and Appendix A in which it is found that the optimum processor is a matched filter, and the experimental findings of Chapter 5 where the autocorrelation function of the temporal changes is observed to be exponential. The processor that experimentally yielded the best performance utilized a gradient preprocessing operation on the images prior to overlaying them, which approximates the derivative type preprocessing operation derived in the example of Chapter 3 where a matched filter is used in the presence of exponentially autocorrelated noise or temporal changes.

Overall, the thesis provides an analytical and experimental investigation into the design of an optimum registration processor. Using the fundamental assumption of spatial congruity between the images, the design problem is approached via parameter estimation theory, where the parameters to be estimated are the relative translations between the images. In this way it is possible to define optimum in terms of a quantitative measure, as in the minimization of the registration error variance of the maximization of the output signal-to-noise ratio. Once the optimum processor has been derived, an analysis of the loss incurred by a deviation from the spatial congruity assumption is performed, since

this is the situation encountered in practice where relative spatial distortions arise due to perturbations in the viewing position of the scanner from one time to the next. Application of the analytically derived optimum processor to the overlay of images in practice is provided by the first experimental analysis in which a model is developed for the temporal-change properties required for evaluation of the optimum processor. Finally, this is followed by the experimental comparison of several algorithms for registering images which acts both to provide a relative performance rating of algorithms implemented by other investigators, plus to give an experimental evaluation of the analytical results found in the derivation of an optimum processor.

CHAPTER 2

VARIANCE OF THE REGISTRATION ERROR

An important part of the development of a registration processor is the ability to quantitatively characterize the registration problem in some manner. In this way, one may utilize this measure of performance to design an optimum processor which maximizes the performance according to the criterion chosen. One such measure of performance is the tolerance to within which one is able to register two images.

This section concerns the derivation of an expression for the variance of the registration error, where the error is the discrepancy between the observed registration position and the true registration location. Two models for the variance of the error in the registration of two different images of the same scene are developed. The method of solution employed is analogous to that used for the determination of the error in the measured delay time in a radar system. For purposes here the radar system model assumes that the returned signal is a delayed version of the original signal corrupted by additive noise. As adapted to the registration of two images, the noise is defined as the difference between the two images at the correct registration position, and is therefore additive. The time delay corresponds to a spatial translation or displacement.

Several analyses of the radar problem have been carried out based upon different premises [15],[29],[44]. These approaches may be

categorized as those which use the probability density function of the noise directly and those which do not. The first case utilizes maximum a posteriori probability, maximum likelihood, or minimum mean square error estimates. All three estimators are based upon knowledge of the noise probability density function. The second case is based only upon the output of a filter which gives a maximum output at the correct time delay when the input is noise free.

An analysis of this sort should prove useful in several respects. The results should give an indication of the best possible registration of two images given the models of the data and noise. Once the models of the parameters involved have been found or assumed, an optimum processor to implement the overlaying procedure may be developed. Comparison of existing registration systems with the results obtained herein may also be performed. However, one must keep in mind the assumptions the entire analysis will be based on, for different assumptions may yield different results.

It is assumed in the following investigation that the useful signal is present, reducing the problem to one of estimation only rather than detection as well as estimation. It is further assumed that the signal shape is known and nonrandom, although the parameter that is to be measured is a random variable. Since the original signal is known, it does not have a probability density function. However, the second signal does contain noise and possibly other perturbations and is therefore a sample function of a random process. The problem will be approached with this in mind.

2.1. Method 1

The solution to the problem of the first case, in which the probability density function of the noise is directly involved, depends upon the cost function which is assigned to the error and the a posteriori distribution, $p_f[m(\tau)]$, of the signal as a function of a parameter, $m(\tau)$, given the received signal, f. A minimum mean square error estimate is the mean of $p_f[m(\tau)]$; an absolute value cost function gives the median of the probability function; the maximum a posteriori estimate yields the maximum of $p_f[m(\tau)]$. The maximum likelihood estimate may be viewed as the same as the maximum a posteriori estimate when there is no prior knowledge of the density function of the parameter, $p[m(\tau)]$, or $p[m(\tau)]$ is assumed uniform over the entire range of interest. All four of the above cost functions will yield the same solution when $p[m(\tau)]$ is uniform and the conditional density function $p_m[\tau(f)]$ is symmetric and unimodal [43]. A Gaussian distribution which has been assumed for $p_f[m(\tau)]$ in several analyses, is a member of this latter class.

There are two basic reasons for the choice of this particular type of probability density function. The first is the availability of a closed form analytical solution. The second is that a Gaussian density function is the model that has been used to represent each of the classes which comprise the total image [36,37].

This derivation of the variance of the registration error is an adaptation of the solution obtained by Zubakov and Wainstein [40]. In this problem one assumes that the additive noise is jointly Gaussian with zero mean. It is also assumed that the density function of the parameter (i.e., the misregistration or displacement of the images) is uniform in the range of interest.

With these assumptions one may construct the likelihood function and then find its peak to determine the optimum estimator.

$$\Lambda(\tau_x,\tau_y) = p_f(\tau_x,\tau_y) = p(\tau_x,\tau_y)\,\frac{p_{\tau_x,\tau_y}(f)}{p(f)} \qquad (2\text{-}1)$$

where,

$\Lambda(\tau_x,\tau_y)$	likelihood function of the displacement parameters, τ_x and τ_y;
$p_f(\tau_x,\tau_y)$	conditional density function of τ_x and τ_y given $f(x,y)$;
$p(\tau_x,\tau_y)$	density function of the parameters τ_x and τ_y;
$p_{\tau_x,\tau_y}(f)$	conditional density function of $f(x,y)$ given the translation parameters τ_x and τ_y;
$p(f)$	density function of $f(x,y)$;
$m(x+\tau_x,y+\tau_y)$	known signal as a function of the spatial coordinates and the displacement parameters;
τ_x,τ_y	translation parameters
$f(x,y)$	$m(x,y) + n(x,y)$ = received signal;
$n(x,y)$	additive noise; assumed independent of the signal.

Since the data that are being analyzed are discrete, it is convenient to use integer subscripts rather than continuous spatial coordinates. A further notational savings is realized by combining the double subscripts into a single subscript. A two dimensional array m_{ij}, $i = 1, \ldots, p$; $j = 1, \ldots, q$, is converted to a one dimensional data set m_h, $h = 1, \ldots, pq$. This conversion loses nothing from the standpoint of the results to be derived.

In this discrete case a continuous function has been sampled and may be denoted,

$$m_h(\tau_x,\tau_y) = m(x_i+\tau_x, y_i+\tau_y)$$

$$n_h = n(x_i, y_j)$$

$$f_h = f(x_i, y_j) = m_h + n_h$$

$$h = 1, \ldots, H$$

$$H = pq = \text{total number of samples.}$$

To arrive at an analytical result, the probability density function of the noise must be known. Because of the many independent contributions to the differences between images being registered, it is reasonable to approximate the density function as being Gaussian. The probability density function of the noise is therefore given by

$$p_{\underline{n}}(\underline{n}) = \frac{1}{(2\pi)^{H/2}|\underline{R}|^{1/2}} \exp\left(-\frac{1}{2}\underline{n}^T\underline{R}^{-1}\underline{n}\right) \qquad (2\text{-}2)$$

where $\underline{R}$ is the covariance matrix of the noise, $R_{gh} = E[n_g n_h]$. The density functions in the likelihood equation then become,

$$p_{\tau_x,\tau_y}(\underline{f}) = p_{\underline{n}}(\underline{f}-\underline{m}(\tau_x,\tau_y))$$

$$\underline{f}^T = (f_1, \ldots, f_H)$$

$$\underline{m}^T = (m_1, \ldots, m_H).$$

The likelihood function is then

$$\Lambda(\tau_x,\tau_y) = p(\tau_x,\tau_y)\left[\frac{1}{p(\underline{f})} \cdot \frac{1}{(2\pi)^{H/2}|\underline{R}|^{1/2}}\right] \cdot \left[\exp\left(\sum_g^H \sum_h^H Q_{gh} f_g m_h(\tau_x,\tau_y) - \frac{1}{2}\sum_g^H \sum_h^H Q_{gh} m_g(\tau_x,\tau_y) m_h(\tau_x,\tau_y)\right)\right]$$

$$Q_{gh} = gh^{\text{th}} \text{ element of } \underline{R}^{-1}. \qquad (2\text{-}3)$$

Since it is only the maximum of $\Lambda(\tau_x,\tau_y)$ which is desired, the problem can be reduced even further. Let $p(\tau_x,\tau_y)$ be a uniform distribution over the area of interest. This is a reasonable assumption since there is no a priori knowledge about the actual distribution. With this assumption, examination of (2-3) shows that the only factor which is not a constant with respect to τ_x and τ_y is,

$$\phi = \sum_g^H \sum_h^H Q_{gh} f_g m_h(\tau_x,\tau_y) \tag{2-4}$$

since,

$$\sum_g^H \sum_h^H Q_{gh} m_g(\tau_x,\tau_y) m_h(\tau_x,\tau_y) \tag{2-5}$$

and $p(\tau_x,\tau_y)$ are constants for all values of τ_x and τ_y, and $p(f)$ does not depend upon τ_x and τ_y. Therefore, the maximum of $\Lambda(\tau_x,\tau_y)$ is determined solely by the maximum of ϕ. The optimum processor is then the one which finds the maximum of ϕ. This type of processor may be viewed as a correlator which is weighted according to the inverse noise covariance function, Q_{gh}. For the case in which the noise is white with spectrum $N_o/2$, the covariance matrix becomes $(N_o/2)\underline{I}$ ($\underline{I}$=identity matrix), and the optimum processor is simply a correlator.

$$\phi = \frac{2}{N_o} \sum_h^H f_h m_h(\tau_x,\tau_y) \tag{2-6}$$

Given that the maximum point (this translation position is denoted by $(\hat{\tau}_x,\hat{\tau}_y)$) of the likelihood function has been found, a measure of the accuracy of the estimate is necessary so that the performance of the estimator may be evaluated. One such measure is the variance of the estimate about the maximum point of $\Lambda(\tau_x,\tau_y)$. For this analysis it is convenient to use $\ln[\Lambda(\tau_x,\tau_y)]$ which is a monotonic function of $\Lambda(\tau_x,\tau_y)$.

The logarithm of the likelihood function is expanded in a second order Taylor series as a function of the delay parameters about its peak in the x-axis and y-axis directions separately. It is assumed that $\ln[\Lambda(\tau_x,\tau_y)]$ can be approximated by a second order polynomial around its peak.

Only the results in the x-axis direction are given since the y-axis direction results are completely analogous.

$$\ln \Lambda(\tau_x,\hat{\tau}_y) \simeq \ln \Lambda(\hat{\tau}_x,\hat{\tau}_y) + \frac{\partial \ln \Lambda(\hat{\tau}_x,\hat{\tau}_y)}{\partial \tau_x}(\tau_x-\hat{\tau}_x) + \frac{1}{2}\frac{\partial^2 \ln(\Lambda\, \hat{\tau}_x,\hat{\tau}_y)}{\partial \tau_x^2}(\tau_x-\hat{\tau}_x)^2 \tag{2-7}$$

where

$$\frac{\partial \ln \Lambda(\hat{\tau}_x,\hat{\tau}_y)}{\partial \tau_x} = \left.\frac{\partial \ln \Lambda(\tau_x,\tau_y)}{\partial \tau_x}\right|_{\substack{\tau_x=\hat{\tau}_x \\ \tau_y=\hat{\tau}_y}}$$

A necessary condition for the maximum point of $\ln \Lambda(\tau_x,\tau_y)$ is that,

$$\frac{\partial \ln \Lambda(\hat{\tau}_x,\hat{\tau}_y)}{\partial \tau_x} = 0 = \frac{\partial \ln \Lambda(\hat{\tau}_x,\hat{\tau}_y)}{\partial \tau_y} \tag{2-8}$$

The Taylor series expansion may then be reduced to

$$\ln \Lambda(\tau_x,\hat{\tau}_y) \simeq \ln \Lambda(\tau_x,\hat{\tau}_y) + \frac{1}{2}\frac{\partial^2 \ln \Lambda(\hat{\tau}_x,\hat{\tau}_y)}{\partial \tau_x^2}(\tau_x-\hat{\tau}_x)^2. \tag{2-9}$$

Rearranging this equation one obtains,

$$\Lambda(\tau_x,\hat{\tau}_y) = \Lambda(\hat{\tau}_x,\hat{\tau}_y)\ \exp\left[-\frac{1}{2}\frac{(\tau_x-\hat{\tau}_x)^2}{\Delta_x^2}\right] \tag{2-10}$$

where

$$\Delta_x^2 = -\left[\frac{\partial^2 \ln \Lambda(\hat{\tau}_x,\hat{\tau}_y)}{\partial\tau_x^2}\right]^{-1} = \text{variance in the x-direction} \tag{2-11}$$

Assuming $p_m(\tau_x,\tau_y)$ to be uniformly distributed,

$$\frac{1}{\Delta_x^2} = \sum_g^H \sum_h^H Q_{gh}[m_g(\hat{\tau}_x,\hat{\tau}_y)-f_g]\frac{\partial^2 m_h(\hat{\tau}_x,\hat{\tau}_y)}{\partial\tau_x^2}$$

$$+ \sum_g^H \sum_h^H Q_{gh}\frac{\partial m_g(\hat{\tau}_x,\hat{\tau}_y)}{\partial\tau_x}\ \frac{\partial m_h(\hat{\tau}_x,\hat{\tau}_y)}{\partial\tau_x}. \tag{2-12}$$

If one further assumes a large signal-to-noise ratio, then

$$\frac{1}{\Delta_x^2} = \sum_g^H \sum_h^H Q_{gh}\frac{\partial m_g(\hat{\tau}_x,\hat{\tau}_y)}{\partial\tau_x}\ \frac{\partial m_h(\hat{\tau}_x,\hat{\tau}_y)}{\partial\tau_x} \tag{2-13}$$

since $[m_g(\hat{\tau}_x,\hat{\tau}_y)-f_g]$ is dependent only upon the noise and is small compared to $m_g(\hat{\tau}_x,\hat{\tau}_y)$.

Greater insight into the solution may be obtained by looking at the result in the frequency domain as opposed to the spatial domain. The transformation yields an interesting answer. The variance becomes,

$$\Delta_x^2 = \frac{1}{\Delta W_x^2 \mu} \tag{2-14}$$

where

ΔW_x^2 effective bandwidth in the x-axis direction;

μ signal-to-noise ratio;

$$\mu = \sum_{u}^{p} \sum_{v}^{q} \frac{|M(u,v)|^2}{S_R(u,v)} \tag{2-15}$$

$$\Delta W_x^2 = \frac{4\pi^2 \sum_{u}^{p} \sum_{v}^{q} \frac{u^2 |M(u,v)|^2}{S_R(u,v)}}{\sum_{u}^{p} \sum_{v}^{q} \frac{|M(u,v)|^2}{S_R(u,v)}} \tag{2-16}$$

$M(u,v)$ Fourier transform of the known signal;

$S_R(u,v)$ noise spectrum.

In the spatial domain,

$$\mu = \sum_{g}^{H} \sum_{h}^{H} Q_{gh} m_g(\hat{\tau}_x, \hat{\tau}_y) m_h(\hat{\tau}_x, \hat{\tau}_y) \tag{2-17}$$

$$\Delta W_x^2 = \frac{\sum_{g}^{H} \sum_{h}^{H} Q_{gh} \frac{\partial m_g(\hat{\tau}_x, \hat{\tau}_y)}{\partial \tau_x} \frac{\partial m_h(\hat{\tau}_x, \hat{\tau}_y)}{\partial \tau_x}}{\sum_{g}^{H} \sum_{h}^{H} Q_{gh} m_g(\hat{\tau}_x, \hat{\tau}_y) m_h(\hat{\tau}_x, \hat{\tau}_y)}. \tag{2-18}$$

With the above assumptions the variance has been reduced to a function of the effective bandwidth and signal-to-noise ratio which are expressed in the frequency domain by equations (2-15) and (2-16), and in the spatial domain by equations (2-17) and (2-18). This implies that if one can estimate the effective bandwidth and the signal-to-noise ratio in the x-axis and y-axis directions, then the variance of the registration error can be estimated.

Now consider the second derivation for the variance which is based upon different assumptions.

2.2. Method 2

A second derivation of the variance of the registration error is developed in this section. In this case, the only assumption about the

signal and processor is that in the absence of noise, the output of the processor will be a maximum at the correct translation [29]. No assumptions about the probability distribution of the noise are needed. As will be seen, the results of this derivation are similar to those obtained in the previous derivation, even though the two approaches are quite unalike.

The signal corresponding to the image to be overlayed is modeled as having two components, the desired signal and additive noise. This signal is passed through a filter and the position where the maximum of the output signal occurs is taken to be the correct registration position. However, since the filter is designed to yield a maximum at the correct delay only in the noise free case, this observed registration position may differ from the true registration location. The discrepancy between these two positions is the registration error.

First consider the parameters involved.

$f(x,y)$	signal;
$m(x,y)$	additive noise;
$f(x,y) + m(x,y)$	data-set to be registered;
$h(x,y)$	filter impulse response;
$g(x,y)$	$f(x,y) * h(x,y)$ = output signal in the absence of noise;
$n(x,y)$	$m(x,y) * h(x,y)$ = output due to the noise input;
$z(x,y)$	$g(x,y) + n(x,y)$ = composite output signal used to estimate the correct registration position;
$(\tilde{x},\tilde{y})$	true registration position;
$(\hat{x},\hat{y})$	estimated registration position.

The derivation proceeds as follows. First expand $g(x,y)$ in a second order Taylor series about $(\tilde{x},\tilde{y})$.

$$g(x,y) \simeq g(\tilde{x},\tilde{y}) + g_x(\tilde{x},\tilde{y})[x-\tilde{x}] + g_y(\tilde{x},\tilde{y})[y-\tilde{y}]$$
$$+ g_{xy}(\tilde{x},\tilde{y})[x-\tilde{x}][y-\tilde{y}] + \tfrac{1}{2} g_{xx}(\tilde{x},\tilde{y})[x-\tilde{x}]^2$$
$$+ \tfrac{1}{2} g_{yy}(\tilde{x},\tilde{y})[y-\tilde{y}]^2 \qquad (2\text{-}19)$$

where the subscripts denote the partial derivatives with respect to the corresponding variables,

$$g_x(\tilde{x},\tilde{y}) = \left.\frac{\partial g(x,y)}{\partial x}\right|_{x=\tilde{x},\ y=\tilde{y}}$$

This subscript notation is used for the remainder of this section. Assume that $(x-\tilde{x})$ and $(y-\tilde{y})$ are small enough so that all higher order terms may be neglected.

Note that a necessary condition for a maximum is

$$\frac{\partial g(\tilde{x},\tilde{y})}{\partial x} = 0 = \frac{\partial g(\tilde{x},\tilde{y})}{\partial y}\ .$$

Substitute this result into the equation for $z(x,y)$.

$$z(x,y) = g(\tilde{x},\tilde{y}) + g_{xy}(\tilde{x},\tilde{y})[x-\tilde{x}][y-\tilde{y}]$$
$$+ \tfrac{1}{2} g_{xx}(\tilde{x},\tilde{y})[x-\tilde{x}]^2$$
$$+ \tfrac{1}{2} g_{yy}(\tilde{x},\tilde{y})[y-\tilde{y}]^2 + n(x,y). \qquad (2\text{-}20)$$

Again use the necessary condition for an observed maximum,

$\partial z(\hat{x},\hat{y})/\partial x = 0 = \partial z(\hat{x},\hat{y})/\partial y$,

$$z_x(\hat{x},\hat{y}) = 0 = g_{xy}(\tilde{x},\tilde{y})[\hat{y}-\tilde{y}]$$
$$+ g_{xx}(\tilde{x},\tilde{y})[\hat{x}-\tilde{x}] + n_x(\hat{x},\hat{y}) \qquad (2\text{-}21)$$

$$z_y(\hat{x},\hat{y}) = 0 = g_{xy}(\tilde{x},\tilde{y})[\hat{x}-\tilde{x}]$$
$$+ g_{yy}(\tilde{x},\tilde{y})[\hat{y}-\tilde{y}] + n_y(\hat{x},\hat{y}). \qquad (2\text{-}22)$$

Arrange these equations in terms of $(\hat{x}-\tilde{x})$ and $(\hat{y}-\tilde{y})$, the error in the registration.

$$(\hat{x}-\tilde{x}) = \frac{g_{xy}n_y - g_{yy}n_x}{g_{xx}g_{yy} - g_{xy}^2} \tag{2-23}$$

$$(\hat{y}-\tilde{y}) = \frac{g_{xy}n_x - g_{xx}n_y}{g_{xx}g_{yy} - g_{xy}^2} \tag{2-24}$$

where the arguments, $(\hat{x},\hat{y})$ and $(\tilde{x},\tilde{y})$ have been left out for notational convenience.

One can now find the variance of the error by taking the expectation of $(\hat{x}-\tilde{x})^2$ and $(\hat{y}-\tilde{y})^2$, where it is assumed that $E[\hat{x}-\tilde{x}] = 0 = E[\hat{y}-\tilde{y}]$.

$$\text{Var}[\hat{x}-\tilde{x}] = E[(\hat{x}-\tilde{x})^2] = \overline{(\hat{x}-\tilde{x})^2} \tag{2-25}$$

$$\text{Var}[\hat{y}-\tilde{y}] = E[(\hat{y}-\tilde{y})^2] = \overline{(\hat{y}-\tilde{y})^2} \tag{2-26}$$

$$\overline{(\hat{x}-\tilde{x})^2} = \frac{g_{xy}^2\overline{n_y^2} - 2g_{xy}g_{yy}\overline{n_y n_x} + g_{yy}^2\overline{n_x^2}}{[g_{xx}g_{yy} - g_{xy}^2]^2} \tag{2-27}$$

$$\overline{(\hat{y}-\tilde{y})^2} = \frac{g_{xy}^2\overline{n_x^2} - 2g_{xy}g_{xx}\overline{n_y n_x} + g_{xx}^2\overline{n_y^2}}{[g_{xx}g_{yy} - g_{xy}^2]^2} \tag{2-28}$$

One may use these equations to calculate the variance of the error, but in doing so, it is found that a filter function must be specified first. This is intrinsic in the parameters in these equations, which is seen more clearly if one writes these terms as a function of the filter (wide sense stationarity is assumed).

$$\overline{n_y^2(\hat{x},\hat{y})} = \iiiint h_y(\hat{x}-\alpha,\hat{y}-\beta)h_y(\hat{x}-\gamma,\hat{y}-\lambda) \cdot R_m(\alpha-\gamma,\beta-\lambda)\,d\alpha\,d\beta\,d\gamma\,d\lambda \tag{2-29}$$

$$\overline{n_y(\hat{x},\hat{y})\,n_x(\hat{x},\hat{y})} = \iiiint h_y(\hat{x}-\alpha,\hat{y}-\beta) \cdot h_x(\hat{x}-\gamma,\hat{y}-\lambda)\,R_m(\alpha-\gamma,\beta-\lambda) \cdot d\alpha\,d\beta\,d\gamma\,d\lambda \tag{2-30}$$

$$\overline{n_x^2(\hat{x},\hat{y})} = \iiiint h_x(\hat{x}-\alpha,\hat{y}-\beta)h_x(\hat{x}-\gamma,\hat{y}-\lambda) \cdot R_m(\alpha-\gamma,\beta-\lambda)d\alpha\,d\beta\,d\gamma\,d\lambda \tag{2-31}$$

$$g_{xx}(\tilde{x},\tilde{y}) = \iint h_{xx}(\tilde{x}-\alpha,\tilde{y}-\beta)\ f(\alpha,\beta)\ d\alpha\,d\beta \tag{2-32}$$

$$g_{yy}(\tilde{x},\tilde{y}) = \iint h_{yy}(\tilde{x}-\alpha,\tilde{y}-\beta)\ f(\alpha,\beta)\ d\alpha\,d\beta \tag{2-33}$$

$$g_{xy}(\tilde{x},\tilde{y}) = \iint h_{xy}(\tilde{x}-\alpha,\tilde{y}-\beta)\ f(\alpha,\beta)\ d\alpha\,d\beta \tag{2-34}$$

where

$$R_m(\alpha-\gamma,\ \beta-\lambda) = \overline{m(\alpha,\beta)m(\gamma,\lambda)} \tag{2-35}$$

One now has an expression for determining the registration error variance. Equations (2-27) and (2-28) will allow one to find the variance of the error for any filter function; however, they seem to bear little resemblance to the results in the first section. To obtain a particular solution, a specific filter function must be chosen. The one that has been picked is intuitively pleasing in two ways: it is an optimum type filter in that it maximizes the signal-to-noise ratio; and it yields an answer in terms of the signal bandwidth and signal-to-noise ratio. In Appendix A it is also shown that this filter minimizes the error variance. This filter is the so called "matched filter."

Let

$$H(u,v) = \frac{F^*(u,v)\ \exp\ (-j2\pi(\tilde{x}u + \tilde{y}v))}{S_m(u,v)} \tag{2-36}$$

$S_m(u,v)$ Fourier transform of $R_m(x,y)$;

$F(u,v)$ Fourier transform of $f(x,y)$;

$H(u,v)$ Fourier transform of $h(x,y)$.

Substituting this filter function into equations (2-27) and (2-28), the results simplify to,

$$\overline{(\hat{x}-\tilde{x})^2} = \left[\frac{g_{xy}^2}{g_{yy}} - g_{xx}\right]^{-1} \tag{2-37}$$

$$\overline{(\hat{y}-\tilde{y})^2} = \left[\frac{g_{xy}^2}{g_{xx}} - g_{yy}\right]^{-1} \tag{2-38}$$

This simplification is seen more easily if one first converts equations (2-29) through (2-34) to the frequency domain and then inserts the matched filter.

One obtains the final result by converting these last two equations to the frequency domain. They then become,

$$\overline{(\hat{x}-\tilde{x})^2} = \left[-\frac{g_{xy}^2}{B_y^2 SNR} + B_x^2 SNR\right]^{-1} \tag{2-39}$$

$$\overline{(\hat{y}-\tilde{y})^2} = \left[-\frac{g_{xy}^2}{B_x^2 SNR} + B_y^2 SNR\right]^{-1} \tag{2-40}$$

where

$$B_x = \left[\frac{4\pi^2 \iint u^2 \frac{|F(u,v)|^2}{S_m(u,v)}\, du\, dv}{\iint \frac{|F(u,v)|^2}{S_m(u,v)}\, du\, dv}\right]^{1/2} \tag{2-41}$$

B_x effective bandwidth of input signal in the x-axis direction;

$$B_y = \left[\frac{4\pi^2 \iint v^2 \frac{|F(u,v)|^2}{S_m(u,v)} \, du \, dv}{\iint \frac{|F(u,v)|^2}{S_m(u,v)} \, du \, dv} \right]^{1/2} \tag{2-42}$$

B_y = effective bandwidth of input signal in the y-axis direction;

$$SNR = \iint \frac{|F(u,v)|^2}{S_m(u,v)} \, du \, dv \tag{2-43}$$

SNR = output signal-to-noise ratio.

It is seen that the variance of the error is again expressible in terms of the effective signal bandwidth and signal-to-noise ratio. These results are similar to those obtained in the first section, but the relationships are not quite as simple.

A further simplication can be obtained by making some additional assumptions. The error variance expressions then will be the same as in the first method. These assumptions concern the term $g_{xy}(\tilde{x},\tilde{y})$ in equations (2-39) and (2-40). If this term equals zero, then the desired result is obtained. Such a condition involves the quantity $[|F(u,v)|^2]/[S_m(u,v)]$ since $g_{xy}(\tilde{x},\tilde{y})$ is a function of this quantity. Let $K(u,v) = [|F(u,v)|^2]/[S_m(u,v)]$ for notational convenience. Since $K(u,v)$ is an even function of u and v, in order for $g_{xy}(\tilde{x},\tilde{y})$ to equal zero it is sufficient that,

$$K(u,v) = K(-u,v) \tag{2-44}$$

or necessary and sufficient that,

$$\int_0^\infty \int_0^\infty uv \, K(u,v) \, du \, dv = \int_0^\infty \int_0^\infty uv \, K(-u,v) \, du \, dv. \tag{2-45}$$

The expressions then become

$$\overline{(\hat{x}-\tilde{x})^2} = \frac{1}{B_x^2 SNR} \tag{2-46}$$

$$\overline{(\hat{y}-\tilde{y})^2} = \frac{1}{B_y^2 SNR} \tag{2-47}$$

which are completely analogous to the results obtained by the first method.

An example of when these last assumptions might apply is the following situation. Let $F(u,v)$ and $S_m(u,v)$ be bandlimited to W_x and W_y in the respective axis directions. And let $[|F(u,v)|^2]/[S_m(u,v)]$ equal a constant. This would occur when the noise spectrum has a shape similar to the signal spectrum. In this case, it might be advantageous to model the two spectra as differing only by a constant factor for simplicity in estimating the variance to be expected. This may be written,

$$\frac{|F(u,v)|^2}{S_m(u,v)} = c, \text{ a constant.} \tag{2-48}$$

From Equation (2-43)

$$SNR = c \int_{-W_y}^{W_x} \int_{-W_y}^{W_y} du\, dv. \tag{2-49}$$

So,

$$c = \frac{SNR}{4W_x W_y}. \tag{2-50}$$

Then from equations (2-41), (2-42) and (2-43),

$$B_x^2\, SNR = 4\pi^2\, c \left[\frac{2W_x^3}{3}\right] (2W_y) \tag{2-51}$$

$$B_y^2\, SNR = 4\pi^2\, c(2W_x) \left[\frac{2W_y^3}{3}\right]. \tag{2-52}$$

Substituting in the expressions for c, the variances are,

$$\overline{(\hat{x}-\tilde{x})^2} = \frac{3}{4\pi^2 W_x^2 SNR} \tag{2-53}$$

$$\overline{(\hat{y}-\tilde{y})^2} = \frac{3}{4\pi^2 W_y^2 SNR} \tag{2-54}$$

The respective standard deviations then are,

$$\text{Standard deviation of } (\hat{x}-\tilde{x}) = \frac{1}{2\pi W_x}\sqrt{\frac{3}{SNR}} \tag{2-55}$$

$$\text{Standard deviation of } (\hat{y}-\tilde{y}) = \frac{1}{2\pi W_y}\sqrt{\frac{3}{SNR}} \tag{2-56}$$

One may obtain a quantitative feel for the values of these expressions by using the sampling intervals for the LANDSAT-1 data in this example. The sampling interval is about 60 meters along the columns and about 80 meters along the lines. Substituting these values in equations (2-55) and (2-56), one finds that,

Standard deviation of error long the

$$\text{lines} = \frac{44.1}{\sqrt{SNR}} \text{ meters} \tag{2-57}$$

Standard deviation of error along the

$$\text{columns} = \frac{33.1}{\sqrt{SNR}} \text{ meters.} \tag{2-58}$$

These results indicate that with the chosen filter, the standard deviation of the registration error is quite small.

2.3. Conclusion

A quantitative measure of the registration processor accuracy in terms of the variance of the error of the registration has been derived.

With the appropriate assumptions, the variance is shown to be inversely proportional to the square of the effective bandwidth times the signal-to-noise ratio. The final expressions are presented again to emphasize both the form and simplicity of their representation.

$$\text{Var } [(\hat{x}-\tilde{x})] = \frac{1}{B_x^2 SNR}$$

$$\text{Var } [(\hat{y}-\tilde{y})] = \frac{1}{B_y^2 SNR}$$

This derivation should prove useful in several respects. First of all it may be a basis for the analysis of different registration systems by providing a way to estimate the expected accuracy of the system. Secondly, it provides a straightforward way of estimating this error.

As a final consideration the basic assumptions needed for the two methods are listed. These assumptions are important and must be realized fully to be sure that they apply to the situation in which they will be utilized. For the first method these assumptions are: the noise is additive and independent of the signal; the joint probability density function of the noise is Gaussian; the a priori distribution of the delay parameters is uniform over the range of interest; the variance may be modeled in the x-axis and y-axis directions separately; the final result is dependent upon a large signal-to-noise ratio [cf. step from equation (2-12) to (2-13)]. The basic assumptions for the second method are: the noise is additive and independent of the signal; the noise spectrum must be known; the chosen filter is the "matched filter;" to obtain results completely analogous to the first method there is one further assumption that must be made about the ratio $[|F(u,v)|^2]/[S_m(u,v)]$ [cf. equations (2-44) and (2-45)].

In particular, note the assumptions related to the probability density function and the spectrum of the noise. The validity of assuming a Gaussian density function and of assuming a particular type of autocorrelation (or spectral density) function is pursued further in succeeding sections. The discussions approach these issues along both analytical and experimental lines, the first to provide a theoretical basis for what should occur, and the second to provide confirmation of these assumptions.

CHAPTER 3

IMPLEMENTATION OF A MATCHED FILTER FOR IMAGE REGISTRATION

In the previous sections it was indicated that the registration processor performance improved as the output signal-to-noise ratio (SNR_o) increased. For example, the variance of the registration error is shown to decrease with an increase in the SNR_o, thus providing a greater registration accuracy (Chapter 2). This result prompts an investigation to find the processor which maximizes the SNR_o thereby improving the system performance. Such an analysis is carried out in this chapter.

The general form for the processor chosen is that of a linear filter whose input is the known signal plus zero mean, additive noise, and whose output is designed to yield a maximum at the correct registration location in the absence of noise. For completeness, a detailed derivation of the filter which yields the maximum SNR_o is provided first. These findings are then utilized in an example illustrating the optimum filter one obtains in the presence of a particular type of noise, where the type of noise reasonably models that observed experimentally (Chapter 5). The analytical approach to this problem is stressed in this section, while its agreement with experimental observation is discussed in Chapters 5 and 6.

The output signal-to-noise ratio at the translation (τ_x,τ_y) is defined as follows.

$$SNR_o = \frac{\left[\int_{-\infty}^{\infty} h(\tau_x - x, \tau_y - y) s(x,y)\ dxdy\right]^2}{E\left\{\left[\int_{-\infty}^{\infty} h(\tau_x - x, \tau_y - y) n(x,y)\ dxdy\right]^2\right\}} \tag{3-1}$$

$h(x,y)$ = processing filter

$s(x,y)$ = known signal

$n(x,y)$ = additive noise

Or equivalently,

$$SNR_o = \frac{\left[\int_{-\infty}^{\infty} h(\tau_x - x, \tau_y - y) s(x,y)\ dxdy\right]^2}{\int_{-\infty}^{\infty}\int_{-\infty}^{\infty} h(\tau_x - x, \tau_y - y) h(\tau_x - \alpha, \tau_y - \beta) R_n(x-\alpha, y-\beta)\ dxdy\ d\alpha d\beta} \tag{3-2}$$

Where $E\{\cdot\}$ denotes expectation and $R_n(\tau_x, \tau_y)$ is the autocorrelation function of the noise.

The filter which maximizes this expression is derived in two basic steps. Let,

$$h(x,y) = \int\int h_w(x-\alpha, y-\beta) h_m(\alpha,\beta)\ d\alpha\ d\beta \tag{3-3}$$

where $h_w(\cdot,\cdot)$ is a prewhitening filter; i.e., for,

$$n_w(x,y) = \int\int h_w(x-\alpha, y-\beta) n(\alpha,\beta)\ d\alpha\ d\beta \tag{3-4}$$

choose $h_w(x,y)$ such that,

$$E[n_w(x,y)\, n_w(\alpha,\beta)] = \delta(x-\alpha, y-\beta) \tag{3-5}$$

and $h_m(\cdot,\cdot)$ is the filter which maximizes the SNR_o with the prewhitened noise and signal. The underlying reason for this approach is that in the presence of white noise, the Schwartz inequality may be applied directly to arrive at the desired filter function in a simple manner. Schematically, the composite filter is as shown in Figure 3-1.

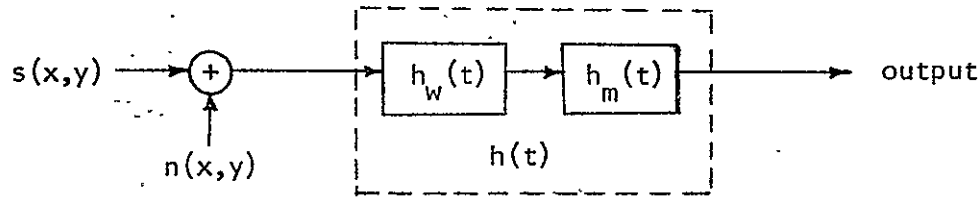

Figure 3-1. Component representation of matched filter.

Since,

$$E[n_w(x,y)n_w(a,b)] = \int_{-\infty}^{\infty}\int_{-\infty}^{\infty} h_w(x-\alpha,y-\beta)h_w(a-\gamma,b-\xi)R_n(\alpha-\gamma,\beta-\xi)\,d\alpha\,d\beta\,d\gamma\,d\xi \tag{3-6}$$

and

$$E[n_w(x,y)n_w(a,b)] = \delta(x-a,y-b)$$

$h_w(x,y)$ is found by solving the integral equation,

$$\delta(x-a,y-b) = \int_{-\infty}^{\infty}\int_{-\infty}^{\infty} h_w(x-\alpha,y-\beta)h_w(a-\gamma,b-\xi)R_n(\alpha-\gamma,\beta-\xi)\,d\alpha\,d\beta\,d\gamma\,d\xi \tag{3-7}$$

which may be equivalently expressed as,

$$\delta(x-a,y-b) = \int_{-\infty}^{\infty}\int H_w(u,v)H_w(-u,-v)S_n(u,v)e^{j2\pi[u(x-a)+v(y-b)]}\,dudv \tag{3-8}$$

where,

$H_w(u,v)$ = Fourier transform of $h_w(x,y)$

$S_n(u,v)$ = Fourier transform of $R_n(\tau_x,\tau_y)$, or the spectral density of the noise

The solution to this integral equation is,

$$H_w(u,v)H_w(-u,-v)S_n(u,v) = 1 \tag{3-9}$$

since $\delta(x,y) = \int_{-\infty}^{\infty}\int 1 \cdot e^{j2\pi(ux + vy)}\,dudv$, by the properties of the Fourier transform.

In the case of a real filter function, which is the situation encountered with the registration of imagery, then,

$$H_w(-u,-v) = H_w^*(u,v) \tag{3-10}$$

so that the solution becomes,

$$|H_w(u,v)|^2 = \frac{1}{S_n(u,v)} \tag{3-11}$$

Once the noise has been prewhitened, the problem reduces to,

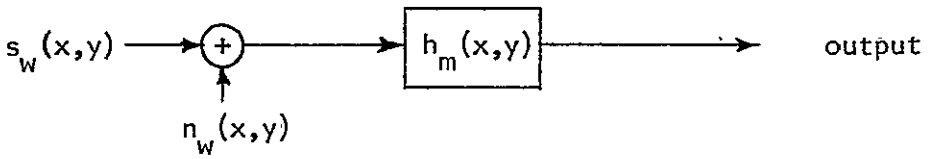

Figure 3-2. Block diagram after prewhitening.

$$s_w(x,y) = \int_{-\infty}^{\infty}\int h_w(x-\alpha,y-\beta)s(\alpha,\beta)\ d\alpha d\beta$$

$$n_w(x,y) = \int_{-\infty}^{\infty}\int h_w(x-\alpha,y-\beta)n(\alpha,\beta)\ d\alpha d\beta$$

where one must find the filter, $h_m(x,y)$, which maximizes the SNR_o.

$$SNR_o = \frac{\left[\int_{-\infty}^{\infty}\int h_m(\tau_x-x,\tau_y-y)s_w(x,y)\ dxdy\right]^2}{E\left\{\left[\int_{-\infty}^{\infty}\int h_m(\tau_x-x,\tau_y-y)n_w(x,y)dxdy\right]^2\right\}} \tag{3-12}$$

Utilizing the whiteness property of $n_w(x,y)$, the SNR_o becomes,

$$SNR_o = \frac{\left[\int_{-\infty}^{\infty}\int h_m(\tau_x-x,\tau_y-y)s_w(x,y)\ dxdy\right]^2}{\int_{-\infty}^{\infty}\int h_m^2(\tau_x-x,\tau_y-y)\ dxdy} \tag{3-13}$$

This expression then has an upper bound which is found by applying the Schwartz inequality.

$$SNR_o \leq \int_{-\infty}^{\infty}\int s_w^2(x,y)\, dxdy \tag{3-14}$$

with equality for,

$$h_m(\tau_x - x, \tau_y - y) = k\, s_w(x,y) \tag{3-15}$$

where k is an arbitrary constant. Letting k = 1, the maximum SNR_o is achieved for,

$$h_m(\tau_x - x, \tau_y - y) = s_w(x,y) \tag{3-16}$$

or equivalently in the frequency domain,

$$H_m(u,v) = S_w(-u,-v)e^{-j2\pi[u\tau_x + v\tau_y]} \tag{3-17}$$

and

$$|H_w(u,v)|^2 = \frac{1}{S_n(u,v)} \tag{3-18}$$

The block diagram in Figure 3-1 may now be replaced by its equivalent form, combining the cascaded filters $h_m(x,y)$ and $h_w(x,y)$, as shown in Figure 3-3.

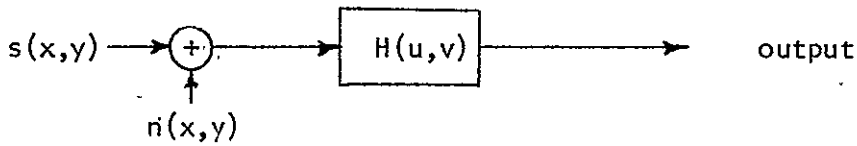

Figure 3-3. Block diagram of matched filter.

where H(u,v) is the Fourier transform of h(x,y) and,

$$H(u,v) = H_w(u,v)H_m(u,v) \tag{3-19}$$

Substitution of the expressions for $H_m(u,v)$ and $H_w(u,v)$ in conjunction with the identity,

$$S_w(u,v) = H_w(u,v)S(u,v) \tag{3-20}$$

$S(u,v)$ = Fourier transform of $s(x,y)$

and the assumption of a real valued signal, allows one to obtain the final expression for the filter which maximizes the SNR_o.

$$H(u,v) = \frac{S^*(u,v)}{S_n(u,v)} e^{-j2\pi[u\tau_x + v\tau_y]} \tag{3-21}$$

Note that the desired filter depends only upon the signal, $S(u,v)$, and the spectral density, $S_n(u,v)$, or autocorrelation function, $R_n(\tau_x,\tau_y)$, of the noise. Since the signal is known, the only additional knowledge required is the noise autocorrelation function.

Before proceeding with the example, first consider an equivalent form for the block diagram of Figure 3-3. Observe that in Figure 3-3 the entire processing filter is lumped under the heading of $H(u,v)$. An equivalent operation is to prewhiten the received signal, prewhiten the known signal, and then crosscorrelate the two. This is illustrated in Figure 3-4.

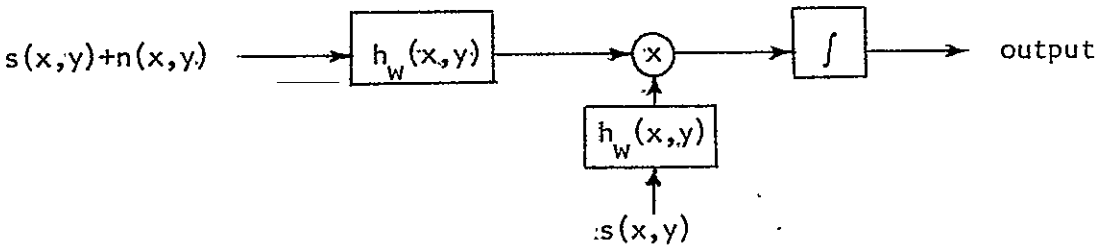

Figure 3-4. Prewhitening representation of matched filter.

The reason for viewing the operations in this manner is because it is analogous to the preprocessing state of image registration, where the two images to be overlayed are first preprocessed and then registered via a crosscorrelation technique.

The following example provides an illustration of the filter required to achieve the maximum SNR_o for noise with a specific type of autocorrelation function. The particular parametric form for the autocorrelation function used was chosen because it was found to provide a reasonable model of the autocorrelation function encountered experimentally (Chapter 5). The interpretation of the operations will follow the block diagram of Figure 3-4, where a prewhitening operation is applied to both the received and known signals. Let,

$$R_n(\tau_x,\tau_y) = A^2 e^{-\alpha|\tau_x| - \beta|\tau_y|} \tag{3-22}$$

Then,

$$S_n(u,v) = \int_{-\infty}^{\infty}\int A^2 e^{-\alpha|\tau_x| - \beta|\tau_y|} e^{-j2\pi[u\tau_x + v\tau_y]} d\tau_x d\tau_y \tag{3-23}$$

Carrying out the integration one obtains the following expression for the spectral density.

$$S_n(u,v) = A^2\left[\frac{2\alpha}{\alpha^2 + 4\pi^2u^2}\right]\left[\frac{2\beta}{\beta^2 + 4\pi^2v^2}\right] \tag{3-24}$$

Since,

$$|H_w(u,v)|^2 = \frac{1}{S_n(u,v)}$$

it follows that

$$|H_w(u,v)|^2 = \frac{1}{4A^2\alpha\beta}[\alpha^2 + 4\pi^2u^2][\beta^2 + 4\pi^2v^2] \tag{3-25}$$

$H_w(u,v)$ is found by factoring the above expression which is of the form $H_w(u,v)H_w(-u,-v)$. Carrying out the factoring operation gives

$$H_w(u,v) = \frac{1}{2A\sqrt{\alpha\beta}}[\alpha + j2\pi u][\beta + j2\pi v] \tag{3-26}$$

At this point one may evaluate $H_w(u,v)$ via two different approaches: a single two-dimensional filter, or two cascaded one-dimensional filters.

Single Two-Dimensional Filter

$$H_w(u,v) = \frac{1}{2A\sqrt{\alpha\beta}} [\alpha\beta + \beta j2\pi u + \alpha j2\pi v - 4\pi^2 uv] \tag{3-27}$$

Cascaded One-Dimensional Filters

$$H_w(u,v) = H_{w_u}(u)\, H_{w_v}(v) \tag{3-28}$$

$$H_{w_u}(u) = \frac{1}{\sqrt{2\alpha A}} [\alpha + j2\pi u] \tag{3-29}$$

$$H_{w_v}(v) = \frac{1}{\sqrt{2\beta A}} [\beta + j2\pi v] \tag{3-30}$$

In the spatial domain these filters become,

Single Two-Dimensional Filter

$$h_w(x,y) = \frac{1}{2A\sqrt{\alpha\beta}} [\alpha\beta\, \delta(x,y) + \beta \frac{d}{dx} + \alpha \frac{d}{dy} + \frac{d^2}{dxdy}] \tag{3-31}$$

Cascaded One-Dimensional Filters

$$h_{w_x}(x) = \frac{1}{\sqrt{2\alpha A}} [\alpha\, \delta(x,y) - \frac{d}{dx}] \tag{3-32}$$

$$h_{w_y}(y) = \frac{1}{\sqrt{2\beta A}} [\beta\, \delta(x,y) - \frac{d}{dy}] \tag{3-33}$$

The important point to be noticed here is that the prewhitening filter is a derivative type processor. This indicates that when one is registering two images by first preprocessing each image and then crosscorrelating, a derivative type operator in the presence of noise with an exponential

autocorrelation function will maximize the SNR_o and thus improve the expected registration performance. This prediction is corroborated by experimental observations which are discussed in Chapter 6.

CHAPTER 4

CHANGES IN THE OUTPUT SIGNAL-TO-NOISE RATIO DUE TO RELATIVE SPATIAL DISTORTIONS BETWEEN IMAGES

In the following analysis the change in the output signal-to-noise ratio (SNR) is computed, for the situation in which the images to be registrated are distorted spatially with respect to each other. The need for such an investigation is prompted by the fact that in the case of LANDSAT imagery, small relative spatial distortions exist between images taken on different orbits over the same area. The probable cause of this lies in small unavoidable perturbations in the satellite's orbit such as altitude, heading, and pitch. Similar, but more pronounced spatial distortions also occur in aircraft scanner imagery.

When the registration problem is modeled as passing the background image containing the temporal changes (received signal plus additive noise) through a filter so as to maximize the SNR at the correct registration position, the processor used essentially correlates a filtered version of the background image (signal plus noise) with a filtered version of the reference image (signal), where the two images to be registered are denoted as the background image and the reference image. The background image is a temporally differing and spatially distorted version of the reference image corrupted by additive noise. One of the parameters that must be chosen in this correlation is the area over which the integration is carried out. For geometrically congruent imagery it

intuitively follows that a larger observation area yields a higher SNR. However, this is not the case when relative spatial distortions dependent upon image size exist between the images. For the case in which the distortion increases with size, as in a simple difference in scale, it is to be expected that beyond a certain image size the SNR will decrease due to the fact that the images cannot be simultaneously matched at widely separated points by translation only. Therefore, when relative distortions exist it should be expected that there is an optimum integration area size which realizes a maximum SNR. This is the problem that is examined in this chapter.

The derivation is divided into two major categories: white noise only is present; or nonwhite noise is present. Within each category an expression for the SNR as a function of the integration area size is derived for both relatively nondistorted and distorted spatial scales between the reference and background images.

The procedure for comparing these two situations involves using the filter which maximizes the SNR when the spatial scales are the same (the matched filter), and then using a distorted spatial scale version of this same filter to observe the effect on the SNR due to relatively distorted spatial scales. The choice of which spatial coordinate system is distorted, reference or background image, is arbitrary since the distortions are only relative. The reason for proceeding in this fashion is that this models quite well what actually happens in practice. Since the relative distortion is unknown beforehand, it cannot be corrected for prior to processing the images, so that the relatively distorted images must be dealt with as they exist.

For two-dimensional signals, in this case imagery, the output signal-to-noise ratio and related parameters are defined as follows.

$$SNR = \frac{\{E[\frac{1}{4T_xT_y}\int_{-T_x}^{T_x}\int_{-T_y}^{T_y} h(\tau_x-x,\tau_y-y)s(x,y)dxdy]\}^2}{E\{[\frac{1}{4T_xT_y}\int_{-T_x}^{T_x}\int_{-T_y}^{T_y} h(\tau_x-x\ \tau_y-y)n(x,y)dxdy]^2\}} \qquad (4\text{-}1)$$

Where,

SNR = output signal-to-noise ratio

$s(x,y)$ = signal; reference image

$n(x,y)$ = additive zero mean noise

$h(x,y)$ = processing filter

$4T_xT_y$ = observation area size

(τ_x,τ_y) = translation

In this expression the SNR is defined as the ratio of the square of the expected value of the output due to the signal and the variance of the output due to the noise. The SNR is a function of the observation area, $4T_xT_y$, through the integration limits.

To proceed, it is necessary that the signal and noise properties be defined more completely to allow for evaluation of the SNR. The necessary assumptions for this analysis are,

(i) $s(x,y)$ and $n(x,y)$ are independent

(ii) $R_s(x-a,y-b) = \overline{s(x,y)s(a,b)}$

(iii) $R_n(x-a,y-b) = \overline{n(x,y)n(a,b)} = \begin{cases} \frac{N_o}{2}\delta(x-a,y-b); & \text{white noise} \\ \frac{N_o}{2}\delta(x-a,y-b)+R_{n_c}(x-a,y-b); & \text{nonwhite noise} \end{cases}$

It is important to note that assumption (iii) states that in the presence

of nonwhite noise, the noise is comprised of a white noise component with autocorrelation function $\frac{N_o}{2}\delta(x-a,y-b)$, and a colored noise component with autocorrelation function $R_{n_c}(x-a,y-b)$. The inclusion of the white noise component is realistic as regards practical measurements and also avoids the possibility of singular detection. Later on in the analysis it is seen that this assumption leads to a solution employing a prewhitening filter as a component of the matched filter for nonwhite noise.

4.1. White Noise With No Relative Spatial Distortion

In this section the SNR will be evaluated for the case where white noise only is present,

$$R_n(\tau_x,\tau_y) = \frac{N_o}{2}\delta(\tau_x,\tau_y) \tag{4-2}$$

and no relative spatial distortions exist between the background and reference images. For evaluation of the SNR (eq. 4-1) a filter must be chosen. In keeping with the analyses of Chapters 2, 3, and Appendix A, a matched filter is employed. In the presence of white noise this filter has an impulse response of the following form,

$$h(\tau_x-x,\tau_y-y) = s(x,y) \tag{4-3}$$

Substitution of this into the expression for the SNR yields,

$$SNR_w = \frac{\{E[\frac{1}{4T_xT_y}\int_{-T_x}^{T_x}\int_{-T_y}^{T_y}s^2(x,y)\,dxdy]\}^2}{E\{[\frac{1}{4T_xT_y}\int_{-T_x}^{T_x}\int_{-T_y}^{T_y}s(x,y)n(x,y)\,dxdy]^2\}} \tag{4-4}$$

where the subscript w denotes white noise. Evaluation of SNR_w is carried out as follows,

$$\{E[\frac{1}{4T_xT_y}\int_{-T_x}^{T_x}\int_{-T_y}^{T_y} s^2(x,y)\,dxdy]\}^2 = \{\frac{1}{4T_xT_y}\int_{-T_x}^{T_x}\int_{-T_y}^{T_y} \overline{s^2(x,y)}\,dxdy\}^2$$

$$= \{\frac{1}{4T_xT_y}\int_{-T_x}^{T_x}\int_{-T_y}^{T_y} R_s(0,0)\,dxdy\}^2$$

$$= R_s^2(0,0) \qquad (4\text{-}5)$$

$$E\{[\frac{1}{4T_xT_y}\int_{-T_x}^{T_x}\int_{-T_y}^{T_y} s(x,y)n(x,y)\,dxdy]^2\}$$

$$= \frac{1}{(4T_xT_y)^2}\iint_{-T_x}^{T_x}\iint_{-T_y}^{T_y} \overline{s(x,y)s(a,b)}\;\overline{n(x,y)n(a,b)}\,dxdy\,dadb$$

$$= \frac{1}{(4T_xT_y)^2}\iint_{-T_x}^{T_x}\iint_{-T_y}^{T_y} R_s(x-a,y-b)\frac{N_o}{2}\delta(x-a,y-b)\,dxdy\,dadb$$

$$= \frac{1}{(4T_xT_y)^2}\frac{N_o}{2}\int_{-T_x}^{T_x}\int_{-T_y}^{T_y} R_s(0,0)\,dxdy$$

$$= \frac{1}{4T_xT_y}\frac{N_o}{2}R_s(0,0) \qquad (4\text{-}6)$$

The SNR is therefore,

$$SNR_w = 4T_xT_y\frac{2R_s(0,0)}{N_o} \qquad (4\text{-}7)$$

Note that SNR_w is proportional to the integration area. This is exactly what is to be expected since a larger integration area allows access to more signal information.

4.2. White Noise With Relative Spatial Distortion

As in the last section the noise is assumed to be white. It is also assumed that relative spatial distortions exist between reference and background images. Thus, since only a spatially distorted version of the

signal is present and the distortions are unknown, the filter is matched to this time distorted signal. The filter is represented as,

$$h(\tau_x - x, \tau_y - y) = s[x+p(x,y), y+q(x,y)] \tag{4-8}$$

where $p(x,y)$ and $q(x,y)$ are functions of x and y that model the relative spatial distortion. With this filter the SNR becomes,

$$SNR_w = \frac{\{E[\frac{1}{4T_xT_y}\int_{-T_x}^{T_x}\int_{-T_y}^{T_y} s[x+p(x,y),y+q(x,y)]\, s(x,y)\ dxdy]^2\}}{E\{[\frac{1}{4T_xT_y}\int_{-T_x}^{T_x}\int_{-T_y}^{T_y} s[x+p(x,y),y+q(x,y)]\, n(x,y)\ dxdy]^2\}} \tag{4-9}$$

This expression may be evaluated as follows

$$\{E[\frac{1}{4T_xT_y}\int_{-T_x}^{T_x}\int_{-T_y}^{T_y} s[x+p(x,y),y+q(x,y)]s(x,y)\ dxdy]\}^2$$

$$= \{\frac{1}{4T_xT_y}\int_{-T_x}^{T_x}\int_{-T_y}^{T_y} \overline{s[x+p(x,y),y+q(x,y)]s(x,y)}\ dxdy\}^2$$

$$= \{\frac{1}{4T_xT_y}\int_{-T_x}^{T_x}\int_{-T_y}^{T_y} R_s[p(x,y),q(x,y)]\ dxdy\}^2 \tag{4-10}$$

$$\{E[\frac{1}{4T_xT_y}\int_{-T_x}^{T_x}\int_{-T_y}^{T_y} s[x+p(x,y),y+q(x,y)]n(x,y)\ dxdy]^2\}$$

$$= \frac{1}{(4T_xT_y)^2}\iint_{-T_x}^{T_x}\iint_{-T_y}^{T_y} \overline{s[x+p(x,y),y+q(x,y)]s[a+p(a,b),b+q(a,b)]}$$

$$\cdot \overline{n(x,y)n(a,b)}\ dadb\ dxdy$$

$$= \frac{1}{(4T_xT_y)^2}\frac{N_o}{2}\iint_{-T_x}^{T_x}\iint_{-T_y}^{T_y} R_s[x+p(x,y)-a-p(a,b),y+q(x,y)-b-q(a,b)]$$

$$\cdot \delta(x-a,y-b)dadb\ dxdy$$

$$= \frac{1}{(4T_xT_y)^2}\frac{N_o}{2}\int_{-T_x}^{T_x}\int_{-T_y}^{T_y} R_s(0,0)\ dxdy$$

$$= \frac{1}{4T_xT_y}\frac{N_o}{2}R_s(0,0) \tag{4-11}$$

The output signal-to-noise ratio is then,

$$SNR_{WD} = 4T_x T_y \frac{2R_s(0,0)}{N_o} \{\frac{1}{4T_x T_y} \int_{-T_x}^{T_x} \int_{-T_y}^{T_y} \frac{R_s[p(x,y),q(x,y)]}{R_s(0,0)} dxdy\}^2 \quad (4\text{-}12)$$

There are several important properties of this expression that should be noted. First, observe the variation of SNR_{WD} with T_x and T_y.

$$\lim_{T_x,T_y \to 0} SNR_{WD} = \lim_{T_x,T_y \to 0} 4T_x T_y \frac{2R_s(0,0)}{N_o} = 0 \quad (4\text{-}13)$$

Furthermore, if $p(x,y)$ and $q(x,y)$ are increasing in t, that is, if,

$$\lim_{x,y \to \infty} |p(x,y)| = \infty = \lim_{x,y \to \infty} |q(x,y)| \quad (4\text{-}14)$$

then,

$$\lim_{T_x,T_y \to \infty} SNR_{WD} = 0 \quad (4\text{-}15)$$

since,

$$\iint_{-\infty}^{\infty} \frac{R_s[p(x,y),q(x,y)]}{R_s(0,0)} dxdy < \infty \quad (4\text{-}16)$$

Therefore, when (4-14) is true, SNR_{WD} has a maximum for some finite integration area. Choice of this integration area will give the maximum possible SNR_{WD}.

Secondly, notice the way in which the SNR is affected by the spatial distortions. An expression equivalent to (4-12) is,

$$SNR_{WD} = SNR_W \{\frac{1}{4T_x T_y} \int_{-T_x}^{T_x} \int_{-T_y}^{T_y} \frac{R_s[p(x,y),q(x,y)]}{R_s(0,0)} dxdy\}^2 \quad (4\text{-}17)$$

Therefore, the signal-to-noise ratio using the spatially distorted filter is less than SNR_W using the nondistorted filter by the factor of,

$$\{\frac{1}{4T_x T_y} \int_{-T_x}^{T_x} \int_{-T_y}^{T_y} \frac{R_s[p(x,y),q(x,y)]}{R_s(0,0)} dxdy\}^2 \leq 1 \quad (4\text{-}18)$$

This follows from (4-17) since,

$$|R_s[p(x,y),q(x,y)]| \leq R_s(0,0) \tag{4-19}$$

for all x and y. Note that this reduction is just the square of the normalized average area under the signal autocorrelation function $R_s[p(x,y),q(x,y)]$ with a spatially distorted scale.

This result indicates that the reduction in the output signal-to-noise ratio for different values of T_x and T_y can be easily estimated with a given distortion model by evaluating the reduction factor given in (4-18). Finally note that SNR_{WD} reduces to SNR_W when there are no relative spatial distortions, i.e., p(x,y) and q(x,y) equal zero.

4.3. Nonwhite Noise With No Relative Spatial Distortion

Analysis of the SNR for nonwhite noise,

$$R_n(\tau_x,\tau_y) = \frac{N_o}{2}\delta(\tau_x,\tau_y) + R_{n_c}(\tau_x,\tau_y) \tag{4-20}$$

requires one more step than in the white noise case. This is embodied in the formulation of the matched filter and involves incorporation of a prewhitening operation into the optimum filter. A derivation of this implementation of the matched filter is given in Chapter 3 where a block diagram (Fig. 3-4) illustrates its construction. The prewhitening operation refers to the filter designed to whiten the input noise.

Addition of the prewhitening filter converts the problem into that where white noise has been assumed. The particular form for this filter depends upon the noise autocorrelation or spectral density function. The background image is passed through the whitening filter and then a second filter is chosen to maximize the SNR of the prewhitened signal plus noise. These two filters in cascade form the matched filter (Fig. 3-3).

This approach requires an alteration of the SNR formula. It is assumed that the received signal plus noise has already been processed by the whitening filter so that it is necessary to deal only with white noise in the choice of the maximization filter.

$$SNR_{NW} = \frac{\{E[\frac{1}{4T_xT_y}\int_{-T_x}^{T_x}\int_{-T_y}^{T_y} h(\tau_x-x,\tau_y-y)s_w(x,y)\,dxdy]\}^2}{E\{[\frac{1}{4T_xT_y}\int_{-T_x}^{T_x}\int_{-T_y}^{T_y} h(\tau_x-x,\tau_y-y)n_w(x,y)\,dxdy]^2\}} \qquad (4\text{-}21)$$

Where,

$$s_w(x,y) = \iint h_w(x-a,y-b)s(a,b)\,dadb \qquad \text{prewhitened signal} \qquad (4\text{-}22)$$

$$n_w(x,y) = \iint h_w(x-a,y-b)n(a,b)\,dadb \qquad \text{prewhitened noise} \qquad (4\text{-}23)$$

The prewhitening filter, $h_w(x,y)$, is designed such that,

$$n_w(x,y)n_w(a,b) = \frac{N_o}{2}\delta(x-a,y-b) \qquad (4\text{-}24)$$

that is, $n_w(x,y)$ is white noise. Conversion of (4-24) to the Fourier transform domain yields the following relationship between the power transfer function of the whitening filter and the noise spectrum.

$$|H_w(u,v)|^2 = \frac{N_o}{2}\frac{1}{S_n(u,v)} \qquad (4\text{-}25)$$

where,

$H_w(u,v)$ = transfer function of the prewhitening filter

$S_n(u,v)$ = noise spectrum

Note that inclusion of the white noise component in the expression for the autocorrelation function, eq. (4-20), insures that $|H_w(u,v)|^2 < \infty$ for all frequencies. This avoids the singular detection problem.

As before, for white noise the filter is matched directly to the signal, which has been passed through the whitening filter in this case.

$$h(\tau_x - x, \tau_y - y) = s_w(x,y) \tag{4-26}$$

With this filter the expression for the SNR becomes,

$$SNR_{NW} = \frac{\{E[\frac{1}{4T_xT_y}\int_{-T_x}^{T_x}\int_{-T_y}^{T_y} s_w^2(x,y)\,dxdy]\}^2}{E\{[\frac{1}{4T_xT_y}\int_{-T_x}^{T_x}\int_{-T_y}^{T_y} s_w(x,y)n_w(x,y)\,dxdy]^2\}} \tag{4-27}$$

which may be evaluated as follows,

$$\{E[\frac{1}{4T_xT_y}\int_{-T_x}^{T_x}\int_{-T_y}^{T_y} s_w^2(x,y)\,dxdy]\}^2 = \{\frac{1}{4T_xT_y}\int_{-T_x}^{T_x}\int_{-T_y}^{T_y} \overline{s_w^2(x,y)}\,dxdy\}^2$$

$$= \{\frac{1}{4T_xT_y}\int_{-T_x}^{T_x}\int_{-T_y}^{T_y} R_{s_w}(0,0)\,dxdy\}^2$$

$$= R_{s_w}^2(0,0) \tag{4-28}$$

where,

$$R_{s_w}(0,0) = \overline{s_w^2(x,y)} = \int_{-\infty}^{\infty}\int\int\int h_w(a,b)h_w(c,e)R_s(a-c,b-e)\,dadbdcde \tag{4-29}$$

is the energy in the prewhitened signal.

$$E\{[\frac{1}{4T_xT_y}\int_{-T_x}^{T_x}\int_{-T_y}^{T_y} s_w(x,y)n_w(x,y)\,dxdy]^2\}$$

$$= \frac{1}{(4T_xT_y)^2}\int\int_{-T_x}^{T_x}\int\int_{-T_y}^{T_y} \overline{s_w(x,y)s_w(a,b)}\;\overline{n_w(x,y)n_w(a,b)}\cdot dxdydadb$$

$$= \frac{1}{(4T_xT_y)^2}\frac{N_o}{2}\int\int_{-T_x}^{T_x}\int\int_{-T_y}^{T_y} \overline{s_w(x,y)s_w(a,b)}\;\delta(x-a,y-b)\,dxdydadb$$

$$= \frac{1}{(4T_xT_y)^2}\frac{N_o}{2}\int_{-T_x}^{T_x}\int_{-T_y}^{T_y} \overline{s_w^2(x,y)}\,dxdy$$

$$= \frac{1}{(4T_xT_y)^2}\frac{N_o}{2}\int_{-T_x}^{T_x}\int_{-T_y}^{T_y} R_{s_w}(0,0)\,dxdy$$

$$= \frac{1}{(4T_xT_y)}\frac{N_o}{2}R_{s_w}(0,0) \tag{4-30}$$

The SNR is then,

$$SNR_{NW} = 4T_xT_y\frac{2R_{s_w}(0,0)}{N_o} \tag{4-31}$$

Note that SNR_{NW} is proportional to the integration area, $4T_xT_y$. This is what is to be expected. Comparing this expression with that obtained for the white noise situation, it is found that the two are analogous, differing only by the signal energy used. For the nonwhite noise case the prewhitened signal energy is used as opposed to the original signal energy.

4.4. Nonwhite Noise With Relative Spatial Distortion

When spatial distortions are present, instead of being able to use $s(x,y)$ in forming the receiving filter, it is necessary to use $s[x+p(x,y),y+q(x,y)]$, a spatially distorted version of the signal, where $p(x,y)$ and $q(x,y)$ functionally model the distortions. In this case the prewhitening filter again is used. However, instead of passing $s(x,y)$ through the whitening filter, $s[x+p(x,y),y+q(x,y)]$ is input to the whitening filter. This corresponds to the situation faced in practice where the time distorted signal is the only version available. The processing filter then is matched to the whitened distorted signal.

$$h(\tau_x-x,\tau_y-y) = z(x,y) = \int_{-\infty}^{\infty}\int h_w(x-a,y-b)s[a+p(a,b),b+q(a,b)]dadb \tag{4-32}$$

$z(x,y)$ = prewhitened spatially distorted signal

For convenience in the derivation, the following equivalent relation for $z(x,y)$ is used.

$$z(x,y) = \int_{-\infty}^{\infty}\int h_w(a,b)s[x-a+p(x-a,y-b),y-b+q(x-a,y-b)]dadb \tag{4-33}$$

Substitution of $z(x,y)$ into the expression for the SNR yields,

$$SNR_{NWD} = \frac{\{E[\frac{1}{4T_xT_y}\int_{-T_x}^{T_x}\int_{-T_y}^{T_y} z(x,y)s_w(x,y)\,dxdy]\}^2}{E\{[\frac{1}{4T_xT_y}\int_{-T_x}^{T_x}\int_{-T_y}^{T_y} z(x,y)n_w(x,y)\,dxdy]^2\}} \tag{4-34}$$

Evaluation of this expression gives,

$$\{E[\frac{1}{4T_xT_y}\int_{-T_x}^{T_x}\int_{-T_y}^{T_y} z(x,y)s_w(x,y)dxdy]\}^2 = \{\frac{1}{4T_xT_y}\int_{-T_x}^{T_x}\int_{-T_y}^{T_y} \overline{z(x,y)s_w(x,y)}dxdy\}^2$$

$$= \{\frac{1}{4T_xT_y}\int_{-T_x}^{T_x}\int_{-T_y}^{T_y} R_{zs_w}(x,y)\,dxdy\}^2 \tag{4-35}$$

where,

$$R_{zs_w}(x,y) = \int_{-\infty}^{\infty}\int\int\int h_w(a,b)h_w(c,e)\overline{s[x-a+p(x-a,y-b),y-b+q(x-a,y-b)]s(x-c,y-e)}$$
$$\cdot\, dadbdcde$$
$$= \int_{-\infty}^{\infty}\int\int\int h_w(a,b)h_w(c,e)R_s[a-c-p(x-a,y-b),b-e-q(x-a,y-b)]dadbdcde \tag{4-36}$$

is the crosscorrelation function between the prewhitened distorted signal and the prewhitened original signal.

$$E\{[\frac{1}{4T_xT_y}\int_{-T_x}^{T_x}\int_{-T_y}^{T_y} z(x,y)n_w(x,y)\,dxdy]^2\}$$
$$= \frac{1}{(4T_xT_y)^2}\int\int_{-T_x}^{T_x}\int\int_{-T_y}^{T_y}\overline{z(x,y)z(a,b)}\;\overline{n_w(x,y)n_w(a,b)}\;dxdydadb$$
$$= \frac{1}{(4T_xT_y)^2}\frac{N_o}{2}\int\int_{-T_x}^{T_x}\int\int_{-T_y}^{T_y}\overline{z(x,y)z(a,b)}\;\delta(x-a,y-b)\;dxdydadb$$
$$= \frac{1}{(4T_xT_y)^2}\frac{N_o}{2}\int_{-T_x}^{T_x}\int_{-T_y}^{T_y}\overline{z^2(x,y)}\;dxdy$$
$$= \frac{1}{4T_xT_y}\frac{N_o}{2}[\frac{1}{4T_xT_y}\int_{-T_x}^{T_x}\int_{-T_y}^{T_y} R_z(x,y)\,dxdy] \tag{4-37}$$

where,

$$R_z(x,y)=\int_{-\infty}^{\infty}\int\int\int \overline{s[x-a+p(x-a,y-b),y-b+q(x-a,y-b)]\,s[x-c+p(x-c,y-e),y-e+q(x-c,y-e)]}$$
$$\cdot\, h_w(a,b)h_w(c,e)\;dadbdcde$$
$$=\int_{-\infty}^{\infty}\int\int\int R_s[a-c-p(x-a,y-b)+p(x-c,y-e),b-e-q(x-a,y-b)+q(x-c,y-e)]$$
$$\cdot\, h_w(a,b)h_w(c,e)\;dadbdcde \qquad (4\text{-}38)$$

is the energy in the prewhitened spatially distorted signal. Note that the independence of $z(x,y)$ and $n_w(x,y)$ in the first step of eq. (4-37) follows from the fact that $z(x,y)$ depends only upon $s(x,y)$ and $n_w(x,y)$ depends only upon $n(x,y)$. Also note that $R_z(x,y)$ is not a function of x and y for a linear distortion (i.e., $p(x,y)$ and $q(x,y)$ are first order polynomials).

The SNR becomes,

$$SNR_{NWD}=4T_xT_y\frac{2R_{s_w}(0,0)}{N_o}\left[\frac{1}{4T_xT_y}\int_{-T_x}^{T_x}\int_{-T_y}^{T_y}\frac{R_z(x,y)}{R_{s_w}(0,0)}dxdy\right]\left[\frac{\frac{1}{4T_xT_y}\int_{-T_x}^{T_x}\int_{-T_y}^{T_y}R_{zs_w}(x,y)dxdy}{\frac{1}{4T_xT_y}\int_{-T_x}^{T_x}\int_{-T_y}^{T_y}R_z(x,y)\,dxdy}\right]^2 \qquad (4\text{-}39)$$

There are several important properties of this expression that should be observed. The expression can be rewritten in the following equivalent form.

$$SNR_{NWD}=SNR_{NW}\left[\frac{1}{4T_xT_y}\int_{-T_x}^{T_x}\int_{-T_y}^{T_y}\frac{R_z(x,y)}{R_{s_w}(0,0)}\;dxdy\right]\left[\frac{\frac{1}{4T_xT_y}\int_{-T_x}^{T_x}\int_{-T_y}^{T_y}R_{zs_w}(x,y)\,dxdy}{\frac{1}{4T_xT_y}\int_{-T_x}^{T_x}\int_{-T_y}^{T_y}R_z(x,y)\,dxdy}\right]^2 \qquad (4\text{-}40)$$

It is evident from (4-40) that use of a spatially distorted signal results in the reduction of SNR_{NW} relative to the undistorted case by a factor of,

$$\left[\frac{1}{4T_xT_y}\int_{-T_x}^{T_x}\int_{-T_y}^{T_y}\frac{R_z(x,y)}{R_{s_w}(0,0)}\,dxdy\right]\left[\frac{\frac{1}{4T_xT_y}\int_{-T_x}^{T_x}\int_{-T_y}^{T_y}R_{zs_w}(x,y)\,dxdy}{\frac{1}{4T_xT_y}\int_{-T_x}^{T_x}\int_{-T_y}^{T_y}R_z(x,y)\,dxdy}\right]^2 \leq 1 \qquad (4\text{-}41)$$

The inequality follows from examination of the expressions for $R_{zs_w}(0,0)$, $R_z(x,y)$, and $R_{zs_w}(x,y)$.

$$|R_z(x,y)| \leq R_{s_w}(0,0) \text{ for all } x,y \qquad (4\text{-}42)$$

$$\left|\int_{-T_x}^{T_x}\int_{-T_y}^{T_y}R_{zs_w}(x,y)\,dxdy\right| \leq \left|\int_{-T_x}^{T_x}\int_{-T_y}^{T_y}R_z(x,y)\,dxdy\right| \text{ for all } T_x \text{ and } T_y \qquad (4\text{-}43)$$

This result shows that the reduction in the output signal-to-noise ratio with a given distortion model for different values of T_x and T_y can be estimated by evaluating the reduction factor, (4-41). It should also be noted that SNR_{NWD} reduces to SNR_{NW} when no distortions are present (i.e., $p(x,y)$ and $q(x,y)$ equal zero).

Next to be considered is the variation of SNR_{NWD} with T_x and T_y.

$$\lim_{T_xT_y \to 0} SNR_{NWD} = 0 \qquad (4\text{-}44)$$

since $\lim_{T_xT_y \to 0} SNR_{WD} = 0$ and $SNR_{NWD} \leq SNR_{NW}$.

Also, if $|p(x,y)|$ and $|q(x,y)|$ are increasing in x and y, that is

$$\lim_{x,y \to \infty} |p(x,y)| = \infty = \lim_{x,y \to \infty} |q(x,y)| \qquad (4\text{-}45)$$

then,

$$\lim_{T_xT_y \to \infty} SNR_{NWD} = 0 \qquad (4\text{-}46)$$

If $R_z(x,y)$ is not a constant function of x and y, then (4-46) follows since $\int_{-T_x}^{T_x}\int_{-T_y}^{T_y}R_z(x,y)\,dxdy$ and $\int_{-T_x}^{T_x}\int_{-T_y}^{T_y}R_{zs_w}(x,y)\,dxdy$ are finite. If $R_z(x,y)$ is

a constant with respect to x and y, then (4-46) is also true since $\int_{-T_x}^{T_x}\int_{-T_y}^{T_y} R_{zs_w}(x,y)\,dxdy < \infty$ for all T_x and T_y while $\lim_{T_xT_y \to \infty} \int_{-T_x}^{T_x}\int_{-T_y}^{T_y} R_z(x,y) = \infty$.

Since SNR_{NWD} is nonnegative for all T_x and T_y, then if (4-45) is true then there must be a maximum of SNR_{NWD} for some finite integration area. These choices of T_x and T_y will yield the maximum SNR_{NWD}. Given a model of the distortions, these values of T_x and T_y may be found by carrying out the required integration in eq. (4-39)

4.5. Examples of the Loss in the Output Signal-To-Noise Ratio Due to Different Types of Spatial Distortion.

In this section several examples are given illustrating the loss in the output signal-to-noise ratio when a processor designed to register spatially congruent imagery is operating in the presence of spatial distortions. The loss in the output signal-to-noise ratio is examined for three types of distortion: the first is a linear scale distortion; the second is the situation where the two images are rotated relative to one another; and the third is one in which relative distortions representative of those observed between multitemporal LANDSAT I images are considered. The first two examples concern general types of distortion. However, the last set of examples where the observed distortions between LANDSAT I images are considered, provides a means of applying the analytical expressions for the loss in the output signal-to-noise ratio to the overlaying of images in practice.

For the examples presented the noise (temporal change) is assumed to be white so that the expressions developed in Section 4.2 may be used. Equation (4-12) is used in a slightly rearranged form to evaluate

the normalized output signal-to-noise ratio (denoted by SNR_N in this section). This equivalent form is,

$$\frac{SNR_{WD}}{2R_s(0,0)/N_o} = 4T^2\left[\frac{1}{4T^2}\int_{-T}^{T}\int_{-T}^{T}\frac{R_s[p(x,y),q(x,y)]}{R_s(0,0)}\,dxdy\right]^2 \tag{4-47}$$

where,

$$T_x = T = T_y$$

and the signal-to-noise ratio has been normalized by $2R_s(0,0)/N_o$.

In order to evaluate (4-47), it is necessary that a model of the signal (image) autocorrelation function be chosen. For these examples an exponential autocorrelation function was used.

$$R_s(x,y) = R_s(0,0)\ \exp\left\{-\frac{|x|}{r} - \frac{|y|}{r}\right\} \tag{4-48}$$

where,

r = characteristic length of the autocorrelation function

Substitution of this expression into (4-47) yields,

$$\frac{SNR_{WD}}{2R_s(0,0)/N_o} = 4T^2\left[\frac{1}{4T^2}\int_{-T}^{T}\int_{-T}^{T}\exp\left[-\frac{|p(x,y)|}{r} - \frac{|q(x,y)|}{r}\right]dxdy\right]^2 \tag{4-49}$$

Given a model of the distortions, p(x,y) and q(x,y), (4-49) can be evaluated to determine the SNR_N.

4.5.1. Linear Scale Distortion.

The first type of spatial distortion examined is that of a linear scale distortion. In matrix notation this is represented as,

$$\begin{bmatrix} x' \\ y' \end{bmatrix} = \begin{bmatrix} 1+c & 0 \\ 0 & 1+c \end{bmatrix}\begin{bmatrix} x \\ y \end{bmatrix} \tag{4-50}$$

where,

(x,y) = reference image coordinate system

(x',y') = coordinate system of image to be overlayed on reference image

c = scale factor distortion

Since,

$$x' = x + p(x,y) = x + cx \tag{4-51}$$

$$y' = y + q(x,y) = y + cy \tag{4-52}$$

from the definition of $p(x,y)$ and $q(x,y)$ in Section 4.2, then,

$$p(x,y) = cx \tag{4-53}$$

$$q(x,y) = cy \tag{4-54}$$

Substitution of these expressions for $p(x,y)$ and $q(x,y)$ into (4-49) yields the equation for the SNR_N in the presence of a linear scale distortion.

$$\frac{SNR_{WD}}{2R_s(0,0)/N_o} = 4T^2\left[\frac{1}{4T^2}\int_{-T}^{T}\int_{-T}^{T}\exp\left[-\frac{|c|}{r}|x| - \frac{|c|}{r}|y|\right]dxdy\right]^2 \tag{4-55}$$

Note that the SNR_N is dependent upon two parameters: $4T^2$, the integration area; and $\frac{|c|}{r}$, the ratio of the scale distortion factor to the characteristic length of the signal (image) autocorrelation function.

Evaluation of (4-55) was carried out by a numerical integration method. Simpson's rule for approximating the integral of a function by the piecewise integrals of quadratic polynomials was used [40]. This procedure proved both straightforward and accurate. With a division of the interval, 2T, into 100 increments it was found that a tolerance of about 0.005% was observed. Also, use of this method of integration was not time consuming and was easy to implement since it only involved calculation of a weighted sum of the integrand at each of the increment endpoints. The general formula for integration via Simpson's rule is shown below for a double integral. The integration is carried out by first

integrating with respect to x and then with respect to y, i.e.,

$$\int_{-T}^{T}\int_{-T}^{T} f(x,y)\ dxdy = \int_{-T}^{T} g(y)\ dy \tag{4-56}$$

where,

$$g(y) = \int_{-T}^{T} f(x,y)\ dx \tag{4-57}$$

Using Simpson's rule the approximate integral is,

$$\int_{-T}^{T}\int_{-T}^{T} f(x,y)dxdy \approx \frac{h}{3}\{4 \sum_{\substack{i=1\\ i\ \text{odd}}}^{N-1} g(-T+ih)+2 \sum_{\substack{i=2\\ i\ \text{even}}}^{N-2} g(-T+ih)+g(-T) + g(T)\} \tag{4-58}$$

where,

$$g(y) = \frac{h}{3}\{4 \sum_{\substack{j=1\\ j\ \text{odd}}}^{N-1} f(-T+jh,y)+2 \sum_{\substack{j=2\\ j\ \text{even}}}^{N-2} f(-T+jh,y) + f(-T,y)+f(T,y)\} \tag{4-59}$$

and,

N = number of divisions of the interval 2T; must be an even number

h = 2T/N, the increment length of each division

For this computation the same number of increments are used for both variables of integration.

Figures 4-1 through 4-4 illustrate the relationship between the SNR_N, the integration area, and the linear scale distortion. Figures 4-1a and 4-1b show the square root of the SNR_N (denoted by $\sqrt{SNR_N}$) for different values of scale distortion as a function of 2T, the square root of the integration area. The reason for this particular choice for ordinate and abscissa is that the $\sqrt{SNR_N}$ in the absence of spatial distortions is linear in 2T with a slope of one. This is evidenced by letting p(x,y) and q(x,y) equal zero in (4-47). In this way it is possible to plot the results on a linear scale.

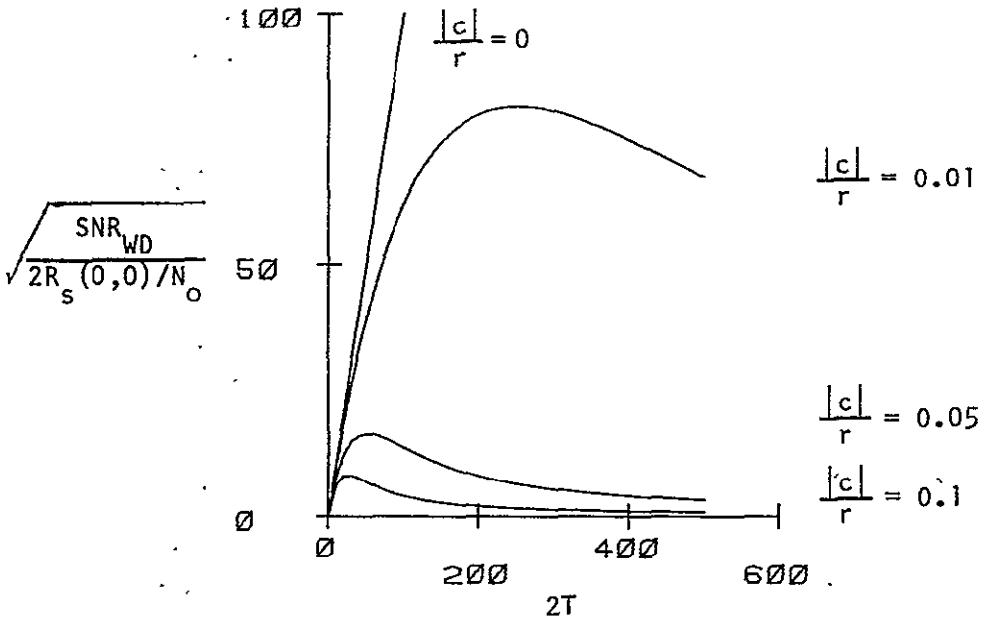

a. $\frac{|c|}{r} = 0, 0.01, 0.05, 0.1$

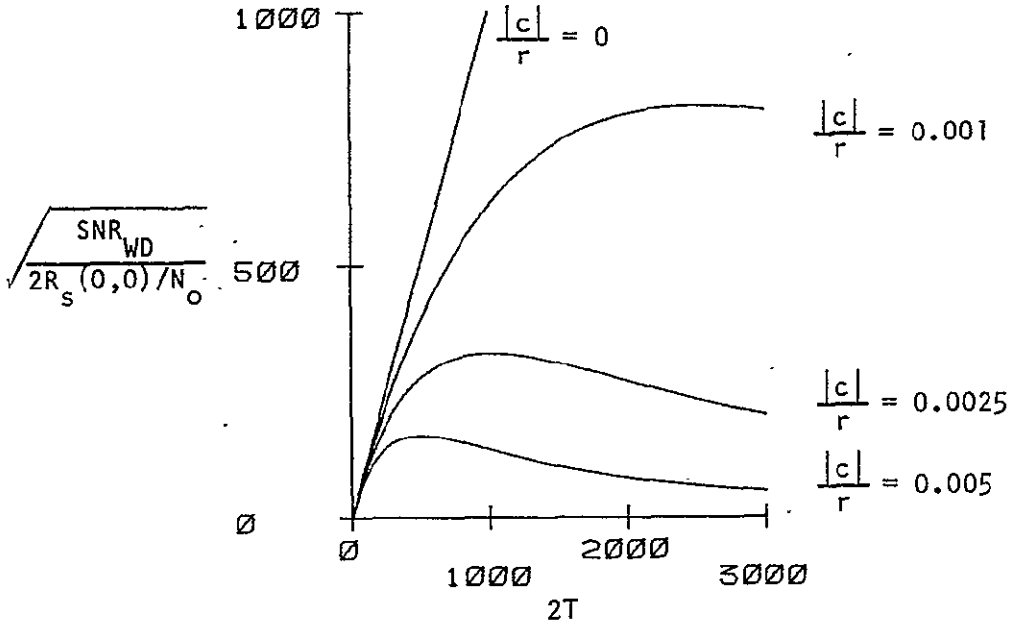

b. $\frac{|c|}{r} = 0, 0.001, 0.0025, 0.005$

Figure 4-1. (Normalized output signal-to-noise ratio)$^{1/2}$ for different values of linear scale distortion vs. (integration area)$^{1/2}$.

Two separate figures are presented so as to illustrate the distortion factor effect over a wide range of values. In Figure 4-1a the $\sqrt{SNR_N}$ versus 2T curves are given for $\frac{|c|}{r}$ equal to 0, 0.01, 0.05 and 0.1. In Figure 4-1b $\frac{|c|}{r}$ equals 0, 0.001, 0.0025 and 0.005. There is considerable convenience in being able to represent the scale factor, c, and the characteristic length, r, in a single term. In this way each curve is representative of a family of values of c and r. For example, a value of $\frac{|c|}{r} = 0.01$ can correspond to a value of 0.01 for $|c|$ and 1.0 for r as well as the combination of 0.02 for $|c|$ and 2.0 for r.

As predicted by the derivation in Section 4.2, in the presence of a scale distortion there is a finite integration area which yields a maximum output signal-to-noise ratio. This is illustrated by the occurrence of a peak in the curves for nonzero c. This result indicates that there is an optimum integration area size to use in the presence of a linear scale distortion when the registration processor is designed for spatially congruent imagery. Given the scale distortion, the optimum choice of integration area size is that which yields the maximum SNR_N. For example, with a distortion of $\frac{|c|}{r} = 0.05$, the maximum SNR_N is found for $2T \approx 50$.

Several other observations also may be made from Figures 4-1a and 4-1b. Again as predicted by (4-47) the $\sqrt{SNR_N}$ is linear in 2T with a slope of one for no scale distortion. Also note that a larger distortion factor requires a smaller integration area to yield the maximum SNR_N. For example, with $\frac{|c|}{r} = 0.01$ the 2T for a maximum SNR_N is 252, whereas for $\frac{|c|}{r} = 0.05$, the 2T for a maximum SNR_N is 50.

Figure 4-2 follows from the observations made in the first figure. Figures 4-1a and 4-1b illustrate that given the scale distortion factor,

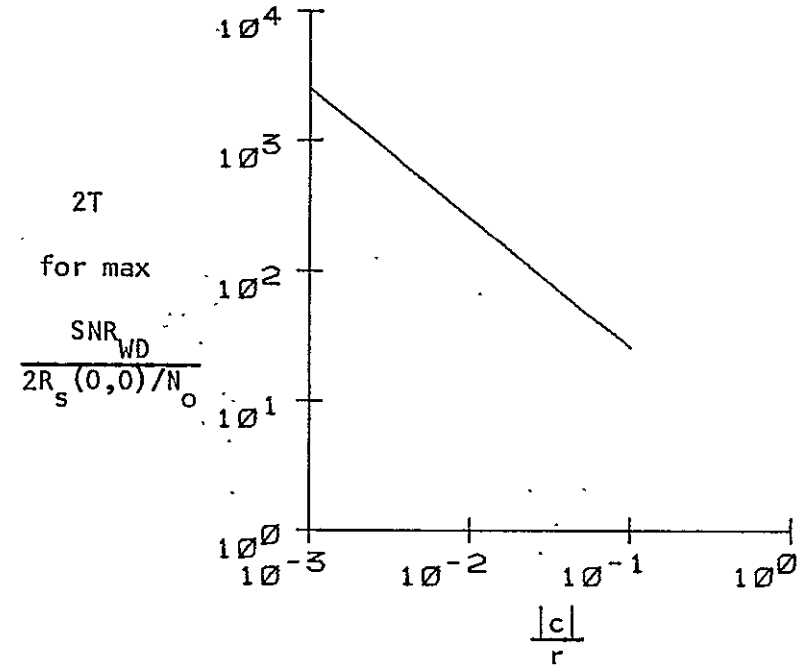

Figure 4-2. (Integration area)$^{1/2}$ yielding the maximum normalized output signal-to-noise ratio vs. linear scale distortion.

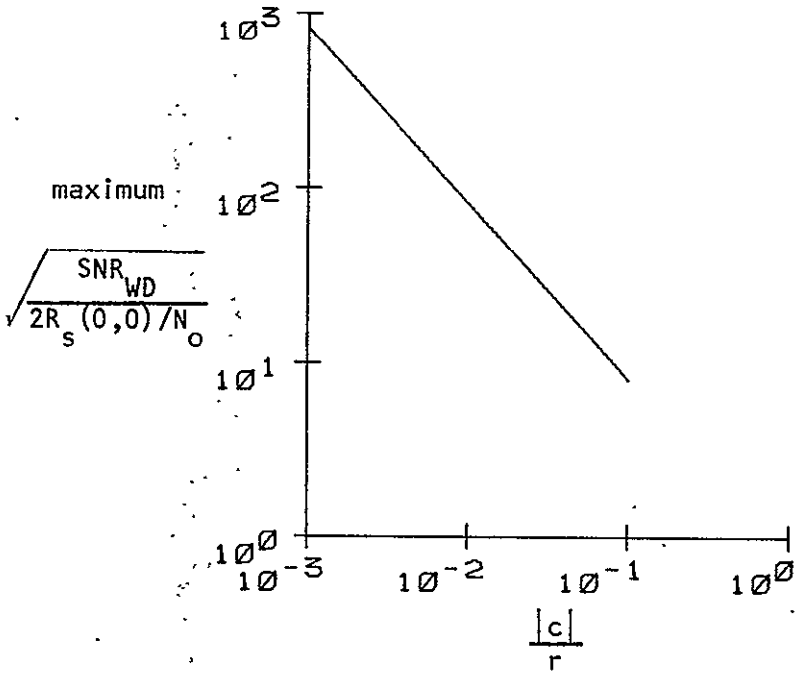

Figure 4-3. Maximum of (normalized output signal-to-noise ratio)$^{1/2}$ vs. linear scale distortion.

Table 4-1. 2T yielding the maximum SNR_N and the maximum $\sqrt{SNR_N}$ for different values of $\frac{|c|}{r}$.

$\frac{\lvert c \rvert}{r}$	2T for max SNR_N	max $\sqrt{SNR_N}$
0.001	2513	814.5
0.0025	1005	325.8
0.005	502	162.9
0.01	252	81.5
0.05	50	16.3
0.1	26	8.1

there is an optimum integration area size yielding the maximum SNR_N. This suggests that given the scale distortion, it is possible to find that integration area giving the maximum output signal-to-noise ratio. Table 4-1 lists a sample of values of the scale distortion and the corresponding 2T yielding the maximum normalized SNR_N. These values were used to generate Figure 4-2 which is a plot of the value of 2T yielding the maximum SNR_N versus the linear scale distortion. Note that the function is linear on a log-log plot. This indicates that the relationship is of the following form,

$$2T = \alpha \left[\frac{|c|}{r}\right]^{\beta} \tag{4-60}$$

where α and β may be determined from the curve or Table 4-1. The values found for α and β are,

$$\alpha \approx 2.52$$

$$\beta = -1$$

Therefore,

$$2T \text{ for max } SNR_N \approx 2.52\left[\frac{|c|}{r}\right]^{-1} \tag{4-61}$$

This result suggests that given the linear distortion factor, the area yielding the maximum output signal-to-noise ratio can be easily computed from (4-61)

Figure 4-3 is a plot of the maximum $\sqrt{SNR_N}$ versus the linear scale distortion. The values in Table 4-1 were used to generate this curve. This graph displays the maximum attainable $\sqrt{SNR_N}$ in the presence of a given scale distortion. As in Figure 4-2, the relationship is linear in a log-log plot which indicates that the maximum SNR_N varies with the scale distortion in the following manner.

$$\sqrt{SNR_N} = \alpha\left[\frac{|c|}{r}\right]^{\beta} \tag{4-62}$$

or equivalently,

$$SNR_N = \{\alpha\left[\frac{|c|}{r}\right]^{\beta}\}^2 \tag{4-63}$$

where α and β may be found directly from the curve or Table 4-1.

$$\alpha \approx 0.8145$$

$$\beta = -1$$

Substitution of these values into (4-63) yields,

$$SNR_N \approx \{0.8145\left[\frac{|c|}{r}\right]^{-1}\}^2 \tag{4-64}$$

Therefore, the maximum possible SNR_N for a given scale distortion may be found directly from (4-64). This provides a straightforward way of estimating the best possible performance in the presence of a given scale distortion.

A third means of analyzing the relationship between the SNR_N and scale distortion is provided in Figure 4-4. This figure is a graph of the $\sqrt{SNR_N}$ for different integration area sizes versus the linear scale distortion. Figure 4-4a illustrates the relationship for 2T equal to 30, 50 and 100, while Figure 4-4b shows the corresponding results for 2T equal to 250, 500 and 1000. For design purposes this may be utilized in the following fashion. If the integration area is given, then the maximum allowable distortion can be determined once a loss criterion in terms of the reduction in the SNR_N due to spatial distortion is decided upon. For example, if an integration area size with 2T = 100 is chosen with a tolerable loss of 19% in the SNR_N, then the maximum allowable distortion is $\frac{|c|}{r} \approx 0.002$. This is found directly from Figure 4-4a. Since a loss of

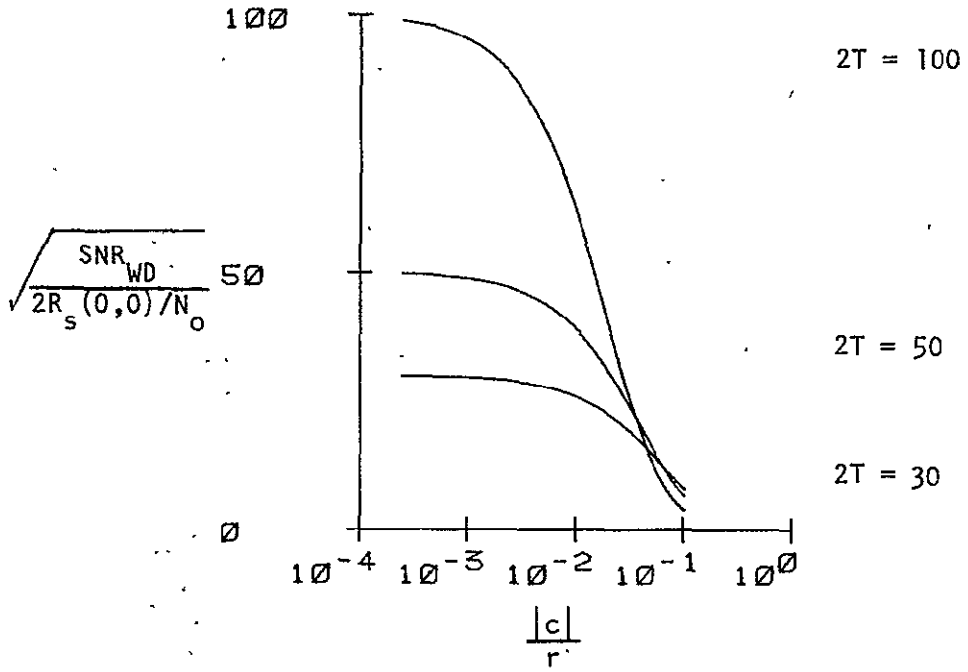

a. 2T = 30, 50, 100

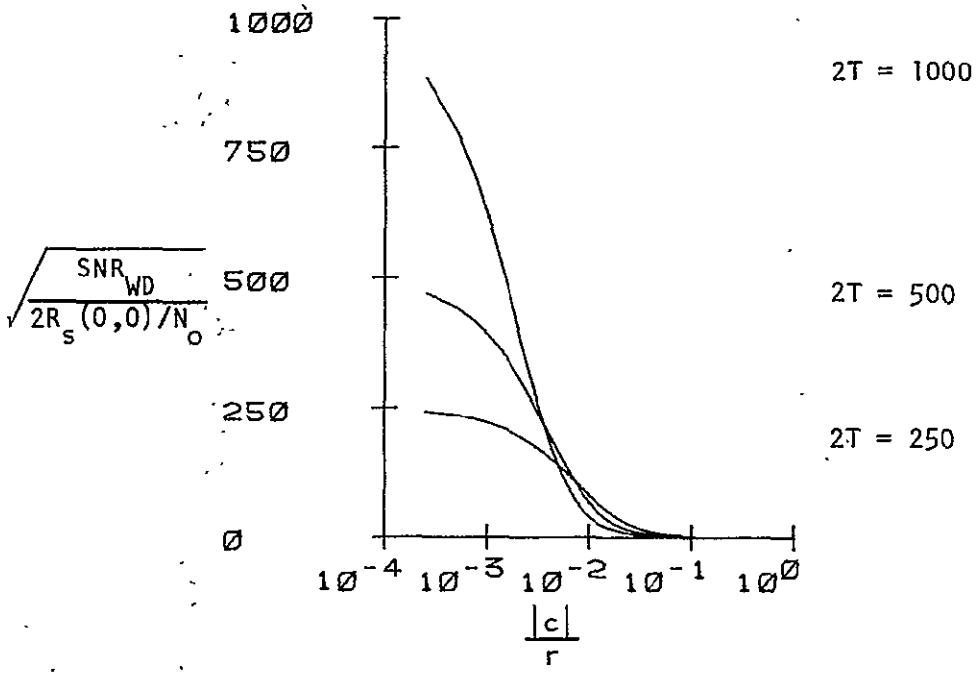

b. 2T = 250, 500, 1000

Figure 4-4. (Normalized output signal-to-noise ratio)$^{1/2}$ for different integration area sizes vs. linear scale distortion.

19% in the SNR_N is equivalent to (0.81) SNR_N, this corresponds to $0.9\sqrt{SNR_N}$. With 2T equal to 100, the $\sqrt{SNR_N}$ has a maximum of 100 (i.e., for c = 0), so that $0.9\sqrt{SNR_N} = 90$. Determination of the scale distortion for a value of $\sqrt{SNR_N} = 90$ on the 2T = 100 curve yields $\frac{|c|}{r} \approx 0.002$.

One other property of the curves may be observed. Note that the curves cross at specified values of linear scale distortion. For example, beyond a certain value of $\frac{|c|}{r}$ the $\sqrt{SNR_N}$ for 2T = 100 is less than that for 2T = 50. This follows from the results obtained in Figure 4-1, where it is shown that for a given distortion there is a value of 2T yielding the maximum SNR_N, all other values of 2T yielding a lesser SNR_N.

Figures 4-1 through 4-4 corroborate the analytical results derived in section 4.2. By utilizing them as outlined above, they provide a means of choosing the optimum integration area size in the presence of linear scale distortion.

4.5.2. Rotation Distortion.

The second general type of distortion examined is that where the two images are rotated relative to one another. This spatial relationship is represented in matrix form by,

$$\begin{bmatrix} x' \\ y' \end{bmatrix} = \begin{bmatrix} 1 + (\cos\theta - 1) & \sin\theta \\ \sin\theta & 1 + (\cos\theta - 1) \end{bmatrix} \begin{bmatrix} x \\ y \end{bmatrix} \qquad (4\text{-}65)$$

where,

(x,y) = reference image coordinate system

(x',y') = coordinate system of image to be registered with the reference image

θ = angle of rotation between the images

Since,

$$x' = x + p(x,y)$$

$$y' = y + q(x,y)$$

from the derivation in section 4.2, therefore,

$$p(x,y) = x(\cos\theta-1) - y\sin\theta \tag{4-66}$$

$$q(x,y) = x\sin\theta + y(\cos\theta-1) \tag{4-67}$$

Substitution of $p(x,y)$ and $q(x,y)$ into (4-49) yields the expression for the SNR_N in the presence of an angular distortion.

$$\frac{SNR_{WD}}{2R_s(0,0)/N_o} = 4T^2\left[\frac{1}{4T^2}\int_{-T}^{T}\int_{-T}^{T}\exp\left[-\frac{|x(\cos\theta-1)-y\sin\theta|}{r} - \frac{|x\sin\theta+y(\cos\theta-1)|}{r}\right]dxdy\right]^2 \tag{4-68}$$

Note that the SNR_N is dependent upon: $4T^2$, the integration area; θ, the angle of rotation; and r, the characteristic length of the image auto-correlation function.

As in section 4.5.1 the integration of (4-68) was carried out by using Simpson's rule approximation to the integral. Refer to 4.5.1 for a description of how this is implemented.

The relationships between the SNR_N, the integration area and angular distortion are illustrated in Figures 4-5 through 4-8. The contention made in section 4.2 that there is an integration area yielding a maximum output signal-to-noise ratio for a given distortion is borne out in Figures 4-5 and 4-6. Both figures show the $\sqrt{SNR_N}$ as a function of 2T. Figures 4-5a and 4-5b illustrate this relationship for several different angular rotations where the characteristic length, r, is equal to 2. Figure 4-6 illustrates the same relationship with a characteristic length of r = 5. In both cases the results reduce to the expected linear

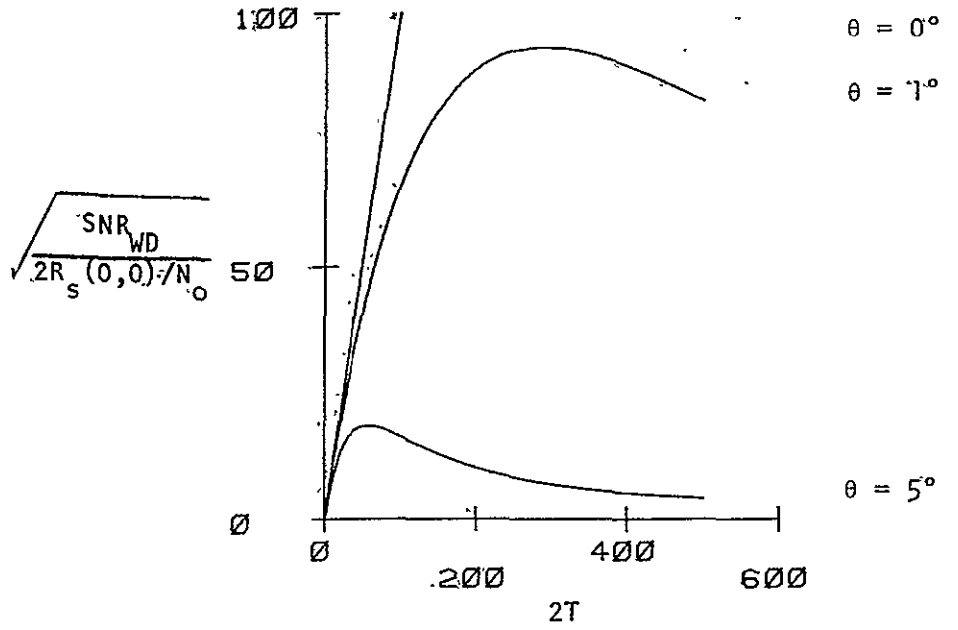

a. $\theta = 0°, 1°, 5°$

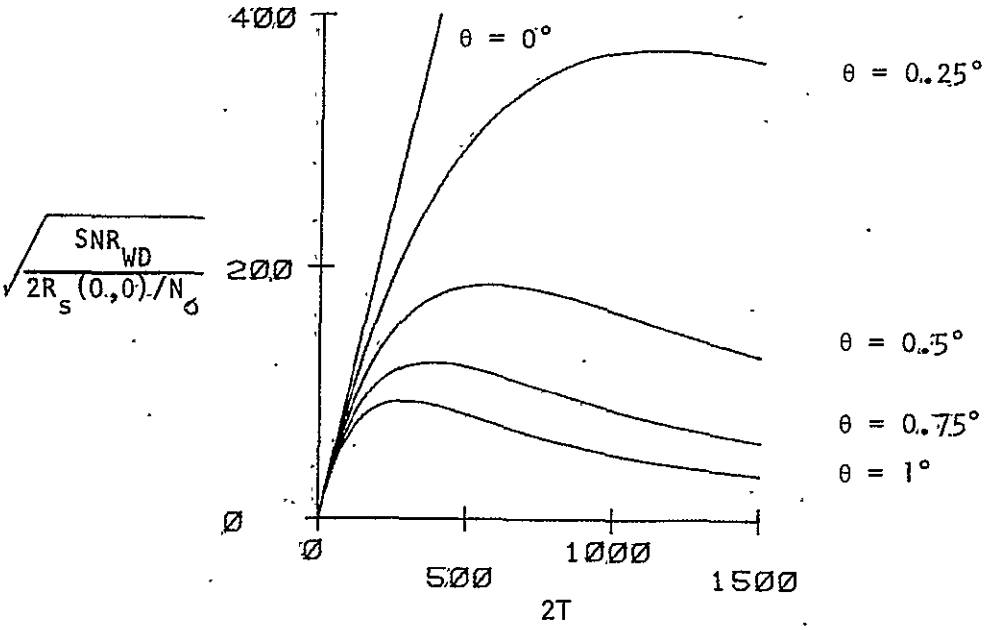

b. $\theta = 0°, 0.25°, 0.5°, 0.75°, 1°$

Figure 4-5. (Normalized output signal-to-noise ratio)$^{1/2}$ for different rotation angles vs. (integration area)$^{1/2}$ ($r = 2.0$).

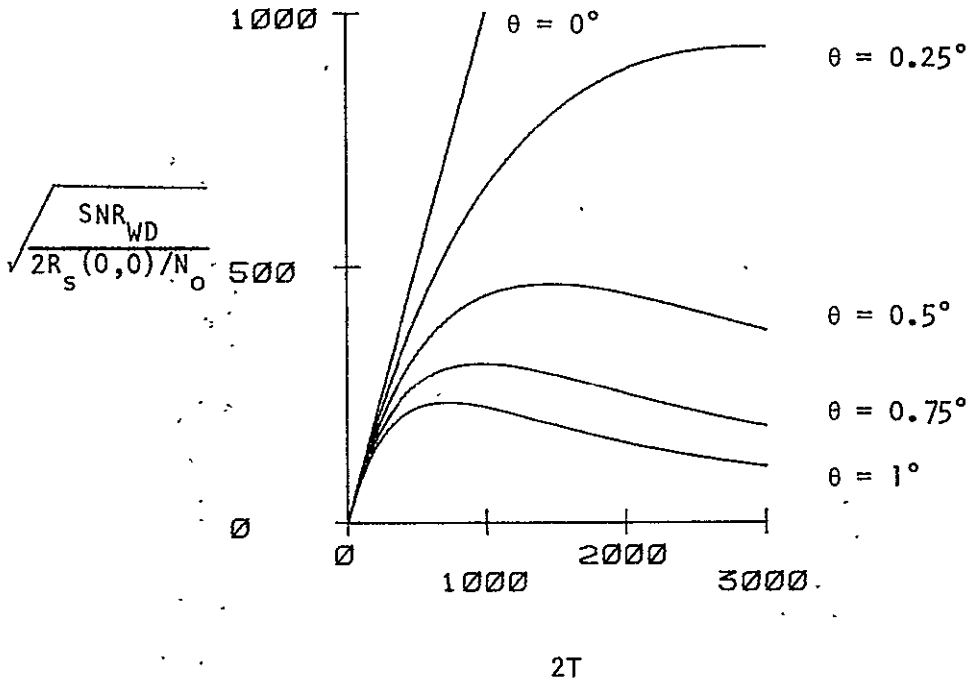

Figure 4-6. (Normalized output signal-to-noise ratio)$^{1/2}$ for different rotation angles vs. (integration area)$^{1/2}$ (r = 5.0).

relationship between the $\sqrt{SNR_N}$ and 2T for no angular distortion, i.e., $\theta = 0$. As was observed for a linear scale distortion, there is an integration area yielding a maximum SNR_N in the presence of an angular distortion, as is evidenced by the peak in each of the curves with nonzero θ. For example, with a rotation angle equal to 1°, a value of $2T \approx 290$ achieves the maximum SNR_N.

For design pruposes in choosing an optimum integration area size, the relationship between the value of 2T yielding the maximum SNR_N versus the angular distortion is given in Figure 4-7. Using this figure, it is a straightforward procedure to choose the integration area size which allows the maximum SNR_N given the value of the angular distortion. This relationship is illustrated for two values of the characteristic length, $r = 2$ and $r = 5$. Note that each is linear on a log-log plot for the values of θ chosen ($0 < \theta \leq 10°$). This indicates that the relationship is of the following form for this range of θ.

$$2T \text{ for max } SNR_N \approx \alpha_r \theta^{\beta_r} \; ; \; 0 < \theta \leq 10° \tag{4-69}$$

where α_r and β_r depend upon r. The data samples used to generate the curves in Figure 4-7 are listed in Table 4-2. Using these values, α_r and β_r become,

$$\alpha_2 \approx 288 \qquad \beta_2 = -1$$

$$\alpha_5 \approx 720 \qquad \beta_5 = -1$$

Therefore, for $r = 2$,

$$2T \text{ for max } SNR_N \approx 288\ \theta^{-1} \tag{4-70}$$

$$0 < \theta \leq 10°$$

and for $r = 5$,

$$2T \text{ for max } SNR_N \approx 720\ \theta^{-1} \; ; \; 0 < \theta \leq 10° \tag{4-71}$$

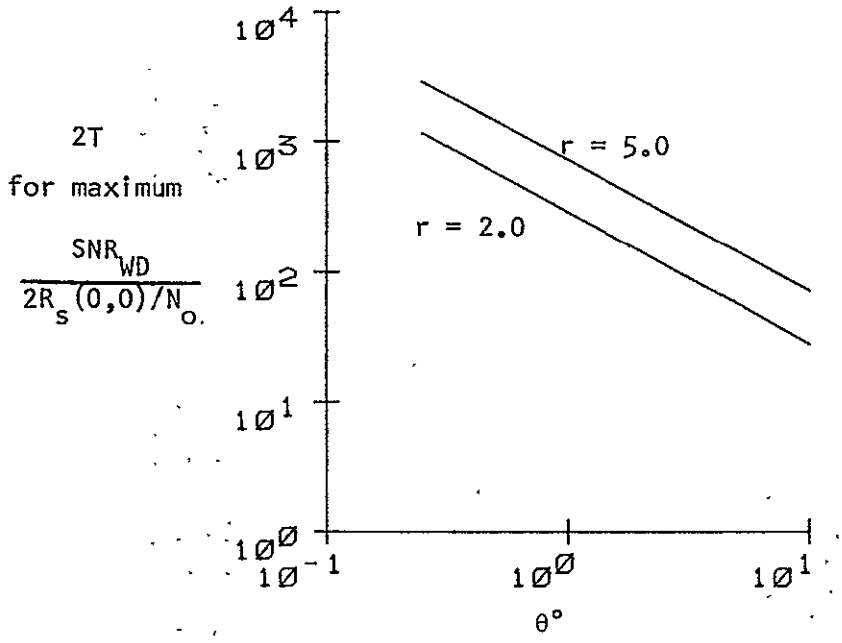

Figure 4-7. (Integration area)$^{1/2}$ yielding the maximum normalized output signal-to-noise ratio for different values of r vs. rotation angle.

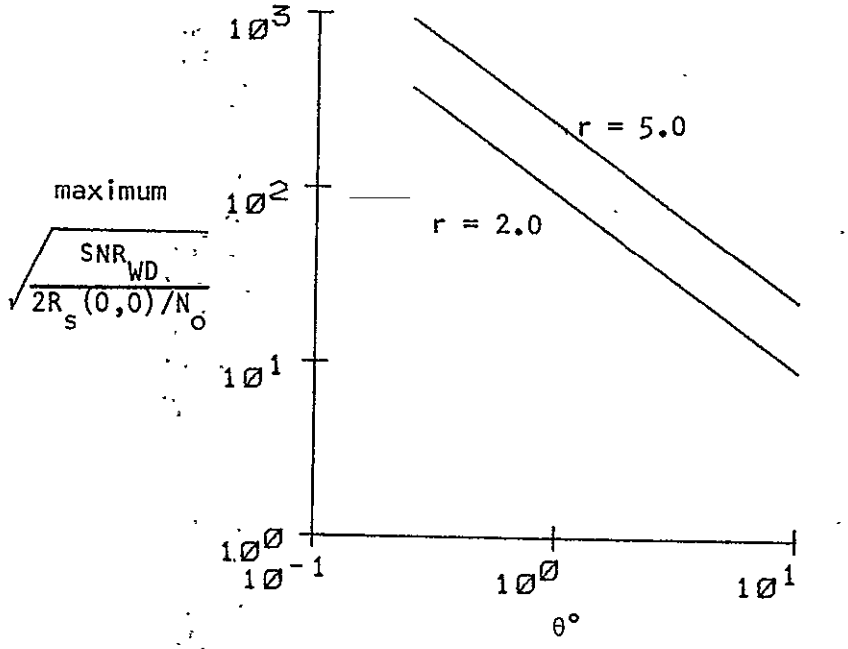

Figure 4-8. Maximum (normalized output signal-to-noise ratio)$^{1/2}$ for different values of r vs. rotation angle.

Table 4-2. 2T yielding the maximum SNR_N for different rotation angles.

	r = 2	r = 5
θ°	2T for max SNR_N	2T for max SNR_N
0.25	1152	2879
0.5	576	1440
0.75	384	960
1.0	288	720
2.0	144	360
3.0	96	240
5.0	58	144
10.0	28	72

Table 4-3. Maximum $\sqrt{SNR_N}$ for different rotation angles.

	r = 2	r = 5
θ°	max $\sqrt{SNR_N}$	max $\sqrt{SNR_N}$
0.25	373.3	933.4
0.5	186.7	466.7
0.75	124.4	311.1
1.0	93.3	233.3
2.0	46.7	116.7
3.0	31.1	77.8
5.0	18.7	46.7
10.0	9.3	23.4

Extrapolation of these last expressions results in a general approximate formula for determining 2T corresponding to the largest SNR_N in the presence of angular distortion for small values of θ.

$$2T \text{ for max } SNR_N \approx 144\ r(\theta^{-1}) \qquad (4\text{-}72)$$
$$0 < \theta \leq 10°$$

This was shown to be true by evaluating (4-72) for different values of r and observing whether the indicated value coincided with that observed. In all cases they agreed. This result indicates that given the angular distortion and characteristic length of the image autocorrelation function, the area yielding the maximum SNR_N can be computed from (4-72) for small values of θ.

Figure 4-8 is a plot of the maximum $\sqrt{SNR_N}$ versus the angular distortion for two values of the characteristic length. These curves were generated from the sample values listed in Table 4-3. This graph displays the maximum attainable $\sqrt{SNR_N}$ in the presence of a given angular distortion. As in Figure 4-7 the relationship is linear in a log-log plot for both values of r over the range of θ used. This indicates that the maximum $\sqrt{SNR_N}$ varies with the rotation angle in the following manner.

$$\sqrt{SNR_N} \approx \alpha_r \theta^{\beta_r} \qquad (4\text{-}73)$$
$$0 < \theta \leq 10°$$

or equivalently,

$$SNR_N \approx \left[\alpha_r \theta^{\beta_r}\right]^2 \qquad (4\text{-}74)$$
$$0 < \theta \leq 10°$$

where α_r and β_r depend upon the characteristic length. The values of α_r and β_r may be found from Table 4-3 or Figure 4-8.

$$\alpha_2 = 93.3 \qquad \beta_2 = -1$$

$$\alpha_5 = 233.3 \qquad \beta_5 = -1$$

Therefore, for r = 2,

$$\max \overline{SNR}_N \approx [93.3\ \theta^{-1}]^2 \qquad (4\text{-}75)$$

$$0 < \theta \leq 10°$$

and for r = 5,

$$\max \overline{SNR}_N \approx [233.3\ \theta^{-1}]^2 \qquad (4\text{-}76)$$

$$0 < \theta \leq 10°$$

These last two expressions may be extrapolated to give the following general expression for the relationship between the maximum $\overline{SNR}_N$ and the angle of rotation for small angular distortions.

$$\max \overline{SNR}_N \approx [46.65\ r\ (\theta^{-1})]^2 \qquad (4\text{-}77)$$

$$0 < \theta \leq 10°$$

This expression was corroborated by evaluating (4-77) for different values of r and testing whether the resulting value for the $\overline{SNR}_N$ was indeed a maximum. In all cases it was.

Figure 4-9 provides a series of curves representing the $\sqrt{\overline{SNR}_N}$ for a given integration area size as a function of the angular distortion. Figure 4-9a illustrates this relationship for a characteristic length of r = 2, while a value of r = 5 was chosen for Figure 4-9b. Curves for 2T = 50, 100, 200 and 400 are displayed for both figures. This representation of the functional relationship between the $\overline{SNR}_N$ and angular distortion may be used for design of the registration processor in the following manner. Given the integration area and percentage loss in the $\overline{SNR}_N$ that is acceptable, the maximum allowable rotation may be found from the curve corresponding to the appropriate integration area. For example,

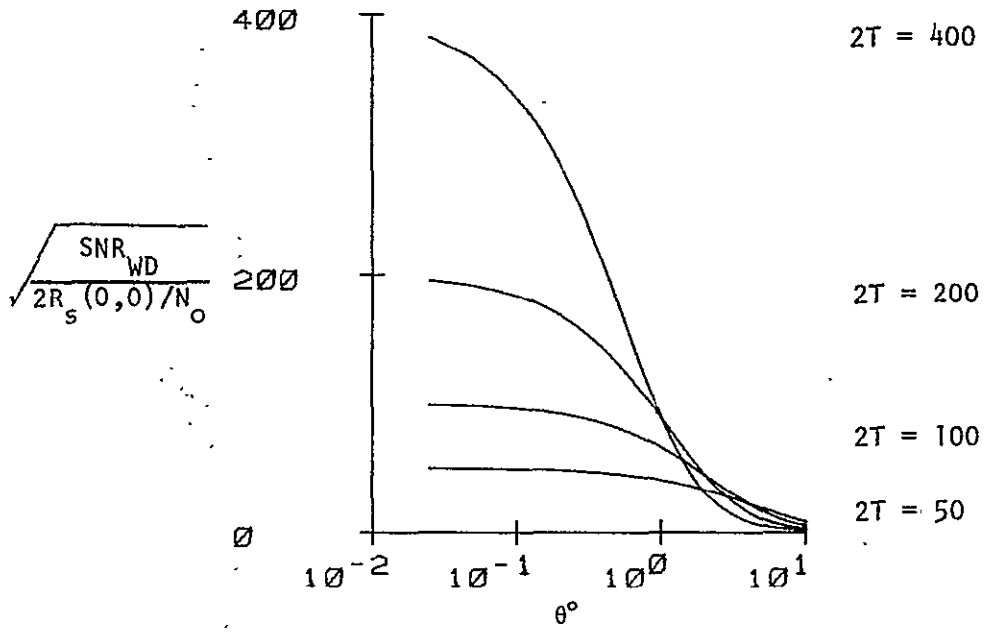

a. r = 2.0

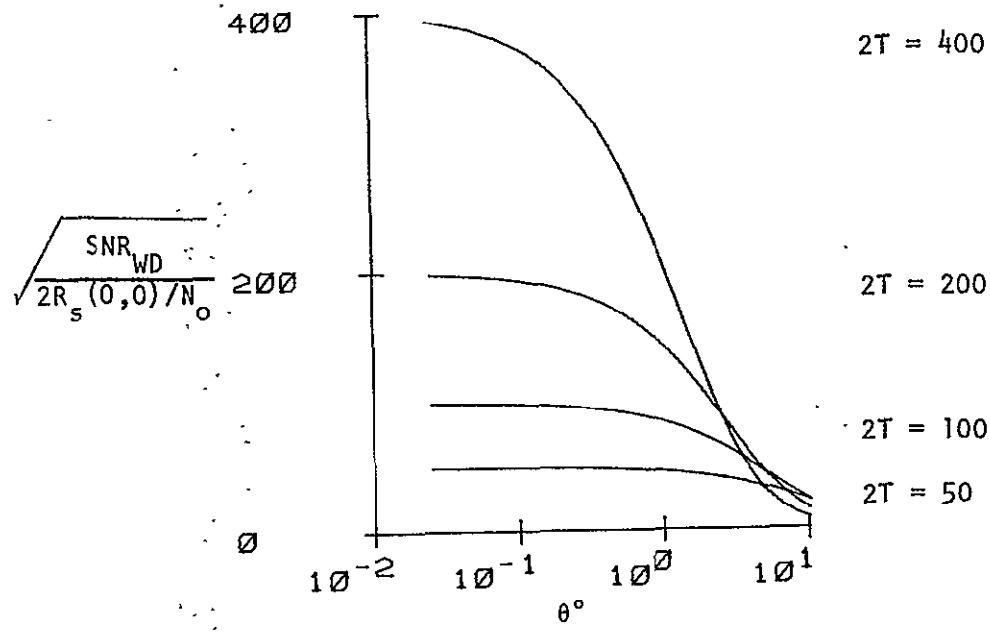

b. r = 5.0

Figure 4-9. (Normalized output signal-to-noise ratio)$^{1/2}$ for different integration area sizes vs. rotation angle.

if the characteristic length is 5 and a loss factor of 0.81 for the SNR_N is acceptable when operating with 2T = 200, then the maximum allowable rotation is 0.15°. This is found directly from Figure 4-9b. A loss factor of 0.81 for the SNR_N corresponds to a loss factor of 0.9 for $\sqrt{SNR_N}$. For 2T = 200, the maximum $\sqrt{SNR_N}$ without any angular distortion is 200, so that a reduction of 0.9(200) equals 180. The maximum allowable rotation is that angle corresponding to a $\sqrt{SNR_N}$ of 180, which is 0.15°.

This concludes the general examples for examining the effect of spatial distortions on the output signal-to-noise ratio. The illustrations presented in Figures 4-1 through 4-9 verified the derived results obtained in section 4.2. It was found that in the presence of a given linear scale or rotational distortion, there is a unique integration area size which yields a maximum output signal-to-noise ratio. Figures 4-1, 4-5 and 4-6 illustrate this while figures 4-2, 4-3, 4-7 and 4-8 present a straightforward way of determining the optimum integration area size and maximum SNR_N achievable. The next section proceeds in a similar fashion with spatial distortions modeling those observed for LANDSAT I images. In this way the method for applying the results of section 4.2 is illustrated for a practical image registration model.

4.5.3. Distortion Model for Temporally Differing LANDSAT I Images.

In this section the distortion model employed in the LARS registration system [1, 5] for overlaying LANDSAT I images is used to evaluate the expression for the SNR_N in the presence of spatial distortions. For multitemporal LANDSAT I images a biquadratic polynomial of the following form is used as the distortion model.

$$\begin{bmatrix} x' \\ y' \end{bmatrix} = \begin{bmatrix} 1+c_{11} & c_{12} & c_{13} & c_{14} & c_{15} \\ c_{21} & 1+c_{22} & c_{23} & c_{24} & c_{25} \end{bmatrix} \begin{bmatrix} x \\ y \\ x^2 \\ y^2 \\ xy \end{bmatrix} \tag{4-78}$$

where,

(x,y) = reference image coordinate system

(x',y') = coordinate system of image to be registered with the reference image

and,

c_{ij} = distortion coefficients; $i = 1,2,;\ j = 1,\ldots,5$

The values of the coefficients are determined by a least squares procedure. The approach followed in the LARS registration system [1, 5] is to overlay a sample of subimages from each full image assuming spatial congruence. This registration of each of the subimages is accomplished by a simple translation because of the assumption that no relative spatial distortions exist between the subimages. However, because the full images are relatively distorted, all of the translations for the subimage overlays are not the same. A least square estimate using a biquadratic polynomial (eq. (4-78)) then is used to find that spatial transformation between the full images which best fits all of the subimage translations simultaneously.

With this model of the spatial distortions, the functions $p(x,y)$ and $q(x,y)$ used in the expression for the output signal-to-noise ratio become,

$$p(x,y) = c_{11}x + c_{12}y + c_{13}x^2 + c_{14}y^2 + c_{15}xy \tag{4-79}$$

$$q(x,y) = c_{21}x + c_{22}y + c_{23}x^2 + c_{24}y^2 + c_{25}xy \tag{4-80}$$

Substitution of these expressions for $p(x,y)$ and $q(x,y)$ into equation (4-49) allows for the evaluation of the SNR_N. In this case, since the specific distortion is given, the SNR_N depends upon two parameters: the integration area, $4T^2$; and the characteristic length of the image autocorrelation function. Again evaluation of (4-49) was performed by using Simpson's rule approximation to the integral.

Two sets of distortion parameters were used in this evaluation of the SNR_N for LANDSAT I imagery. The coefficient sets chosen were those used in the operational registration of images. In this way the method of using the analytical results of section 4.2 for the situation encountered in practice is exemplified. The LANDSAT I imagery registered and corresponding distortion coefficients for the two overlays are listed in Table 4-4.

The relationship between the $\sqrt{SNR_N}$ and the integration area for different values of the characteristic length is displayed in Figures 4-10a and 4-10b. Figure 4-10a contains the results for the first set of coefficients and Figure 4-10b for the second set. Note that for each curve in both figures there is a value of 2T yielding a maximum SNR_N. This indicates that there is an optimum integration area where a maximum SNR_N is realized in the presence of the distortion models chosen.

In each figure the series of curves illustrates the dependence of the integration area size yielding the maximum SNR_N on the characteristic length of the image autocorrelation function. For example, when the first distortion model is used (Fig. 4-10a), a value of $2T = 70$ will give the maximum SNR_N for $r = 2$, whereas for $r = 5$ a value of $2T = 180$ must be chosen. Therefore, choice of an optimum integration area size is determined by the value of r.

Table 4-4. LANDSAT I images registered and the corresponding distortion coefficients.

Set 1

	LARS Run #	Lines	Columns
Reference run	72053602	(1350,2200)	(1350,2250)
Overlay run	73070100	(1450,2340)	(1650,2700)

Distortion coefficients

c_{11} = -0.05694005	c_{21} = -0.02044661
c_{12} = 0.01516939	c_{22} = -0.08017300
c_{13} = 0.00001908	c_{23} = -0.00000123
c_{14} = -0.00000280	c_{24} = 0.00001501
c_{15} = -0.00000445	c_{25} = 0.00001334

Set 2

	LARS Run #	Lines	Columns
Reference run	72053602	(1350,2200)	(1350,2250)
Overlay run	75009000	(1490,2340)	(1425,2325)

Distortion coefficients

c_{11} = -0.08289302	c_{21} = 0.01898512
c_{12} = -0.02288279	c_{22} = -0.11859888
c_{13} = 0.00000824	c_{23} = 0.00000147
c_{14} = -0.00001332	c_{24} = 0.00003922
c_{15} = 0.00003550	c_{25} = -0.00001333

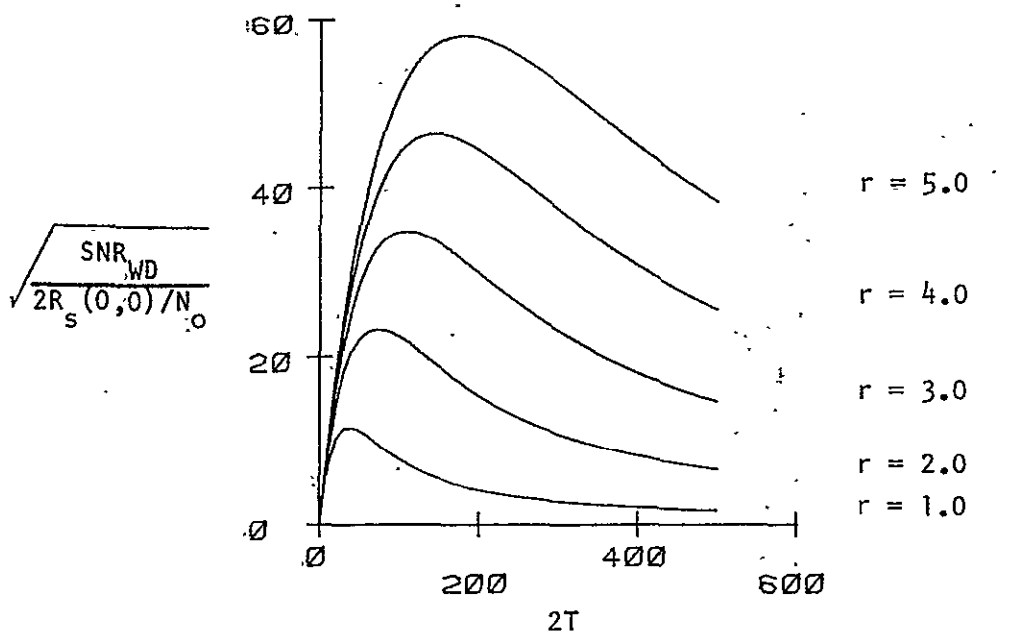

a. First spatial distortion model (set 1).

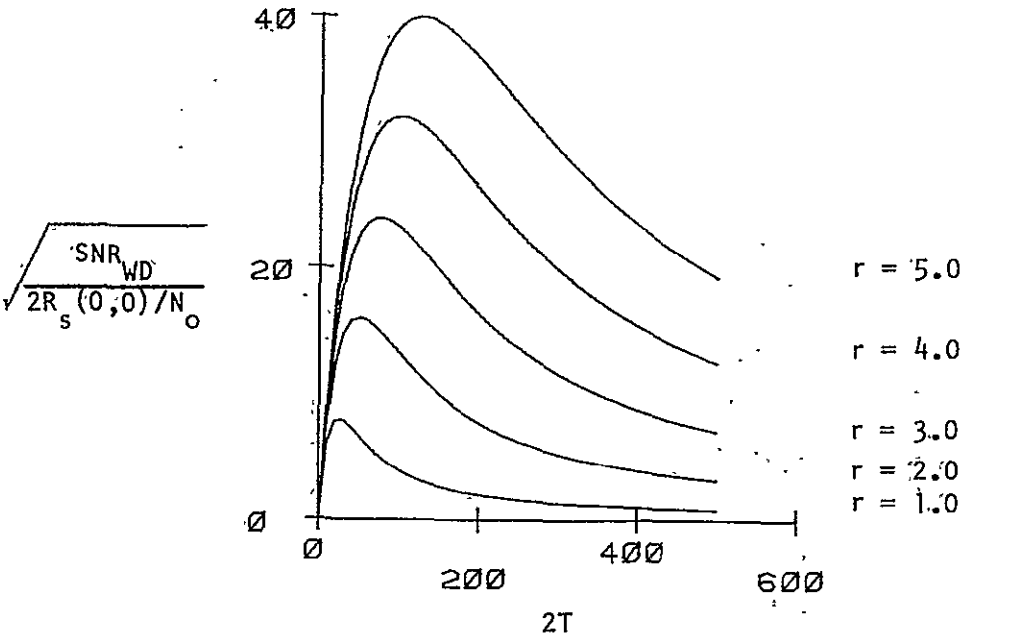

b. Second spatial distortion model (set 2).

Figure 4-10. $(\text{Normalized output signal-to-noise ratio})^{1/2}$ for different values of r vs. $(\text{integration area})^{1/2}$ (LANDSAT I images)

This dependence upon r required that an estimate of the image autocorrelation function be made so that a value of r could be determined. This was carried out by first picking several test sites from the images to be registered. The subimage size chosen for each of these test sites was 111 lines by 111 columns.

The next step in estimating the image autocorrelation function required a preprocessing operation on the images. Since the examples in this section are applications of the analysis in section 4.2, it is necessary that the noise (temporal changes) be white. In Chapter 5 it is experimentally observed that the noise is nonwhite with an exponential autocorrelation function. In this situation it is necessary that the images first be passed through a filter designed to whiten the noise and then these preprocessed images be registered (refer to Figure 3-4). With an exponential autocorrelation function for the temporal changes it is shown in the example in Chapter 3 that a derivative type operator must be applied in the preprocessing stage. In compliance with this analytical result a gradient operator was applied to each of the images, where,

$$|\text{Gradient } X_{i,j}| = \{(X_{i,j+1} - X_{i,j-1})^2 + (X_{i+1,j} - X_{i-1,j})^2\}^{1/2} \qquad (4\text{-}81)$$

$X_{i,j}$ = image sample value at coordinate (i,j)

The autocorrelation function estimate then was made from the gradient images. The following expression was used to estimate the autocorrelation function.

$$R_{\ell,k} = \frac{1}{N^2} \sum_{i=1}^{N-\ell} \sum_{j=1}^{N-k} (X_{i+\ell,j+k} - \bar{X})(X_{i,j} - \bar{X}) \qquad (4\text{-}82)$$

$\ell = 0, 1, \ldots, M$

$k = 0, 1, \ldots, M$

where,

$\bar{X}$ = mean of the image

$X_{i,j}$ = image sample value at coordinate (i,j)

N^2 = number of data points in the image

M = maximum shift for the autocorrelation function estimate

Figures 4-11 through 4-15 contain examples of the resulting autocorrelation surfaces and contours of these surfaces. In Figures 4-11a through 4-15a each of the autocorrelation surfaces are displayed, where each number denotes a value of the surface at the corresponding shift position and the (0,0) lag position is in the center of the displayed surface. The scale for each of the surfaces has been normalized by the factor $100/R_{0,0}$.

Although Figures 4-11a through 4-15a present the complete surfaces, the general shape of the surfaces is better illustrated by the contour plots in Figures 4-11b through 4-15b. In these figures, contours at levels $R_{0,0}$, $R_{0,0}e^{-1}$, and $R_{0,0}e^{-2}$ are displayed. In this way it is a straightforward procedure to determine whether the surfaces are of exponential form, and if so, what is the characteristic length, r. If the contours are equally spaced, then the surface is exponential and the characteristic length is the distance between the contours. From these figures it is seen that an exponential model for the autocorrelation surface is a reasonable model with a characteristic length ranging between 1 and 3.

Using this range of r and the curves presented in Figures 4-10a and 4-10b, the range for 2T yielding the maximum SNR_N is,

$40 \leq 2T \leq 110$ for distortion coefficient set 1

AUTOCORRELATION FUNCTION ESTIMATE

```
 1  2  2  2  1  1  1  0  0  0  0  0  0  1  0  1  0  1  0 -2 -1  0  1  1  2  2  3 -1 -1  0  0  0  0
 0  1  1  0  0  0  0  0  0  0  1  1  1  2  1  1  1  1  0  0  0  0  1  1  1  1  0  0 -1 -1  0 -1 -1
 0  0  1  0  0  0  0  0  0  2  2  2  3  3  3  2  1  2  0  0  0  1  1  1  1  1  0  0  0  0 -1 -1 -1
 0  0  2  2  1  1  0  1  1  2  3  3  3  2  2  3  3  1  0  0  1  1  1  1  0  1  0  0  0  0 -1  0
 0  0  0  1  1  1  0  0  1  2  3  3  3  2  2  2  2  1  0  0  0  0  1  0  0  0  0 -1 -1  0  0  0  0
 0  0  0  0  0  0  0  1  2  2  1  1  1  1  2  3  2  2  1  1  1  0  0  0 -1 -1  0 -1  0  0  0  0  0
 1  1  0 -1 -1 -1  0  0  1  1  0  0  0  1  1  2  2  2  2  2  1  0  0  0 -1 -2 -1 -1 -1  0  0  0 -1
 1  0  0 -1 -1 -1  0  0  0  1  0  0  0  2  3  2  3  3  3  3  2  2  1  0 -1 -2 -2 -1 -1 -1  0  0 -1
 0  0  0 -1 -1 -1 -1  0  0  0  0  0  1  3  4  4  6  4  4  4  4  2  1  0 -2 -2 -3 -1 -1 -1  0 -1 -1
-1 -1 -1 -1 -2 -2 -2 -2  0  0  0  0  0  1  2  5  7  6  5  4  3  2  0 -1 -2 -3 -2 -2 -2 -2 -2 -2 -2
-1  0 -1 -1 -2 -2 -3 -2  0  1  1  1  1  2  3  5  8  7  6  5  4  2  1  0 -2 -3 -2 -2 -2 -1 -1 -2 -2
 0  0  0  0  0 -1 -1  0  1  1  2  1  2  4  5  7  9  7  6  7  6  3  1  0 -1 -2 -2 -2  0 -1 -1 -1 -2
 0  0  0  0  0 -1  0  0  2  1  2  2  3  5  7  9 11 10  8  6  4  2  2  0 -2 -2 -2  0 -1 -1 -1 -2 -2
-1 -1  0  0  0  0  0  0  1  1  1  2  4  7 10 13 17 14 10  8  6  3  2  1  0 -1  0  0  0 -1  0  0 -1
-2 -2  0  0  0  0  0  0  0  1  1  3  7 10 14 20 23 19 14 10  7  4  3  3  2  0  0  0  0  0  0  0  0
-2 -2 -1  0  0  0 -1  0  2  1  2  3  7 13 21 35 42 35 27 13  7  3  3  4  2  0  0  1  0  0  0  0  0
 0  0  1  1  2  0  0  1  3  5  3  4  7 15 26 51100 51 26 15  7  4  3  5  3  1  0  0  2  1  1  0  0
 0  0  0  0  0  1  0  0  2  4  3  3  7 13 22 35 47 35 21 13  7  3  2  1  2  0 -1  0  0  0 -1 -2 -2
 0  0  0  0  0  0  0  0  2  3  3  4  7 10 14 19 23 20 14 10  7  3  1  1  0  0  0  0  0  0  0 -2 -2
-1  0  0 -1  0  0  0 -1  0  1  2  3  6  8 10 14 17 13 10  7  4  2  1  1  1  0  0  0  0  0  0 -1 -1
-2 -2 -1 -1 -1  0 -2 -2 -2  0  2  2  4  6  8 10 11  9  7  5  3  2  2  1  2  0  0 -1  0  0  0  0  0
-2 -1 -1 -1  0 -2 -2 -2 -1  0  1  3  6  7  6  7  9  7  5  4  2  1  2  1  1  0 -1 -1  0  0  0  0  0
-2 -2 -1 -1 -2 -2 -2 -3 -2  0  1  2  4  5  6  7  8  5  3  2  1  1  1  1  0 -2 -3 -2 -2 -1 -1  0 -1
-2 -2 -2 -2 -2 -2 -2 -3 -2 -1  0  2  3  4  5  6  7  5  2  1  0  0  0  0  0 -2 -2 -2 -2 -1 -1 -1 -1
-1 -1  0 -1 -1 -1 -1 -2 -2  0  1  2  4  4  4  4  6  4  4  3  1  0  0  0  0  0 -1 -1 -1 -1  0  0  0
-1  0  0 -1 -1 -1 -2 -2 -1  0  1  2  2  3  3  3  3  2  3  2  0  0  0  1  0  0  0 -1 -1 -1  0  0  1
-1  0  0  0 -1 -1 -1 -2 -1  0  0  0  1  2  2  2  2  2  1  1  0  0  0  1  1  0  0 -1 -1 -1  0  1  1
 0  0  0  0  0 -1  0 -1 -1  0  0  0  1  1  1  2  2  3  2  1  1  1  1  2  2  1  0  0  0  0  0  0  0
 0  0  0  0 -1 -1  0  0  0  0  1  0  0  0  0  1  2  2  2  2  3  3  3  2  1  0  0  1  1  1  0  0  0
 0 -1  0  0  0  0  0  1  0  1  1  1  1  0  0  1  3  3  2  2  3  3  3  2  1  1  0  1  1  2  2  0  0
-1 -1 -1  0  0  0  0  1  1  1  1  1  0  0  0  0  1  2  3  3  3  2  2  2  0  0  0  0  0  0  1  0  0
-1 -1  0 -1 -1  0  0  1  1  1  1  0  0  0  0  1  1  1  1  2  1  1  1  0  0  0  0  0  0  0  1  1  0
 0  0  0  0 -1 -1  0  2  2  1  1  0 -1 -2  0  1  0  1  0  1  0  0  0  0  0  0  1  1  1  2  2  2  1
```

	NORMALIZED SCALE	ACTUAL VALUE		SHIFT POSITION (LINE,COLUMN)
MAXIMUM =	100	18.905	AT	(0, 0)
MINIMUM =	-3	-0.671		(6, -9)

SCALE CONVERSION - 1 UNIT NORMALIZED SCALE = 0.189 UNITS ACTUAL SCALE
0 ON NORMALIZED SCALE = 0 ON ACTUAL SCALE

Original Imagery

LARS Run #	Channel	Spectral Band	Area
72053626	4	0.8 - 1.1 μm	Line(104,216),Column(104,216)

Figure 4-11a. Autocorrelation surface for the magnitude of the gradient of the image.

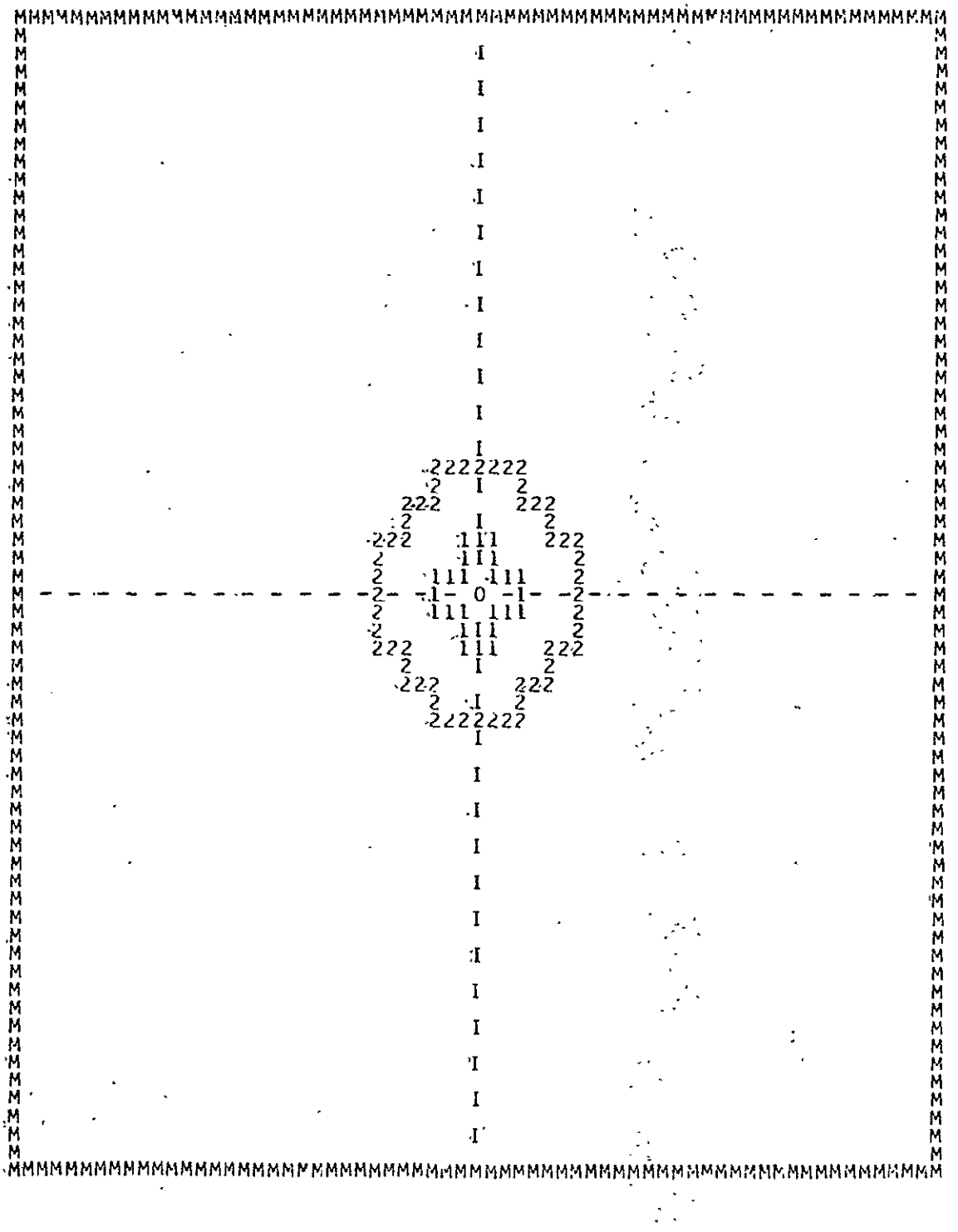

Figure 4-11b. Autocorrelation surface contour for the magnitude of the gradient of the image.

AUTOCORRELATION FUNCTION ESTIMATE

```
-2 -1  0  0  0 -1  0  0  0  0 -1  0  0  0  0  0  1  0  0  0 -1 -1  0 -1 -1  0  0  0  0  0  0 -1 -1
 0  0  0  0  0  0  0  0  0  0  0  0  1  0 -1  0  0  0 -1 -2 -2 -1  0  0  0  0  0  0  0  0  0  0 -1
-1 -1 -1 -2 -1 -1  0  0  0  0  0  0  1  0  0  0  0  0  0 -1 -1  0  0  0  0  0  1  0  0  0  0 -1  0
 0  0 -1 -1 -2 -1  0  0  1  1  0  1  1  0  0  1  1  0 -1 -1 -1  0  0  0  0  0  0  0  0  0  0  0  0
 0  0 -1 -1  0  0  0  1  1  1  1  0  1  0 -1 -1 -1 -2 -4 -3 -2 -2 -1 -1 -1  0  0  1  0  0  0  0  1
 0  0  0  0  0  1  2  2  2  2  2  1  0  0  0 -1 -1 -1 -1 -1 -2 -2 -1 -1 -1  0  0  0  0  0  0  0  1
 0  0  0  0  0  2  3  3  3  2  2  1  1  0  0  0  0  0  0 -1 -1 -1  0  0 -1  0  0  0  0  0  0 -1  0
 0  0  0  0  0  0  2  3  2  1  0  0  1  1  0  0  0 -1 -1 -1 -1 -1 -1 -1 -1  0  0 -1  0 -1 -1 -1 -1
 0  0  0  0  0  0  0  1  1  1  1  0  1  1  0  0  0  0 -2 -1  0 -1  0 -1 -1 -2 -2 -1 -1 -1 -1 -1  0
 0  0  0  0  0  0  0  0  0  0  0 -1  0  0  0  0 -1 -2 -3 -2 -1  0  0  0 -1 -2 -1 -1 -2 -1  0  0  0
 0 -1 -1 -1 -1  0 -1 -1  0  0  0  0  0  0  0  0  0 -1 -1  0  1  2  1  0  0  0  0  0  0  0  0  0
-1 -1  0  0  0  0  0  0  1  2  1  1  0  1  1  2  4  2  0  0  0  1  2  2  0 -1  0  0  0  0  0  0  0
-1 -1 -1  0  0  0  1  0  1  3  2  1  1  2  3  5  5  3  2  2  1  1  1  1  0  0  0 -1  0  0  0  1
-2 -1 -1 -1  0  0  2  1  1  4  4  3  3  4  5  8 13  8  4  5  3  2  3  1  1  1  1  0  0  0  0  1
 0  0  0  0  0  1  1  2  2  3  4  4  5  6  9 14 18 15  8  7  5  4  3  2  1  1  0  1  0  0  0 -1  0
 0  0  0  0  1  2  3  2  2  4  6  6  7 11 17 31 37 31 18 11  8  7  5  4  3  3  3  2  1  0  0  0  1
 1  0  0  1  2  3  4  4  4  5  7  9 11 15 21 47100 47 21 15 11  9  7  5  4  4  4  3  2  1  0  0  1
 1  0  0  0  1  2  3  3  3  4  5  7  8 11 18 31 37 31 17 11  7  6  6  4  2  2  3  2  1  0  0  0  0
 0 -1  0  0  0  1  0  1  1  2  3  4  5  7  8 15 18 14  9  6  5  4  4  3  2  2  1  1  0  0  0  0  0
 1  0  0  0  0  0  1  1  1  1  3  2  3  5  4  8 13  8  5  4  3  3  4  4  1  1  2  0  0 -1 -1 -1 -2
 1  0  0  0 -1  0  0  0  0  1  1  1  1  2  2  3  5  5  3  2  1  1  2  3  1  0  1  0  0  0 -1 -1 -1
 0  0  0  0  0  0  0 -1  0  2  2  1  0  0  0  2  4  2  1  1  0  1  1  2  1  0  0  0  0  0  0 -1 -1
 0  0  0  0  0  0  0  0  0  1  2  1  0 -1 -1  0  0  0  0  0  0  0  0  0  0 -1 -1  0 -1 -1 -1 -1  0
 0  0  0 -1 -2 -1 -1 -2 -1  0  0  0 -1 -2 -3 -2 -1  0  0  0  0 -1  0  0  0  0  0  0  0  0  0  0  0
 0 -1 -1 -1 -1 -1 -2 -2 -1 -1  0 -1  0 -1 -2  0  0  0  0  1  1  0  1  1  1  1  0  0  0  0  0  0  0
-1 -1 -1 -1  0 -1  0  0 -1 -1 -1 -1 -1 -1 -1 -1  0  0  0  1  1  0  0  1  2  3  2  0  0  0  0  0  0
 0 -1  0  0  0  0  0  0 -1  0  0 -1 -1 -1  0  0  0  0  0  0  1  1  2  2  3  3  3  2  0  0  0  0  0
 1  0  0  0  0  0  0  0 -1 -1 -1 -2 -2 -1 -1 -1 -1 -1  0  0  0  1  2  2  2  2  2  1  0  0  0  0  0
 1  0  0  0  0  1  0  0 -1 -1 -1 -2 -2 -3 -4 -2 -1 -1 -1  0  1  0  1  1  1  1  0  0  0 -1 -1  0  0
 0  0  0  0  0  0  0  0  0  0  0  0 -1 -1 -1  0  1  1  0  0  1  1  0  1  1  0  0 -1 -2 -1 -1  0  0
 0 -1  0  0  0  0  1  0  0  0  0  0 -1 -1  0  0  0  0  0  0  1  0  0  0  0  0  0 -1 -1 -2 -1 -1 -1
-1  0  0  0  0  0  0  0  0  0  0 -1 -2 -2 -1  0  0  0 -1  0  1  0  0  0  0  0  0  0  0  0  0  0  0
-1 -1  0  0  0  0  0  0 -1 -1  0 -1 -1  0  0  0  1  0  0  0  0  0 -1  0  0  0  0 -1  0  0  0 -1 -2
```

	NORMALIZED SCALE	ACTUAL VALUE		SHIFT POSITION (LINE,COLUMN)
MAXIMUM =	100	14.312	AT	(0, 0)
MINIMUM =	-4	-0.590		(12, -2)

SCALE CONVERSION - 1 UNIT NORMALIZED SCALE = 0.143 UNITS ACTUAL SCALE
0 ON NORMALIZED SCALE = 0 ON ACTUAL SCALE

Original Imagery

LARS Run #	Channel	Spectral Band	Area
72053626	4	0.8 - 1.1 μm	Line(304,416),Column(104,216)

Figure 4-12a. Autocorrelation surface for the magnitude of the gradient of the image.

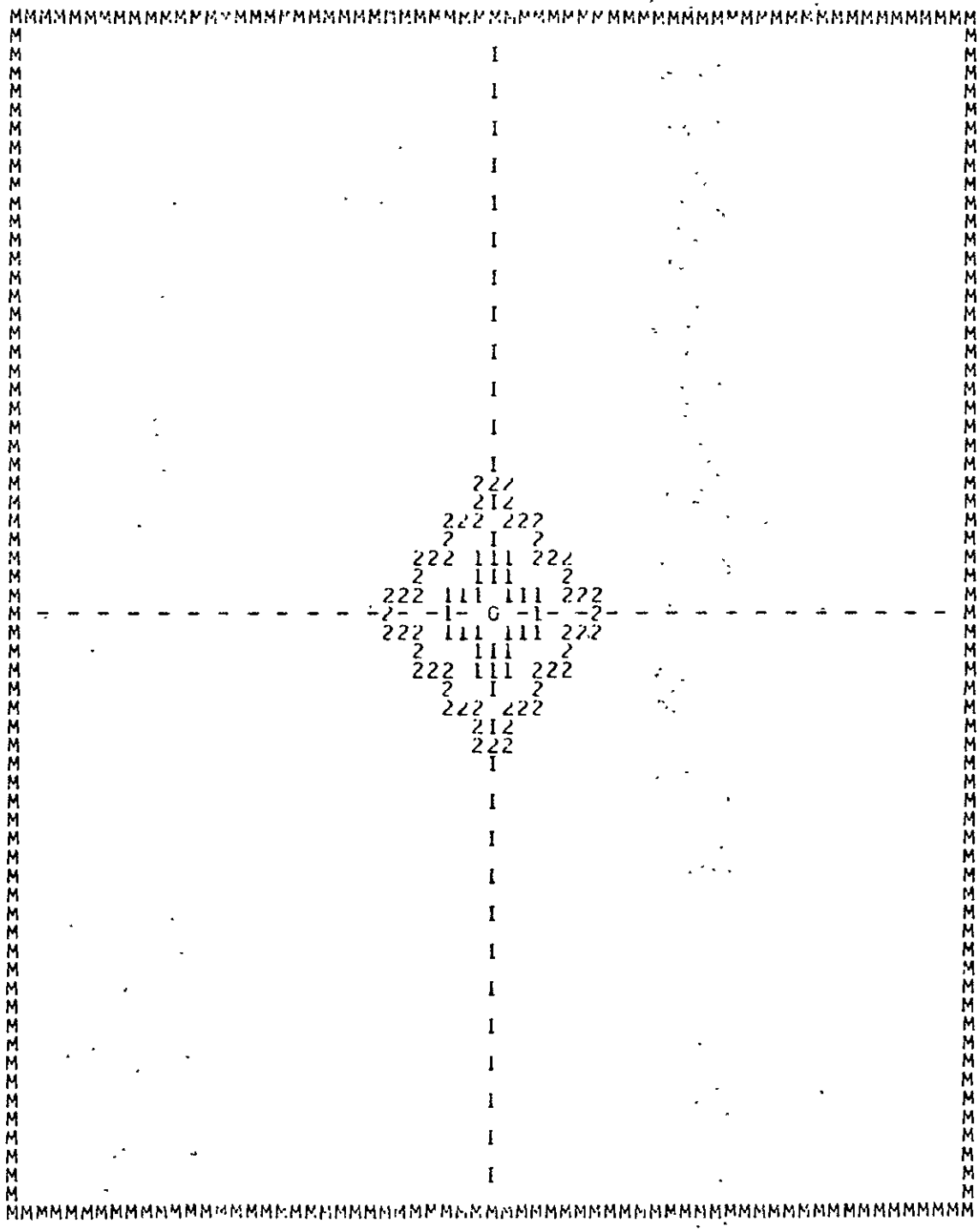

Figure 4-12b. Autocorrelation surface contour for the magnitude of the gradient of the image.

AUTOCORRELATION FUNCTION ESTIMATE

-1	0	0	0	0	0	0	0	1	0	0	-1	-1	0	1	2	2	2	3	3	3	3	3	3	3	3	2	0	0	0	-1
-1	0	0	0	-1	-1	-1	0	1	0	0	-1	0	0	1	1	2	3	4	3	3	3	3	4	4	3	2	2	0	0	0	0	0
0	0	0	0	-1	-1	-1	0	1	0	0	0	0	0	1	2	4	5	4	3	2	3	4	5	3	2	2	2	1	0	0	-1	-1
1	0	0	0	-1	-1	-1	0	0	0	0	0	0	0	1	3	4	5	4	4	3	3	3	4	3	3	2	1	0	0	-1	0	0
0	0	-1	-2	-2	-1	-1	0	0	0	0	1	0	1	2	3	5	5	5	4	4	4	4	3	3	2	1	1	0	0	0	0	-1
0	0	-1	-2	-3	-2	-1	0	0	0	1	1	1	1	3	4	5	6	6	6	6	6	5	3	3	2	1	0	0	0	0	0	-1
0	-1	-1	-2	-2	-2	-1	0	0	0	0	2	3	4	4	5	6	8	9	8	7	5	4	4	3	2	1	0	0	0	0	0	0
0	-1	-2	-2	0	0	-1	0	0	0	1	2	4	5	6	6	8	9	10	9	7	5	4	4	3	2	1	0	0	0	0	0	0
-1	-1	-1	-1	0	0	-1	0	0	-1	1	3	4	6	8	9	9	10	10	8	8	6	5	4	3	4	2	1	0	0	1	0	0
0	0	0	0	0	0	-1	-1	-1	-1	1	4	5	8	9	9	10	11	10	9	8	7	5	4	3	2	3	2	2	1	0	0	0
0	0	0	0	1	0	0	0	0	0	2	4	7	10	10	10	12	13	12	11	10	7	6	5	3	1	1	2	1	1	0	0	0
1	1	1	2	2	1	0	0	1	1	3	6	8	10	12	13	15	15	14	13	10	9	7	5	2	0	0	0	1	0	0	0	0
2	2	3	2	2	2	1	1	1	3	4	7	10	12	14	17	19	19	17	13	11	9	7	5	2	0	0	0	0	1	0	0	0
3	3	2	3	3	3	2	2	3	3	5	9	11	15	18	23	27	26	19	14	12	10	7	4	2	0	0	0	0	0	0	0	0
2	2	3	4	3	2	1	2	2	3	5	9	12	16	23	31	37	34	24	17	13	10	7	4	2	1	0	0	1	0	0	0	0
1	3	3	3	3	2	2	2	2	2	5	9	13	19	29	46	57	49	29	19	14	11	7	4	1	1	0	1	2	2	1	1	0
2	2	2	2	2	1	1	1	2	3	7	10	14	20	30	60	100	60	30	20	14	10	7	3	2	1	1	1	2	2	2	2	2
0	1	1	2	2	1	0	1	1	4	7	11	14	19	29	49	57	46	29	19	13	9	5	2	2	2	2	2	3	3	3	3	1
0	0	0	0	1	0	0	1	2	4	7	10	13	17	24	34	37	31	23	16	12	9	5	3	2	2	1	2	3	4	3	2	2
0	0	0	0	0	0	0	0	2	4	7	10	12	14	19	26	27	23	18	15	11	9	5	3	3	2	2	3	3	3	2	3	3
0	0	0	1	0	0	0	0	2	5	7	9	11	13	17	19	19	17	14	12	10	7	4	3	1	1	1	2	2	2	3	2	2
0	0	0	0	1	0	0	0	2	5	7	9	10	13	14	15	15	13	12	10	8	6	3	1	1	0	0	1	2	2	1	1	1
0	0	0	1	1	2	1	1	3	5	6	7	10	11	12	13	12	10	10	10	7	4	2	0	0	0	0	0	1	0	0	0	0
0	0	0	1	2	2	3	2	3	4	5	7	8	9	10	11	10	9	9	8	5	4	1	-1	-1	-1	-1	0	0	0	0	0	0
0	0	1	0	0	1	2	4	3	4	5	6	8	8	10	10	9	9	8	6	4	3	1	-1	0	0	-1	0	0	-1	-1	-1	-1
0	0	0	0	0	0	1	2	3	4	4	5	7	9	10	9	8	6	6	5	4	2	1	0	0	0	-1	0	0	-2	-2	-1	0
0	0	0	0	0	0	1	2	3	4	4	5	7	8	9	8	6	5	4	4	3	2	0	0	0	0	-1	-2	-2	-2	-1	-1	0
-1	0	0	0	0	0	1	2	3	3	5	6	6	6	6	6	5	4	3	1	1	1	1	0	0	0	-1	-2	-3	-2	-1	0	0
-1	0	0	0	0	1	1	2	3	3	4	4	4	4	5	5	5	3	2	1	0	1	0	0	0	0	-1	-1	-2	-2	-1	0	0
0	0	-1	0	0	1	2	3	3	4	3	3	3	4	4	5	4	3	1	0	0	0	0	0	0	0	-1	-1	-1	0	0	0	1
-1	-1	0	0	1	2	2	2	3	5	4	3	2	3	4	5	4	2	1	0	0	0	0	0	1	0	-1	-1	-1	0	0	0	0
0	0	0	0	0	2	2	3	4	4	3	3	3	3	4	3	2	1	1	0	0	-1	0	0	1	0	-1	-1	-1	0	0	0	-1
-1	0	0	0	0	2	3	3	3	3	3	3	3	3	3	2	2	2	1	0	-1	-1	0	0	1	0	0	0	0	0	0	0	-1

	NORMALIZED SCALE	ACTUAL VALUE		SHIFT POSITION (LINE,COLUMN)
MAXIMUM =	100	24.923	AT	(0, 0)
MINIMUM =	-3	-0.801		(11, 12)

SCALE CONVERSION - 1 UNIT NORMALIZED SCALE = 0.249 UNITS ACTUAL SCALE
0 ON NORMALIZED SCALE = 0 ON ACTUAL SCALE

Original Imagery

LARS Run #	Channel	Spectral Band	Area
72053626	8	0.8 - 1.1 μm	Line(104,216),Column(304,416)

Figure 4-13a. Autocorrelation surface for the magnitude of the gradient of the image.

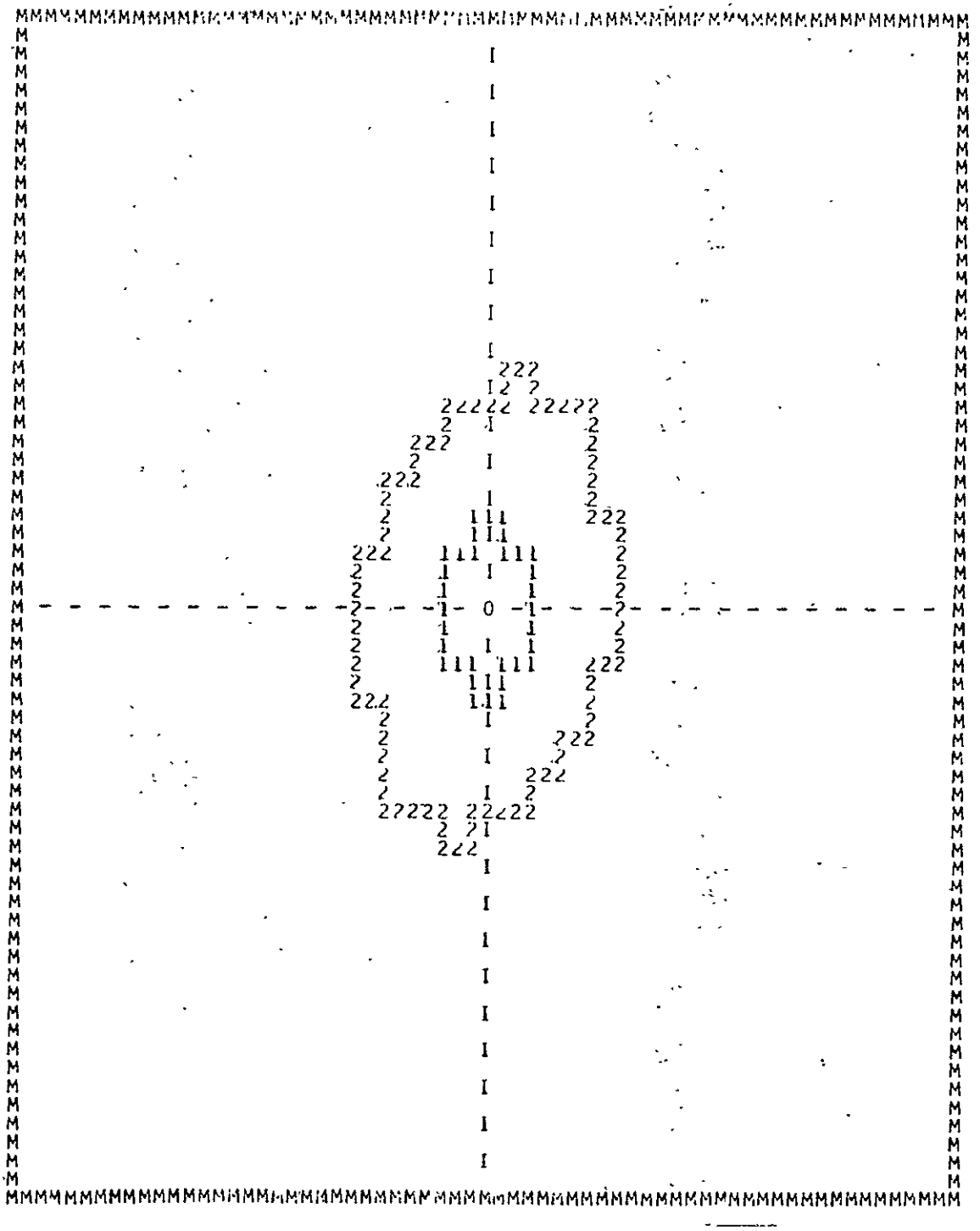

Figure 4-13b. Autocorrelation surface contour for the magnitude of the gradient of the image.

AUTOCORRELATION FUNCTION ESTIMATE

-1	0	0	0	1	0	0	0	0	0	0	0	0	1	2	1	2	1	0	-1	-2	0	0	0	1	2	1	1	1	0	1	1	0
-1	0	0	1	1	1	1	1	1	0	0	0	0	1	2	3	1	1	0	0	0	-1	0	1	1	1	2	2	1	1	1	0	0
0	0	1	1	1	1	0	0	0	0	0	0	0	0	0	0	2	1	0	0	0	0	-1	0	0	1	1	1	1	1	1	0	0
0	1	1	1	2	1	0	0	-1	-1	0	0	0	0	-1	0	2	1	1	0	0	0	0	0	0	0	0	0	0	1	1	1	0
0	1	2	1	1	2	1	0	0	0	-2	-1	-1	-1	0	1	1	0	1	1	0	-1	0	0	0	0	0	1	0	0	2	2	2
0	0	1	2	2	1	1	0	0	0	-1	-2	0	0	0	0	1	1	0	0	0	-1	0	0	0	0	1	1	0	1	2	3	1
-1	-1	0	0	0	1	0	0	0	0	-1	-2	0	0	-1	-1	0	0	0	0	0	0	0	1	1	1	2	1	1	3	3	3	2
-1	-2	0	0	0	0	1	0	0	0	0	0	0	0	-2	-2	-1	0	0	0	0	-1	0	1	1	1	3	1	1	1	3	4	1
0	0	0	0	0	0	1	1	1	1	1	1	1	0	0	0	1	1	0	0	0	1	0	0	0	0	0	0	0	0	2	1	2
-1	0	0	0	0	0	1	1	1	1	1	1	0	0	0	0	0	0	0	0	1	1	1	0	0	0	0	0	0	0	0	0	-1
-1	0	1	1	1	0	0	1	0	0	0	0	1	0	0	0	1	1	0	0	0	0	1	2	0	0	1	0	0	0	0	0	0
0	0	2	2	1	0	0	0	0	0	0	0	0	1	0	2	3	3	2	1	1	1	2	2	1	0	0	1	0	0	0	0	-2
0	0	1	2	2	2	2	2	1	0	0	0	1	1	3	4	6	5	4	3	2	2	2	3	2	1	0	0	0	0	0	0	-2
0	1	1	0	1	1	2	1	0	0	0	1	2	4	5	8	10	8	7	5	3	2	3	2	1	1	0	0	-1	0	0	0	-1
1	1	2	1	0	1	2	1	0	1	0	1	3	6	11	14	19	14	10	7	5	3	3	2	1	0	0	0	0	0	0	0	-1
0	0	1	1	0	1	0	0	1	2	3	4	6	11	17	31	33	31	18	11	7	6	5	4	1	0	0	0	-1	0	-1	0	-2
-1	0	0	0	0	0	0	0	0	1	5	6	9	13	21	44	100	44	21	13	9	6	5	3	0	0	0	0	0	0	0	0	-1
-2	0	-1	0	-1	0	0	0	1	4	5	6	7	11	18	31	33	31	17	11	6	4	3	2	1	0	0	1	0	1	1	0	0
-1	0	0	0	0	0	0	0	1	2	3	3	5	7	10	14	19	14	11	6	3	1	0	1	0	1	2	1	0	1	2	1	1
-1	0	0	0	-1	0	0	1	1	2	3	2	3	5	7	8	10	8	5	4	2	1	0	0	0	1	2	1	1	0	1	1	0
-2	0	0	0	0	0	0	1	2	3	2	2	2	3	4	5	6	4	3	1	1	0	0	0	1	2	2	2	2	2	1	0	0
-2	0	0	0	0	1	0	0	1	2	2	1	1	1	2	3	3	2	0	1	0	0	0	0	0	0	0	0	1	2	2	0	0
0	0	0	0	0	0	1	0	0	2	1	0	0	0	0	1	1	0	0	0	1	0	0	0	0	1	0	0	1	1	1	0	-1
-1	0	0	0	0	0	0	0	0	0	1	1	1	0	0	0	0	0	0	0	0	1	1	1	1	1	1	0	0	0	0	0	-1
2	1	2	0	0	0	0	0	0	0	0	1	0	0	0	1	1	0	0	0	1	1	1	1	1	1	1	0	0	0	0	0	0
1	4	3	1	1	1	3	1	1	1	0	-1	0	0	0	0	-1	-2	-2	0	0	0	0	0	0	0	1	0	0	0	0	-2	-1
2	3	3	3	1	1	2	1	1	1	0	0	0	0	0	0	0	-1	-1	0	0	-2	-1	0	0	0	0	1	0	0	0	-1	-1
1	3	2	1	0	1	1	0	0	0	0	-1	0	0	0	1	1	0	0	0	0	-2	-1	0	0	0	1	1	2	2	1	0	0
2	2	2	0	0	1	0	0	0	0	0	-1	0	1	1	0	1	1	0	-1	-1	-1	-2	0	0	0	1	2	1	1	2	1	0
0	1	1	1	0	0	0	0	0	0	0	0	0	0	1	1	2	0	-1	0	0	0	0	-1	-1	0	0	1	2	1	1	1	0
0	0	1	1	1	1	1	1	0	0	-1	0	0	0	0	1	2	0	0	0	0	0	0	0	0	0	0	1	1	1	1	0	0
0	0	1	1	1	2	2	1	1	1	0	-1	0	0	0	1	1	3	2	1	0	0	0	0	1	1	1	1	1	1	0	0	-1
0	1	1	0	1	1	1	2	1	0	0	0	-2	-1	0	1	2	1	2	1	0	0	0	0	0	0	0	1	0	0	0	0	-1

	NORMALIZED SCALE	ACTUAL VALUE		SHIFT POSITION (LINE,COLUMN)
MAXIMUM =	100	4.047	AT	(0, 0)
MINIMUM =	-2	-0.105		(5,-16)

SCALE CONVERSION - 1 UNIT NORMALIZED SCALE = 0.040 UNITS ACTUAL SCALE
0 ON NORMALIZED SCALE = 0 ON ACTUAL SCALE

Original Imagery

LARS Run #	Channel	Spectral Band	Area
72053626	12	0.8 - 1.1 μm	Line(304,416),Column(104,216)

Figure 4-14a. Autocorrelation surface for the magnitude of the gradient of the image.

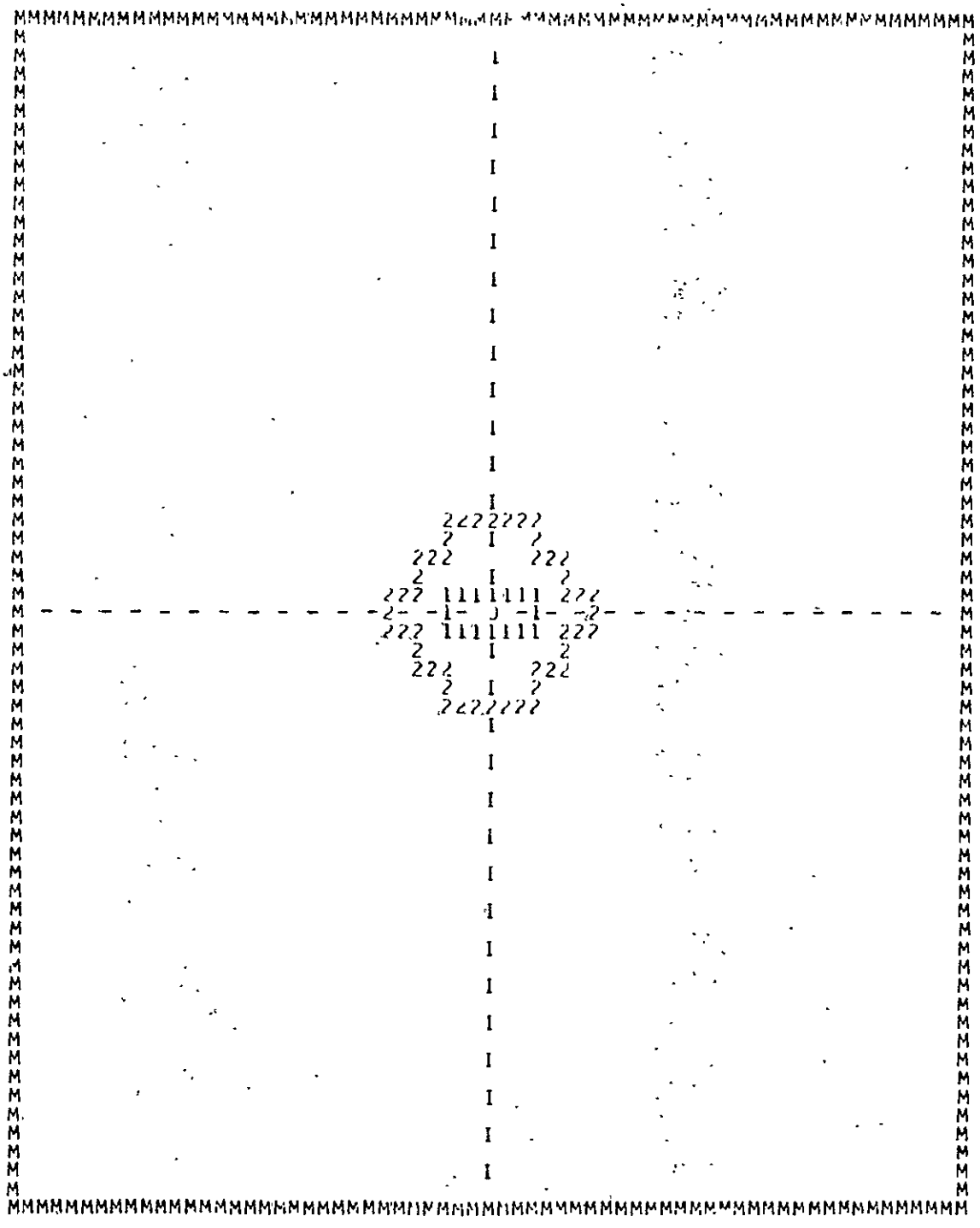

Figure 4-14b. Autocorrelation surface contour for the magnitude of the gradient of the image.

AUTOCORRELATION FUNCTION ESTIMATE

-2	-1	0	-1	-1	0	0	0	0	0	0	0	-1	-2	-1	-1	0	0	0	0	0	0	0	0	0	0	0	1	1	0	1	0	1
0	0	0	0	-1	-1	0	0	0	0	0	0	0	0	0	0	0	0	0	0	1	0	0	0	0	0	0	1	0	0	0	0	1	1
-1	0	-1	-1	-1	-1	-1	-1	-1	0	0	0	0	0	0	0	1	0	0	0	1	0	0	0	0	0	1	1	0	0	0	0	0
-1	0	0	0	0	0	0	0	0	-1	0	0	1	0	0	0	0	0	0	-1	0	0	0	-1	0	0	0	0	0	0	-1	-1	-1	0
0	1	0	0	0	1	0	1	0	0	0	0	1	1	1	1	0	0	0	0	0	0	0	0	0	0	0	0	0	0	-1	-1	-1	0
1	1	1	0	0	0	1	1	0	0	1	2	2	1	0	1	1	1	1	0	0	0	1	0	0	0	0	0	-1	-1	-1	0	0
1	1	0	1	0	0	1	1	1	2	1	3	2	1	0	1	1	1	1	0	0	0	0	1	1	0	0	-1	-1	-1	-1	0	0
0	0	0	0	0	1	1	1	1	1	2	2	1	1	0	1	2	1	1	0	0	1	1	0	0	1	0	-1	-1	-1	-1	0	0
0	0	0	1	2	1	0	0	0	0	2	2	2	0	0	1	1	1	0	0	0	1	2	1	1	1	0	0	0	0	0	0	0
0	1	1	2	2	2	2	0	0	0	0	2	1	2	1	2	3	2	1	1	1	2	1	1	2	2	1	0	0	0	0	0	0
1	0	2	2	2	2	2	0	0	0	1	2	3	1	2	3	4	4	3	3	3	2	2	2	3	2	1	0	0	0	1	2	0
0	1	1	2	2	2	2	1	1	1	2	2	3	2	3	6	7	6	6	3	3	4	4	3	2	2	1	1	1	2	2	1	1
1	0	1	1	3	4	3	3	2	2	3	4	3	6	8	8	9	9	7	6	5	5	4	3	2	1	1	0	1	2	2	1	1
0	1	1	3	3	4	4	4	3	3	3	5	7	9	11	13	16	13	11	9	7	5	4	2	1	2	1	0	0	0	1	2	1
0	0	2	2	3	3	4	4	2	3	4	5	8	11	15	20	24	21	15	12	9	7	5	4	3	3	2	1	1	1	1	2	3
1	1	2	3	3	3	2	2	3	4	6	7	10	15	23	36	37	36	22	14	11	8	5	4	5	4	3	2	2	3	3	3	2
2	2	3	4	3	2	3	4	4	5	6	8	13	18	26	47	100	47	26	18	13	8	6	5	4	4	3	2	3	4	3	2	2
2	3	3	3	2	2	3	4	5	4	5	8	11	14	22	36	37	36	23	15	10	7	6	4	3	2	2	3	3	3	2	1	1
3	2	1	1	1	1	2	3	3	4	5	7	9	12	15	21	24	20	15	11	8	5	4	3	2	4	4	3	3	2	2	0	0
1	2	1	0	0	0	1	2	1	2	4	5	7	9	11	13	16	13	11	9	7	5	3	3	3	4	4	4	3	3	1	1	0
1	1	2	2	1	0	1	1	2	3	4	5	5	6	7	9	9	8	8	6	3	4	3	2	2	3	3	4	3	1	1	0	1
1	1	2	2	1	1	1	2	2	3	4	4	3	3	6	6	7	6	3	2	3	2	2	1	1	1	2	2	2	2	1	1	0
0	2	1	0	0	0	1	2	3	2	2	2	3	3	3	4	4	3	2	1	3	2	1	0	0	0	2	2	2	2	2	0	1
0	0	0	0	0	0	1	2	2	1	1	2	1	1	1	2	3	2	1	2	1	2	0	0	0	0	2	2	2	2	1	1	0
0	0	0	0	0	0	0	1	1	1	2	1	0	0	0	1	1	1	0	0	2	2	2	0	0	0	0	1	2	1	0	0	0
0	0	-1	-1	-1	-1	0	1	0	0	1	1	0	0	1	1	2	1	0	1	1	2	2	1	1	1	1	1	0	0	0	0	0
0	0	-1	-1	-1	-1	0	0	1	1	0	0	0	0	1	1	1	1	0	1	2	3	1	2	1	1	1	0	0	1	0	1	1
0	0	-1	-1	-1	0	0	0	0	0	1	0	0	0	1	1	1	1	0	1	2	2	1	0	0	1	1	0	0	0	1	1	1
0	-1	-1	-1	0	0	0	0	0	0	0	0	0	0	0	0	0	1	1	1	1	0	0	0	0	1	0	1	0	0	0	1	0
0	-1	-1	-1	0	0	0	0	0	0	-1	0	0	0	-1	0	0	0	0	0	1	0	0	-1	0	0	0	0	0	0	0	0	-1
0	0	0	0	0	1	1	0	0	0	0	0	1	0	0	0	1	0	0	0	0	0	0	0	-1	-1	-1	-1	-1	-1	-1	0	-1
1	1	0	0	0	0	1	0	0	0	0	0	0	1	0	0	0	0	0	0	0	0	0	0	0	0	0	-1	-1	0	0	0	0
1	0	1	0	1	1	0	0	0	0	0	0	0	0	0	0	0	-1	-1	-2	-1	0	0	0	0	0	0	0	-1	-1	0	-1	-2

	NORMALIZED SCALE	ACTUAL VALUE		SHIFT POSITION (LINE,COLUMN)
MAXIMUM =	100	4.912	AT	(0, 0)
MINIMUM =	-2	-0.111		(16, 3)

SCALE CONVERSION - 1 UNIT NORMALIZED SCALE - 0.049 UNITS ACTUAL SCALE
0 ON NORMALIZED SCALE = 0 ON ACTUAL SCALE

Original Imagery

LARS Run #	Channel	Spectral Band	Area
72053626	12	0.8 - 1.1 μm	Line(304,416),Column(304,416)

Figure 4-15a. Autocorrelation surface for the magnitude of the gradient of the image.

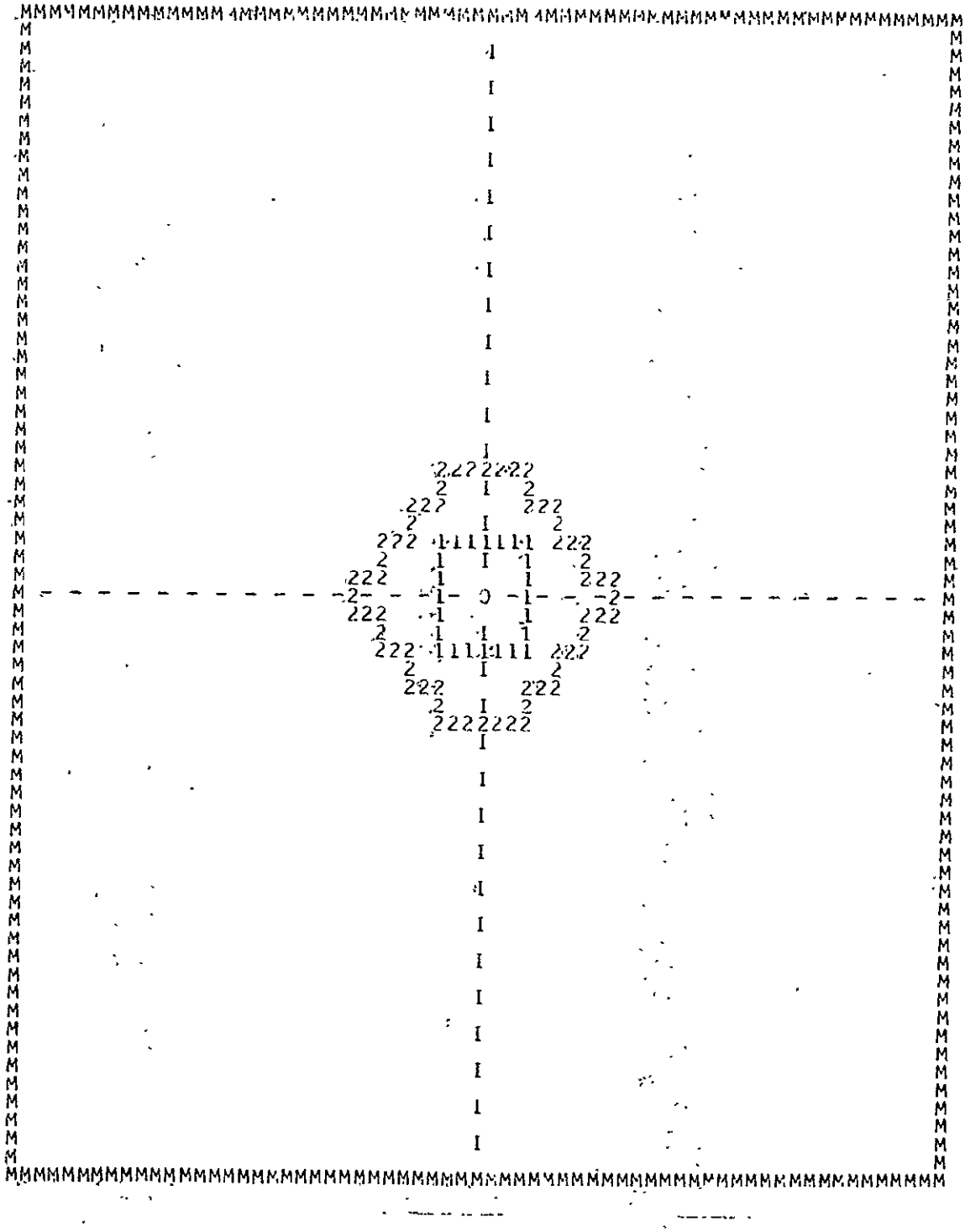

Figure 4-15b. Autocorrelation surface contour for the magnitude of the gradient of the image.

and,

$$30 \leq 2T_x \leq 70 \text{ for distortion coefficient set 2}$$

Therefore, it is possible to choose an optimum integration area size for the registration processor based upon the distortion model and image autocorrelation function characteristics observed for actual satellite images.

4.6. Conclusion

In the situation where relative spatial distortions exist between images to be registered, expressions have been derived for estimating the loss in the output signal-to-noise ratio due to these spatial distortions. These results are in terms of a reduction factor (eqs. (4-18) and (4-41)) applied to the SNR had the spatial distortions not been present. For distortions that are increasing with image size (eqs. (4-14) and (4-45)) there is a finite integration area that yields the maximum SNR. Determination of this integration area may be found by evaluating expressions (4-12) and (4-39) with an appropriate model of the distortions. This evaluation is a straightforward procedure which may be accomplished by numerical integration methods as is shown in section 4.5. This is performed for both general linear distortions such as a scale change or rotation, plus two distortion models for LANDSAT I images. These latter examples illustrate the direct application of this analysis to practical image registration.

CHAPTER 5

TEMPORAL CHANGE PROPERTIES

In one important application of image registration, one would like to match spatially as close as possible two temporally differing images of the same scene so that they may be compared on a point by point basis. Assuming that there are no relative spatial distortions between the images, the registration process reduces to finding the relative translation between the images. However, since the images have been taken at different times, one can expect that changes in the scene have occurred, so that the two images will vary in the intensity levels as well as their relative translation. This variation in intensity levels contributes significantly to the uncertainty in finding the relative translation.

In the development of a registration processor, these changes have been modeled as additive noise. One image is assumed to be the signal and the second image the signal plus noise (temporal changes).

Several approaches to the image registration problem have utilized statistical parameter estimation theory, where the parameters to be estimated are the translations along the respective coordinate axes (Chapter 2). A central part of this type of analysis is that one be able to characterize the noise properties, where the properties in question are determined by the particular approach that is taken. This is illustrated in Chapter 2 where an expression for the variance of the error of the registration processor is derived. Two lines of approach are presented,

both of whose validity depends upon certain assumptions. The first method requires knowledge of the probability density function of the noise and the second assumes that the autocorrelation function or spectral density of the noise is known.

These requirements prompted the development of a model of the temporal change characteristics. The particular properties of concern are those that have been encountered in the analysis and development of a registration processor. These are the probability density function and the autocorrelation or spectral density function of the noise.

5.1. Probability Density Function of the Temporal Changes

The first analysis is that of the probability density function of the noise. Since the noise is defined as being the additive change that has occurred between registered images, this investigation necessitated the registration of a series of images and then a subtraction of the image pairs to generate the difference image, or additive noise, for each time pair. Test sites for this study were chosen from LANDSAT imagery over Kansas, Montana, Missouri, and Indiana, and are tabulated in Table 5-1. These particular test sites were picked because multitemporal imagery that had been previously registered [35] was readily available.

The probability density function of the noise for each test site was estimated by generating a histogram of each of the corresponding difference images and then normalizing the histogram by dividing by the total number of points in the difference image to obtain an approximation to the probability density function.

Table 5-1. Test sites for temporal change investigation.

a. Kansas

LARS Run #	73046000		73064000		74024100		74024200	
Date Data Taken	7/6/73		8/29/73		5/26/74		7/1/74	
Area #	Line Center	Column Center	Line Center	Column Center	Line Center	Column Center	Line Center	Column Center
1	111	445*	116	389	294	393	218	336
			115	389*	293	392	218	336
					294	392*	218	336
2	116	570*	121	514	300	518	223	462
			121	514*	299	518	223	463
					300	518*	224	462
3	211	435*	216	380	395	383	318	327
			216	380*	395	384	317	327
					396	384*	319	327
4	111	1495*	120	1440	297	1447	219	1398
			120	1440*	298	1447	219	1398
					298	1447*	219	1398
5	352	210*	358	154	537	157	459	98
			358	154*	537	157	459	98
					538	157*	459	98
6	100	170*	104	113	282	116	206	57
			105	114*	283	116	208	58
					284	118*	208	59
7	100	310*	104	254	282	257	207	199
			104	254*	284	257	207	199
					284	258*	208	200

Table 5-1a, cont.

LARS Run #	73046000		73064000		74024100		74024200	
Date Data Taken	7/6/73		8/29/73		5/26/74		7/1/74	
Area #	Line Center	Column Center	Line Center	Column Center	Line Center	Column Center	Line Center	Column Center
8	250	170*	255	114	434	117	356	60
			255	114*	434	117	357	57
					434	118*	357	59
9	250	310*	255	255	434	258	357	200
			255	254*	434	257	356	199
					434	258*	356	200
10	400	360*	407	304	586	308	507	250
			405	304*	584	307	505	250
					584	308*	505	250
11	400	510*	407	455	587	459	507	403
			405	454*	584	458	505	402
					584	458*	504	401

*Reference location for corresponding line and column centers which are tabulated to the right.

5-lb. Hill County, Montana

LARS Run Number 73124700

LARS Channel # is	1-4		21-24		17-20		9-12		5-8	
Date Data Taken	5/5/73		5/23/73		6/10/73		7/16/73		8/3/73	
Area #	Line Center	Column Center	Line Center	Column Center	Line Center	Column Center	Line Center	Column Center	Line Center	Column Center
1	110	410*	110	410	110	409	109	410	110	410
			110	410*	110	409	109	410	110	410
					110	410*	109	411	110	412
							110	410*	111	410
2	170	130*	170	129	170	129	170	128	170	128
			170	130*	170	130	170	129	170	129
					170	130*	170	130	170	129
							170	130*	170	130
3	415	150*	415	150	415	149	414	149	415	148
			415	150*	415	149	415	150	415	148
					415	150*	415	150	415	149
							415	150*	415	149

*Reference location for corresponding line and column centers which are tabulated to the right.

55-1c. Missouri

LARS Run Number 72033804

LARS Channel # is	1-4		5-8		9-12	
Date Data Taken	9/13/72		8/26/72		10/1/72	
Area #	Line Center	Column Center	Line Center	Column Center	Line Center	Column Center
1	200	200*	201	200	201	200
			200	200*	199	201
2	200	400*	202	399	201	400
			200	400*	199	401
3	200	600*	202	599	201	599
			200	600*	199	601
4	200	800*	202	799	200	800
			200	800*	199	800
5	200	1000*	201	1000	200	1000
			200	1000*	200	1000
6	400	200*	401	199	401	200
			400	200*	400	200
7	400	400*	401	399	400	400
			400	400*	400	401
8	400	600*	401	600	400	600
			400	600*	400	601
9	400	800*	401	800	400	800
			400	800*	399	800
10	400	1000*	401	999	400	999
			400	1000*	399	1000
11	600	200*	601	200	600	600
			600	200*	599	199

Table 5-1c, cont.

LARS Channel # is	1-4		5-8		9-12	
Date Data Taken	9/13/72		8/26/72		10/1/72	
Area #	Line Center	Column Center	Line Center	Column Center	Line Center	Column Center
12	600	400*	601	400	600	400
			600	400*	599	400
13	600	600*	601	599	600	601
			600	600*	599	601
14	600	800*	601	800	600	800
			600	800*	599	800
15	600	1000*	600	1000	600	1000
			600	1000*	600	1000
16	800	200*	800	200	800	200
			800	200*	800	200
17	800	400*	800	400	800	401
			800	400*	800	400
18	800	600*	800	600	800	601
			800	600*	799	601
19	800	800*	801	800	799	800
			800	800*	799	800
20	800	1000*	801	1000	800	1001
			800	1000*	799	1000

*Reference location for corresponding line and column centers which are tabulated to the right.

5-1d. Tippecanoe County, Indiana

LARS Run Number 72053603

LARS Channel # is	1-4		5-8		9-12	
Date Data Taken	9/30/72		10/19/72		11/29/72	
Area #	Line Center	Column Center	Line Center	Column Center	Line Center	Column Center
1	200	200*	199	201	199	203
			200	200*	200	202
2	200	400*	199	401	200	402
			200	400*	200	401
3	200	600*	200	601	200	602
			200	600*	201	600
4	200	800*	200	801	199	799
			200	800*	201	801
5	400	200*	399	200	398	201
			400	200*	399	200
6	400	400*	400	401	399	401
			400	400*	399	400
7	400	600*	400	600	399	600
			400	600*	400	600
8	400	800*	400	800	401	800
			400	800*	401	799
9	600	200*	599	200	599	200
			600	200*	599	200
10	600	400*	599	400	599	399
			600	400*	599	399
11	600	600*	600	600	599	599
			600	600*	599	599

Table 5-1d, cont.

LARS Channel # is	1-4		5-8		9-12	
Date Data Taken	9/30/72		10/19/72		11/29/72	
Area #	Line Center	Column Center	Line Center	Column Center	Line Center	Column Center
12	600	800*	600	800	600	799
			600	800*	600	799

*Reference location for corresponding line and column centers which are tabulated to the right.

$$\Pr[\text{Difference image has value } x] = \frac{\text{No. of points in the difference image having value } x}{\text{Total no. of points in the difference image}}$$

These probability density functions were then plotted for a visual comparison. For the initial phase of this examination a sample size of 111 lines by 111 columns was chosen for each test site.

Before examining the resulting probability density functions, first consider some of the types of density functions that one might expect. Referring to Chapter 2 where an expression for the variance of the registration error is derived, the first method of approaching the problem, that is, via a maximum a posteriori estimate of the translation parameters, requires the assumption that the noise be normally distributed. In the light of this method of analysis, a Gaussian distribution would be highly desirable.

In previous analyses of multispectral imagery, [36,37] an image is modeled as being comprised of different homogeneous classes, each of which is normally distributed. Thus when considering two temporally differing images, the difference image is composed of the change that has occurred for each of the different classes. Since each class has a Gaussian distribution, the change for each class is also normally distributed. This follows from the property that the difference of two normally distributed data sets also has a Gaussian distribution.

One may formalize this line of reasoning in the following manner. Let D be the entire difference image, and D_i be the additive noise for the ith class. Since the noise for a particular class is Gaussian, the probability density function of D_i is,

$$p_{D_i}(x) = \frac{1}{\sqrt{2\pi}\,\sigma_i} \exp\left\{-\frac{(x-\mu_i)^2}{2\sigma_i^2}\right. \tag{5-2}$$

where,

$$p_{D_i}(x) = p_D(x|D_i) \tag{5-3}$$

the probability density of the difference image given that one considers only the D_ith class. The probability density of the entire difference image is then,

$$p_D(x) = \sum_i p_{D_i}(x)\ Pr[D_i] \tag{5-4}$$

which is a weighted sum of Gaussian density functions, where $Pr[D_i]$ is the probability of occurrence of the D_ith class and,

$$\sum_i Pr[D_i] = 1 \tag{5-5}$$

Given this formulation, what are reasonable forms for $p_D(x)$? First consider the case where all the D_i are identically distributed. Letting,

$$\sigma^2 = Var[D_i]$$

$$\mu = E[D_i]$$

then,

$$p_D(x) = \frac{1}{\sqrt{2\pi}\,\sigma} \exp\left\{-\frac{(x-\mu)^2}{2\sigma^2}\right. \tag{5-6}$$

so that D has a Gaussian distribution. This simplistic assumption yields a straightforward and compact expression for the difference image density function, however, it is not a reasonable assumption in many instances. In these cases one must retain the weighted expression for $p_D(x)$. For

example, one class may decrease in reflectivity over a period of time while a second class may increase in its reflectance. Underlying reasons for this will depend upon the type of imagery that is being considered. With agricultural data, the classes being different crop types, one type of crop may reach maturity in a given time period while a second cover type has not changed in appearance. Another example would be that of different harvesting times for different crops. Or if one is examining a scene containing a body of water, the changes over the water may be independent of those over the surrounding land, so that the two classes, water and land, will not necessarily have the same amount of change over the same period of time.

This latter formulation for the probability density function more closely coincides with experimental observation, where the density function is modeled as a weighted sum of Gaussian density functions. This is borne out by examination of the probability density function estimates of the generated difference images. In conjunction with the examination of the histogram plots, also consider examples of the corresponding difference images. By observation of these images one can obtain a better feeling for the resulting probability density function estimates. The particular examples given represent a cross section of those density functions encountered. Figures 5-1 through 5-5 contain examples of the difference images and their corresponding probability density function estimates. Note that they are categorized according to the observed density function estimates.

Figures 5-1 and 5-2 contain examples of difference images whose probability density functions have a single mode. Referring back to the

a. Difference Image

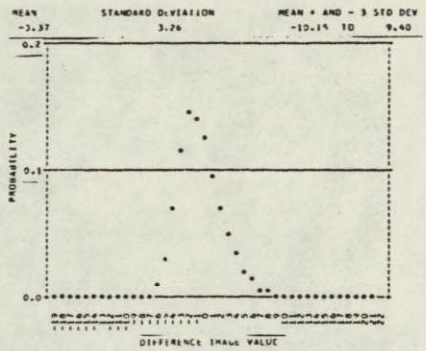

b. Probability density function

VALUE	NUMBER POINTS	VALUE	NUMBER POINTS
-19	2	1	1130
-18	0	2	924
-17	1	3	644
-16	1	4	462
-15	0	5	317
-14	2	6	210
-13	3	7	116
-12	3	8	69
-11	5	9	55
-10	8	10	23
-9	19	11	17
-8	32	12	14
-7	47	13	8
-6	172	14	10
-5	426	15	9
-4	889	16	7
-3	1474	17	14
-2	1808	18	6
-1	1775	19	4
0	1564	20	1

c. Histogram listing

Original Imagery

LARS Run #	Channel	Spectral Band	Area
73064000	4	0.8 - 1.1 μm	Line(65,175),Column(1385,1495)
74024100	4	0.8 - 1.1 μm	Line(243,353),Column(1392,1502)

Figure 5-1. Difference image with single mode probability density function.

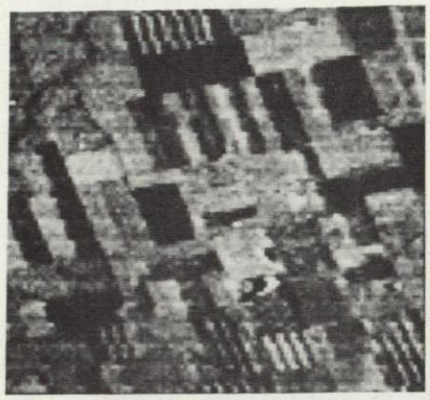

a. Difference Image

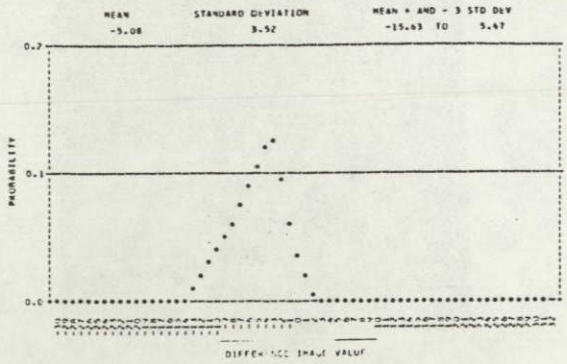

b. Probability density function

VALUE	NUMBER POINTS	VALUE	NUMBER POINTS
-30	1	1	260
-29	0	2	117
-28	0	3	38
-27	0	4	14
-26	0	5	8
-25	0	6	4
-24	3	7	3
-23	1	8	1
-22	1	9	0
-21	0	10	0
-20	0	11	0
-19	3	12	0
-18	4	13	0
-17	8	14	0
-16	13	15	2
-15	34	16	0
-14	56	17	0
-13	162	18	0
-12	255	19	0
-11	416	20	0
-10	526	21	0
-9	655	22	0
-8	784	23	0
-7	965	24	0
-6	1164	25	0
-5	1350	26	0
-4	1484	27	0
-3	1567	28	0
-2	1207	29	0
-1	775	30	1
0	439	31	0

c. Histogram listing

Original Imagery

LARS Run #	Channel	Spectral Band	Area
73124700	4	0.8 - 1.1 μm	Line(55,165),Column(355,465)
73124700	20	0.8 - 1.1 μm	Line(55,165),Column(354,464)

Figure 5-2. Difference image with single mode probability density function.

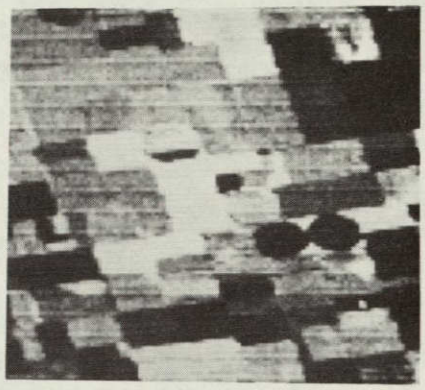

a. Difference Image

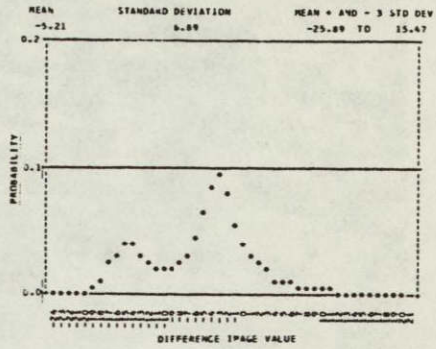

b. Probability density function

VALUE	NUMBER POINTS	VALUE	NUMBER POINTS
-24	1	-2	1002
-23	2	-1	721
-22	1	0	503
-21	19	1	377
-20	51	2	321
-19	92	3	260
-18	179	4	172
-17	314	5	155
-16	376	6	127
-15	498	7	123
-14	501	8	111
-13	416	9	86
-12	344	10	92
-11	282	11	71
-10	261	12	57
-9	297	13	35
-8	350	14	16
-7	416	15	10
-6	569	16	3
-5	839	17	4
-4	1084	18	7
-3	1172	19	2

c. Histogram listing

Original Imagery

LARS Run #	Channel	Spectral Band	Area
73064000	4	0.8 - 1.1 μm	Line(161,271),Column(325,435)
74024200	4	0.8 - 1.1 μm	Line(262,372),Column(272,382)

Figure 5-3. Difference image with dual mode probability density function.

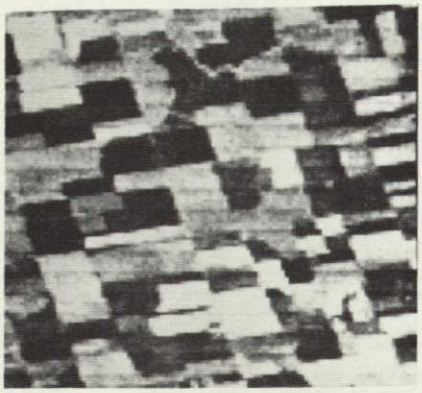

a. Difference Image

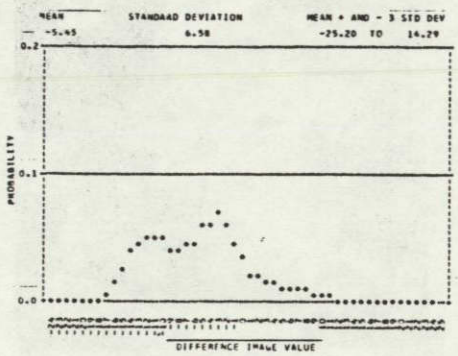

b. Probability density function

VALUE	NUMBER POINTS	VALUE	NUMBER POINTS
-24	1	0	447
-23	4	1	289
-22	5	2	226
-21	9	3	185
-20	6	4	195
-19	30	5	161
-18	60	6	177
-17	113	7	166
-16	200	8	125
-15	365	9	95
-14	503	10	90
-13	616	11	62
-12	633	12	59
-11	643	13	32
-10	629	14	17
-9	549	15	7
-8	551	16	5
-7	577	17	4
-6	612	18	0
-5	774	19	3
-4	795	20	5
-3	879	21	4
-2	798	22	2
-1	577	23	1

c. Histogram listing

Original Imagery

LARS Run #	Channel	Spectral Band	Area
73064000	4	0.8 - 1.1 μm	Line(350,460),Column(249,359)
74024200	4	0.8 - 1.1 μm	Line(450,560),Column(195,305)

Figure 5-4. Difference image with nondistinct dual mode probability density function.

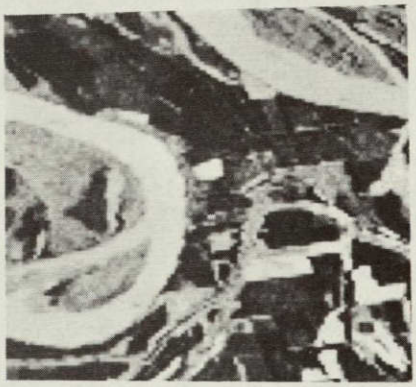

a. Difference Image

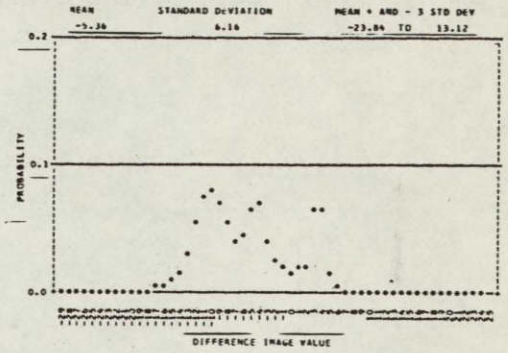

b. Probability density function

VALUE	NUMBER POINTS	VALUE	NUMBER POINTS
-29	1	-2	328
-28	0	-1	287
-27	5	0	242
-26	3	1	261
-25	6	2	277
-24	3	3	835
-23	6	4	840
-22	6	5	245
-21	11	6	86
-20	13	7	61
-19	19	8	34
-18	50	9	16
-17	76	10	21
-16	100	11	12
-15	129	12	5
-14	239	13	5
-13	406	14	3
-12	715	15	6
-11	951	16	3
-10	994	17	3
-9	870	18	3
-8	735	19	3
-7	536	20	3
-6	408	21	2
-5	841	22	4
-4	864	23	1
-3	548	24	0

c. Histogram listing

Original Imagery

LARS Run #	Channel	Spectral Band	Area
72033804	4	0.8 - 1.1 μm	Line(545,655),Column(945,1055)
72033804	8	0.8 - 1.1 μm	Line(545,655),Column(945,1055)

Figure 5-5. Difference image with multimodal probability density function.

equation form for the density function, this indicates that the mean of the noise for each of the classes is the same, i.e.,

$$p_D(x) = \Sigma \Pr[D_i] \frac{1}{\sqrt{2\pi}\,\sigma_i} \exp\left\{-\frac{(x-\mu)^2}{2\sigma_i^2}\right. \tag{5-7}$$

Observe that while the field structure of the scene is visible, there is little differentiability between the fields in terms of the gray level representation of each. It is this non-uniqueness of the gray level intervals for each class that yields the single mode probability density function.

Figure 5-3 illustrates the situation where the density function is dual modal. This type of density function is indicated in the difference image by the predominance of essentially two gray levels. Also note that the difference image contains the field structure of the scene, which supports the hypothesis that the temporal change is somewhat class dependent.

Figures 5-4 and 5-5 contain other examples of the types of density functions encountered. A multimodal example is presented in Figure 5-4, and Figure 5-5 illustrates a case in which the modes are not separated.

Although each of these examples differs in the type of density function observed, they all have a common factor. The basic field structure of each of the scenes is still intact in the difference images. The conclusion one may draw from this observation is that the temporal changes are dependent in part upon the different classes within the scene.

5.2. Autocorrelation Function of the Temporal Changes

In the earlier analysis (Chapter 2) it was found that a suitable model of the autocorrelation function was required in the derivation of a registration processor. Both approaches to the problem necessitated knowledge of this nature. The probabilistic approach based upon the premise of normally distributed noise inherently requires a model of the autocorrelation function simply by the functional form of the probability density function.

$$p_{\underline{n}}(\underline{n}) = \frac{1}{(2\pi)^{N/2}|\underline{\Lambda}|^{1/2}} \exp\{-\frac{1}{2}\underline{n}^T\underline{\Lambda}^{-1}\underline{n}\} \qquad (5\text{-}8)$$

$\underline{n}$ = noise; assumed zero mean here

$\underline{\Lambda}$ = autocorrelation function (matrix) of the noise

Note that the autocorrelation matrix and autocovariance matrix are the same for zero mean noise.

One also comes across the need for an autocorrelation function model while approaching the registration problem via the second method. The basic design criterion utilized in this approach is that the processor be a linear filter which yields a maximum output at the correct registration position in the absence of noise. In order to obtain the compact expression for the variance of the registration error, i.e., as the reciprocal of the output signal-to-noise ratio times the square of the effective bandwidth (Equations 2-46 and 2-47), a particular form for the processing filter was chosen, the matched filter, which maximizes the output signal-to-noise ratio (Equation 2-36). When one examines the expression for this type of filter in the frequency domain, one finds that it depends upon the reciprocal of the spectral density function of the noise which is determined uniquely by the autocorrelation function of the noise.

Therefore, one again finds that knowledge of the autocorrelation function of the noise is essential.

Determination of an approximate functional form for the autocorrelation function was carried out by experimentally estimating the autocorrelation functions of the series of difference images which were generated for the probability density function estimates (cf. Table 5-1 for the areas used). Since the noise is modeled as being additive, it is just the difference between two registered images. The following expression was used to estimate the autocorrelation functions. Note that it is an asymptotically unbiased estimator.

$$R_{\ell,k} = \frac{1}{N^2} \sum_{i=1}^{N-\ell} \sum_{j=1}^{N-k} (x_{ij} - \bar{x})(x_{i+\ell,j+k} - \bar{x}) \qquad (5\text{-}9)$$

$$\ell = 0, 1, \ldots, L$$

$$k = 0, 1, \ldots, K$$

Where,

$R_{\ell,k}$ = autocorrelation function estimate at shift (ℓ,k)

$x_{i,j}$ = (i,j) th element of the difference image

$\bar{x}$ = mean of the difference image

L,K = maximum shift along the lines and columns respectively

N^2 = number of data samples in the difference image.

The results obtained are best illustrated by viewing several examples of the estimated autocorrelation surfaces. Figures 5-6a through 5-11a contain several different surface estimates. The sample image size chosen is 111 lines by 111 columns with a maximum shift of 16 lines or columns. The amplitude of the surface is represented on a normalized scale, where zero on the scale corresponds to a value of zero for the autocorrelation function estimate, and the scale increment is $100/\max|R_{\ell,k}|$.

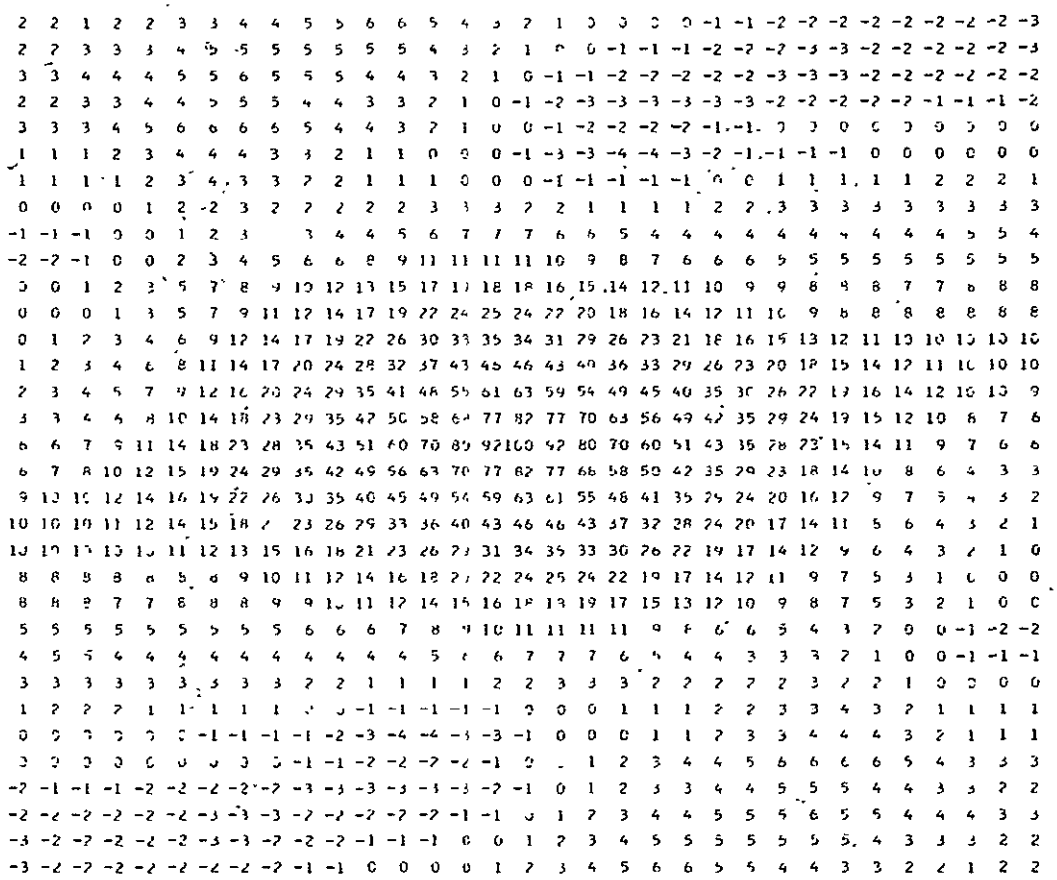

	NORMALIZED SCALE	ACTUAL VALUE		SHIFT POSITION (LINE,COLUMN)
MAXIMUM =	10	41.301	AT	(0, 0)
MINIMUM =	-4	-2.508		(11, -3)

SCALE CONVERSION - 1 UNIT NORMALIZED SCALE = 0.618 UNITS ACTUAL SCALE
0 ON NORMALIZED SCALE = 0 ON ACTUAL SCALE

Original Imagery

LARS Run #	Channel	Spectral Band	Area
73046000	4	0.8 - 1.1 μm	Line(56,166),Column(390,500)
73064000	4	0.8 - 1.1 μm	Line(61,171),Column(334,444)

Figure 5-6a. Difference image autocorrelation surface.

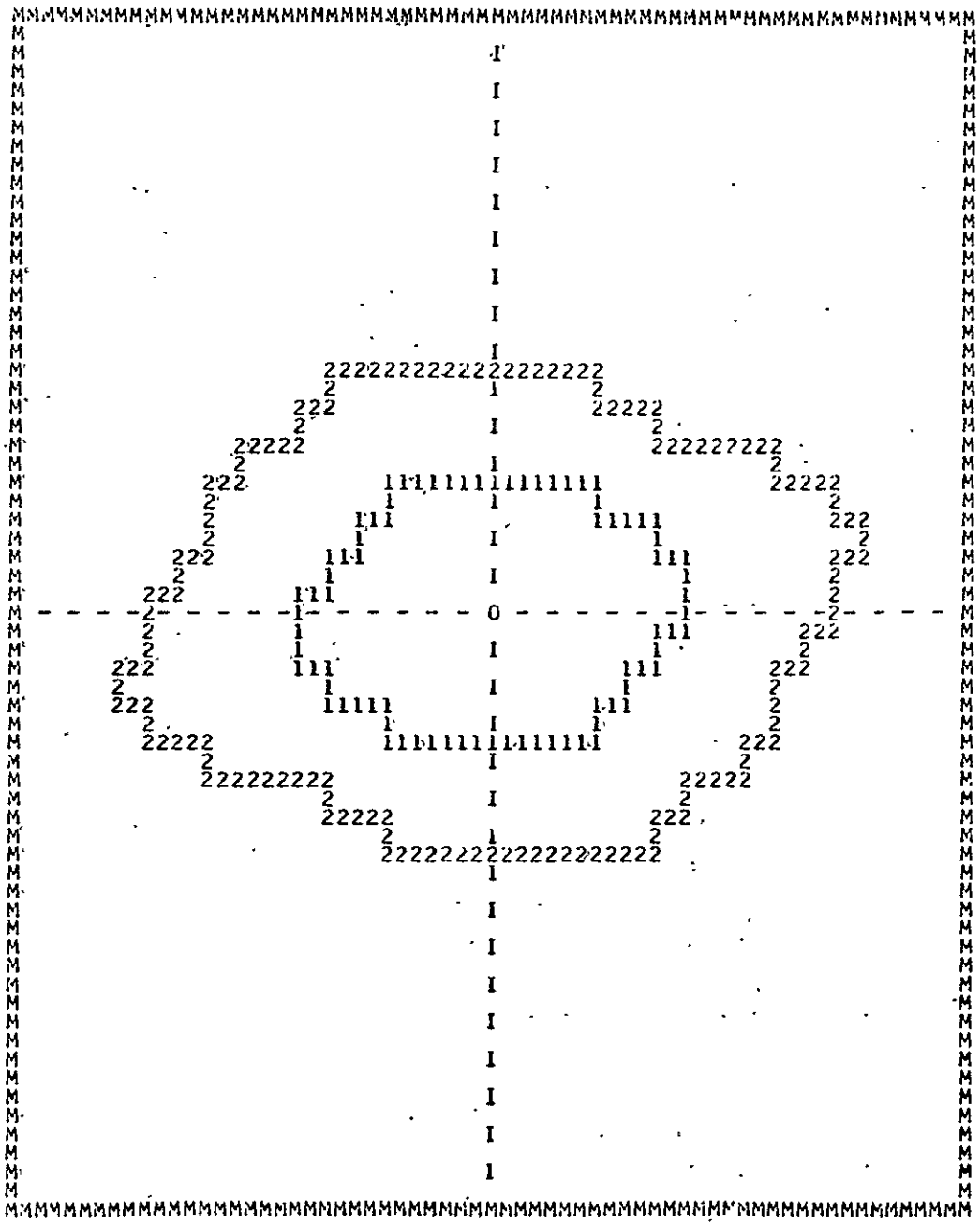

Figure 5-6b. Difference image autocorrelation surface contour.

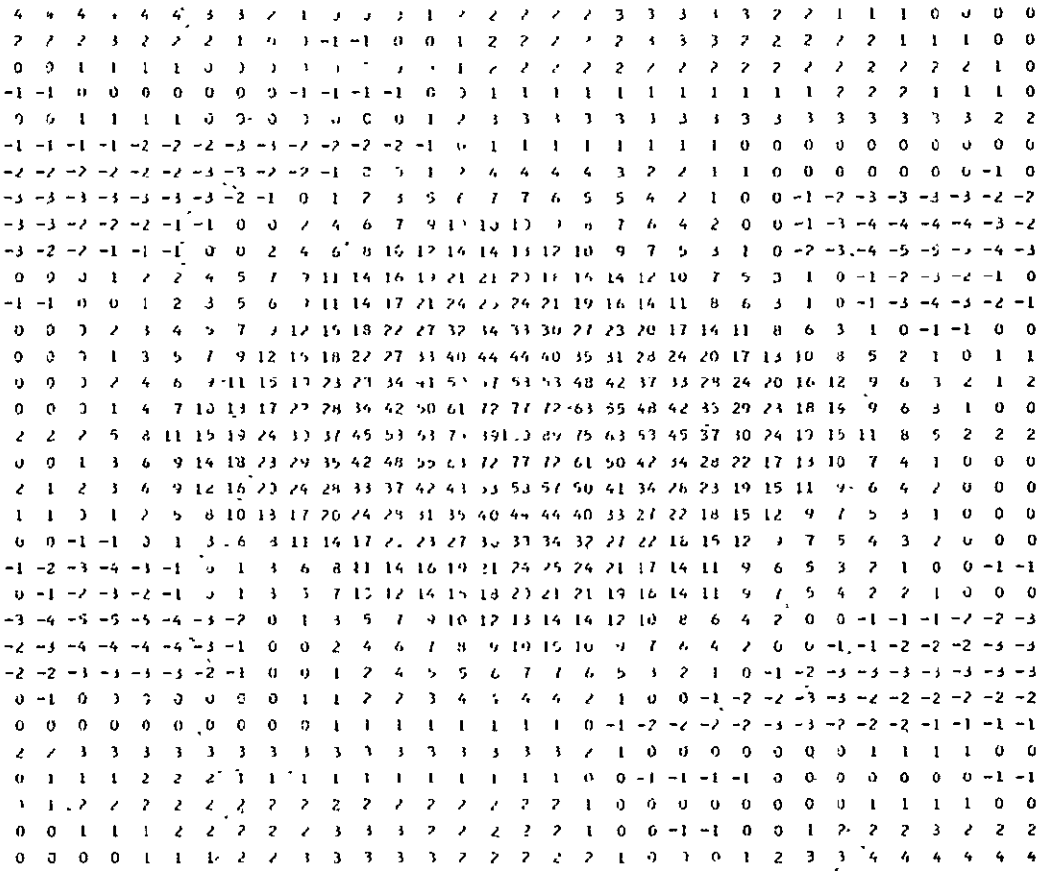

	NORMALIZED SCALE	ACTUAL VALUE		SHIFT POSITION (LINE,COLUMN)
MAXIMUM =	100	41.023	AT	(0, 0)
MINIMUM =	-5	-2.368		(7,-12)

SCALE CONVERSION = 1 UNIT NORMALIZED SCALE = 0.413 UNITS ACTUAL SCALE
0 ON NORMALIZED SCALE = 0 ON ACTUAL SCALE

Original Imagery

LARS Run #	Channel	Spectral Band	Area
73046000	4	0.8 - 1.1 μm	Line(61,171),Column(515,625)
73064000	4	0.8 - 1.1 μm	Line(66,176),Column(459,569)

Figure 5-7a. Difference image autocorrelation surface.

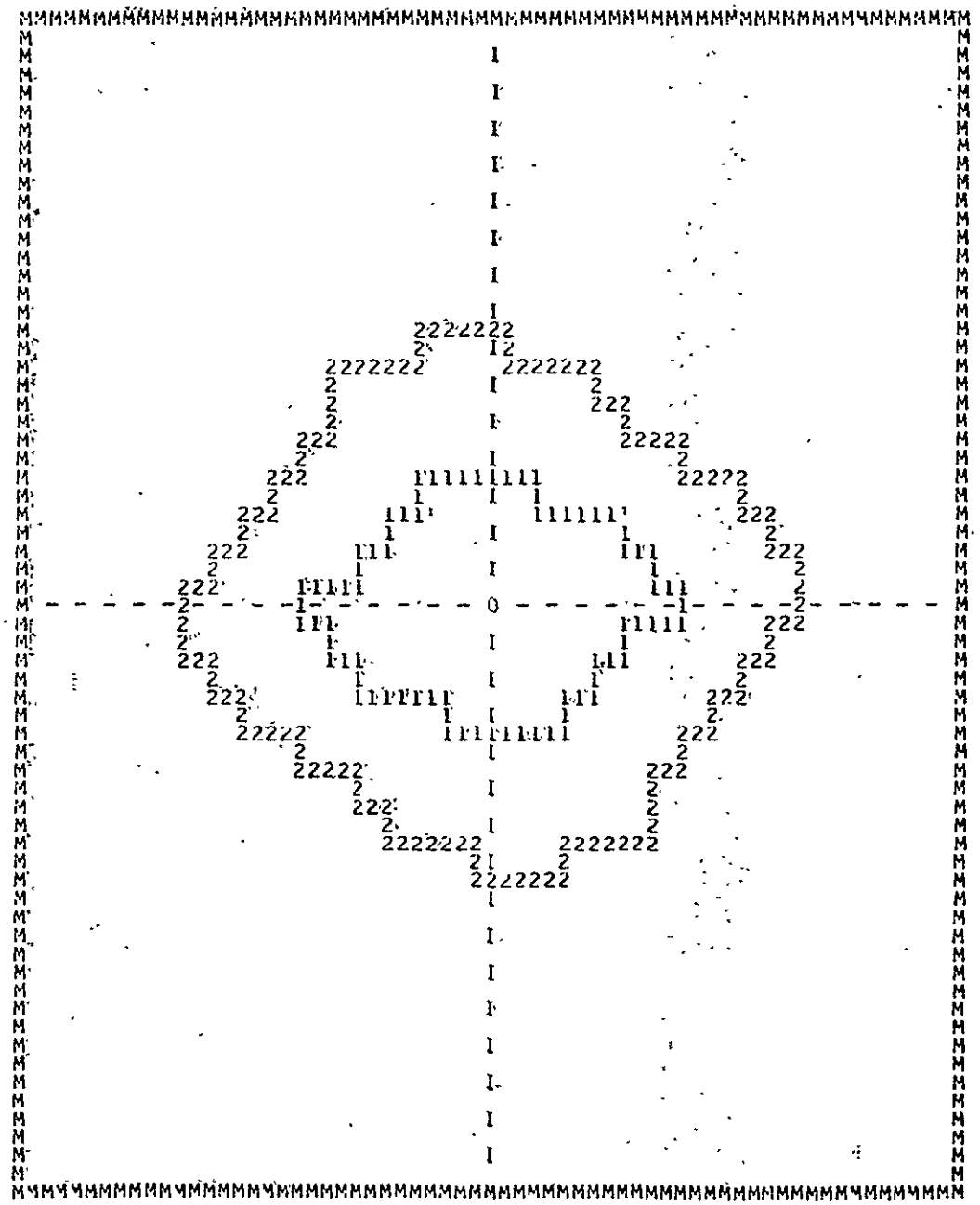

Figure 5-7b. Difference image autocorrelation surface contour.

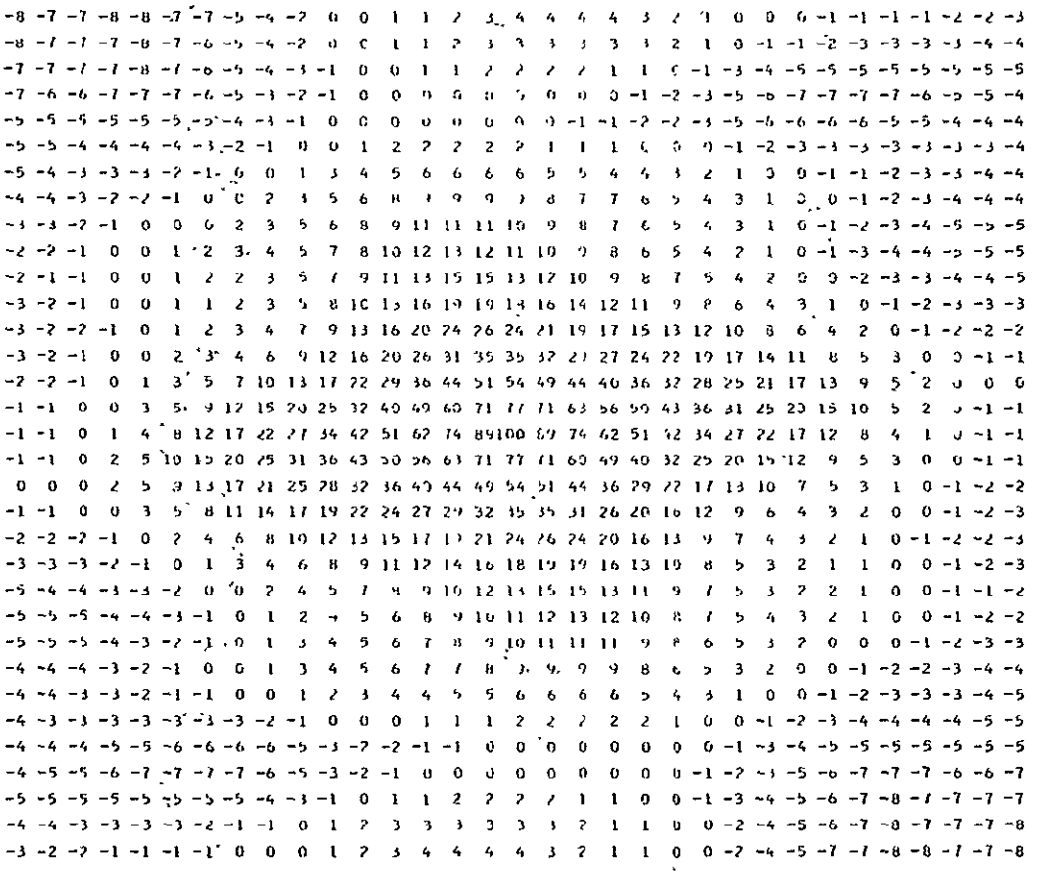

	NORMALIZED SCALE	ACTUAL VALUE		SHIFT POSITION (LINE,COLUMN)
MAXIMUM =	100	39.628	AT	(0, 0)
MINIMUM =	-8	-2.950		(14, 121)

SCALE CONVERSION - 1 UNIT NORMALIZED SCALE = 0.356 UNITS ACTUAL SCALE
0 ON NORMALIZED SCALE = 0 ON ACTUAL SCALE

Original Imagery

LARS Run #	Channel	Spectral Band	Area
73046000	4	0.8 - 1.1 μm	Line(345,455),Column(305,415)
74024100	4	0.8 - 1.1 μm	Line(531,641),Column(253,363)

Figure 5-8a. Difference image autocorrelation surface.

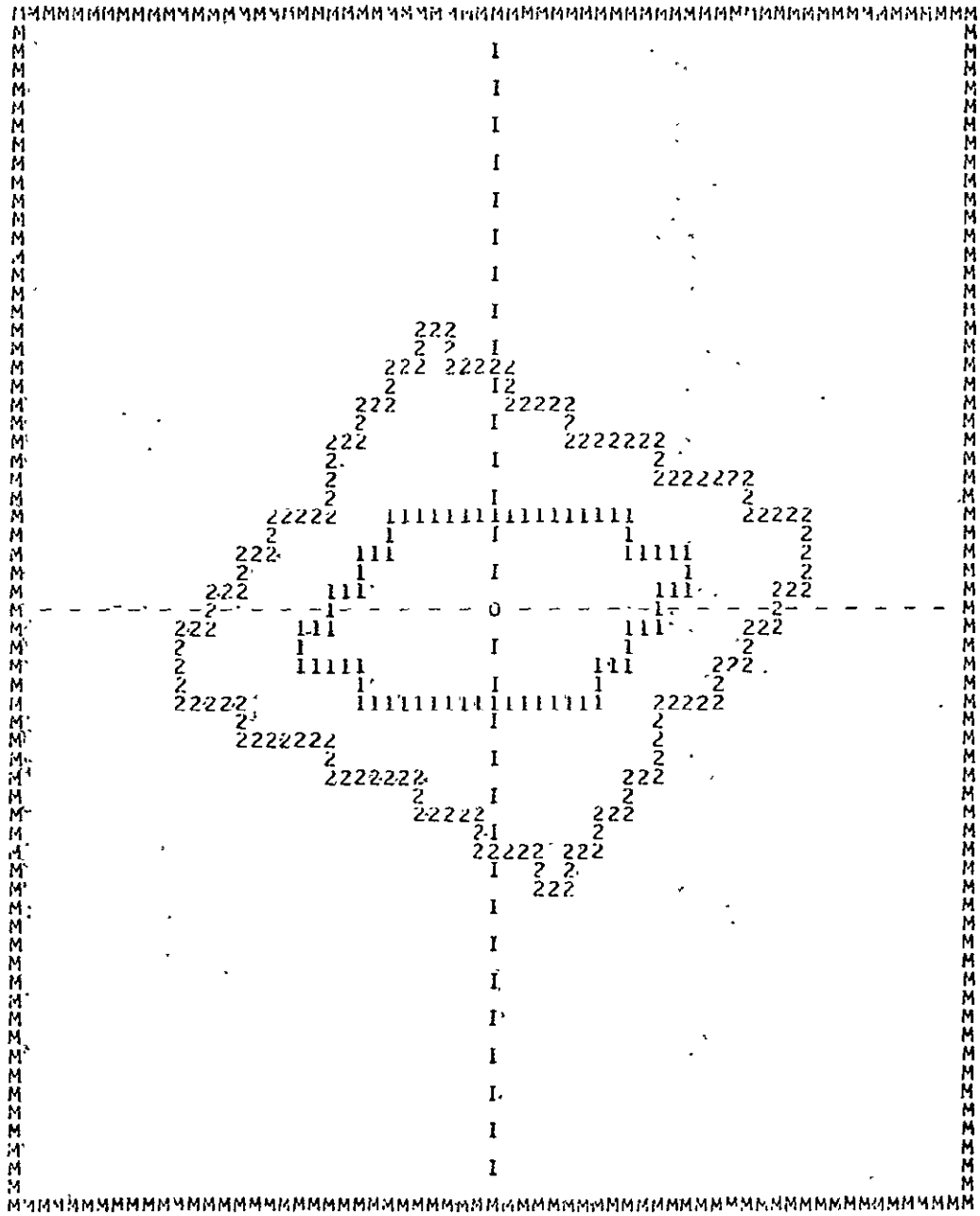

Figure 5-8b. Difference image autocorrelation surface contour.

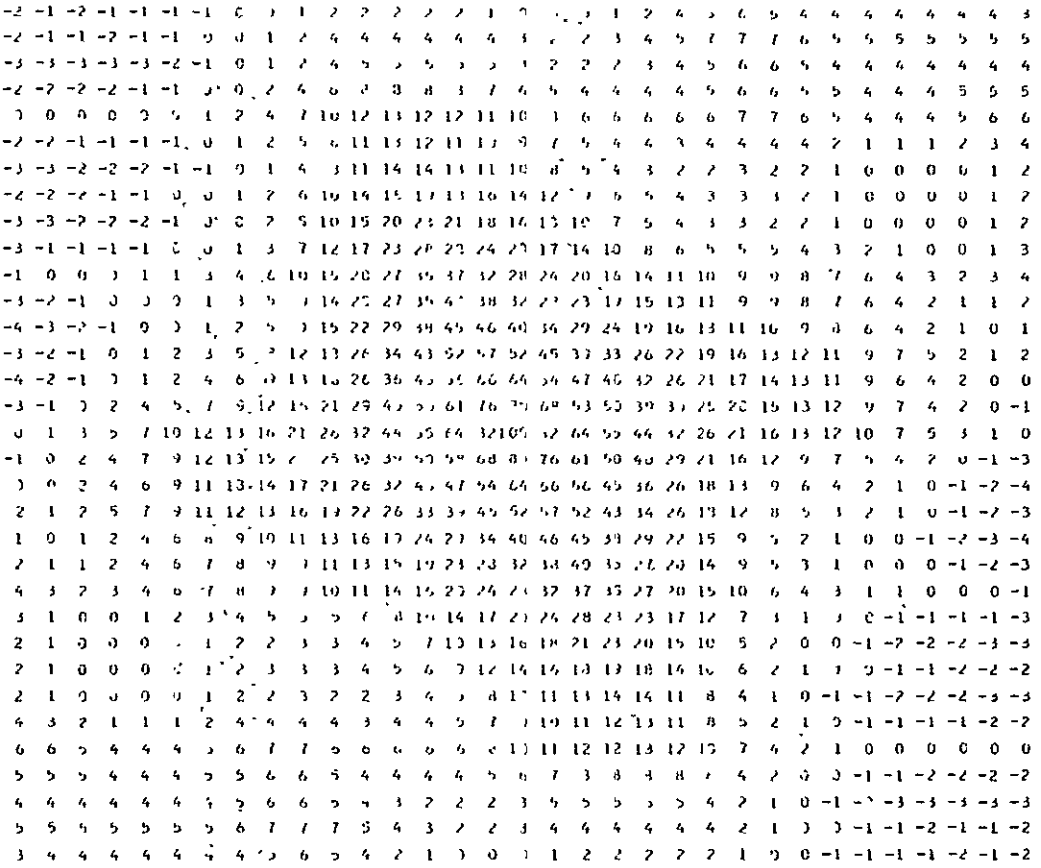

	NORMALIZED SCALE	ACTUAL VALUE		SHIFT POSITION (LINE,COLUMN)
MAXIMUM =	10	13.511	AT	(0, 0)
MINIMUM =	-4	-0.400		(2, 16)

SCALE CONVERSION - 1 UNIT NORMALIZED SCALE = 0.136 UNITS ACTUAL SCALE
0 ON NORMALIZED SCALE = 0 ON ACTUAL SCALE

Original Imagery

LARS Run #	Channel	Spectral Band	Area
73124700	4	0.8 - 1.1 μm	Line(55,165),Column(355,465)
73124700	8	0.8 - 1.1 μm	Line(55,165),Column(355,465)

Figure 5-9a. Difference image autocorrelation surface.

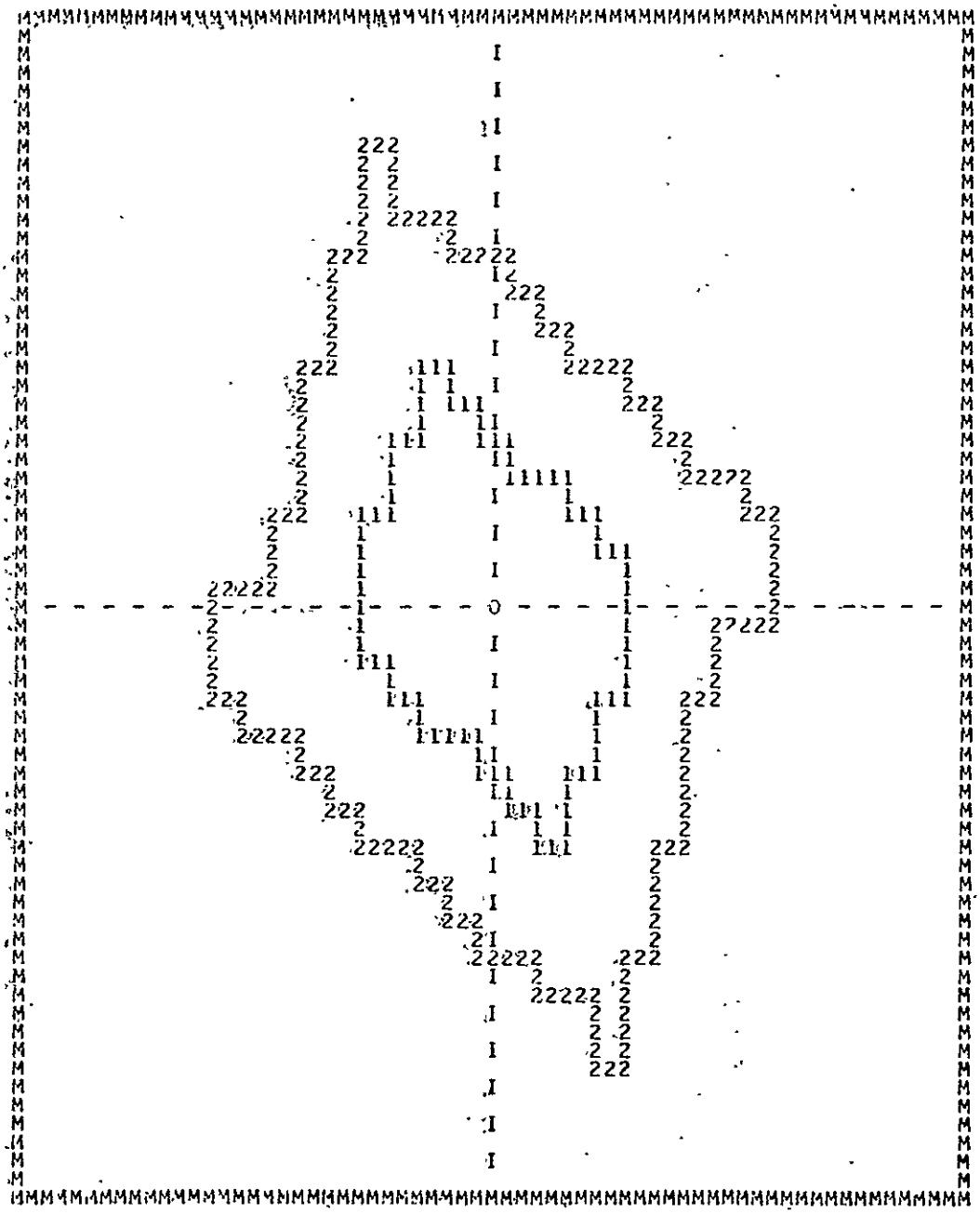

Figure 5-9b. Difference image autocorrelation surface contour.

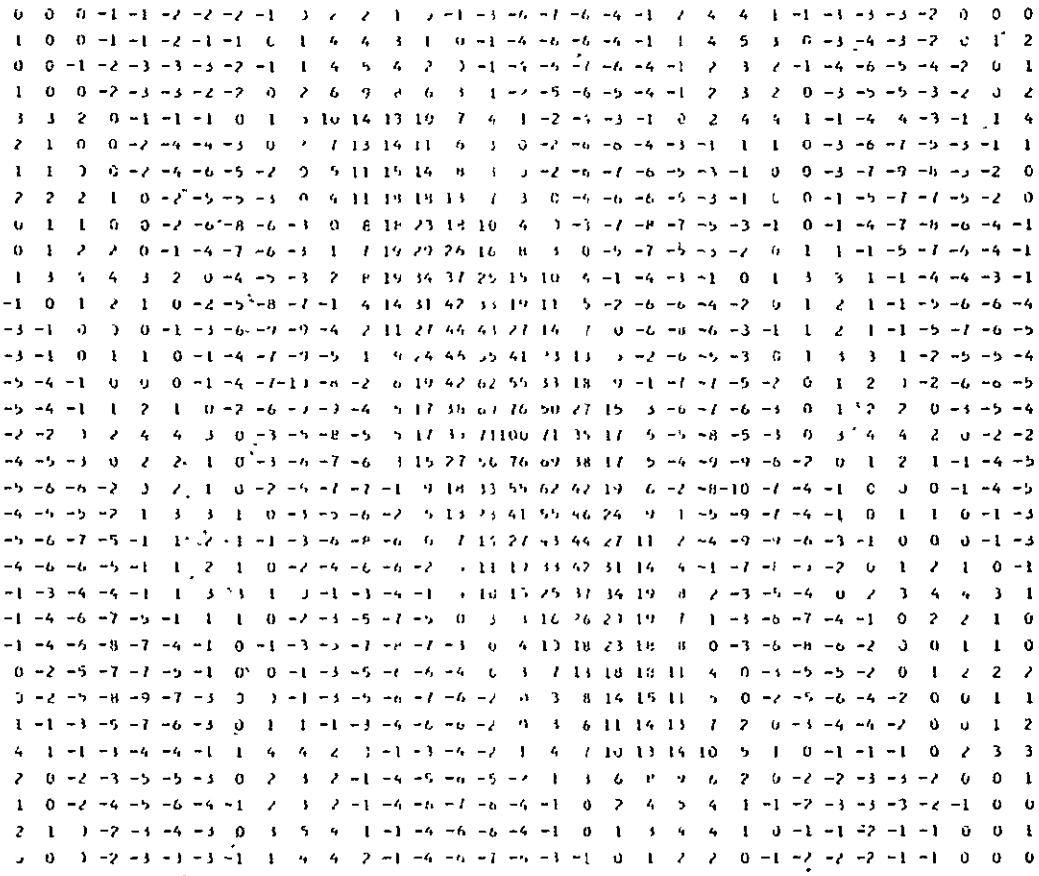

	NORMALIZED SCALE	ACTUAL VALUE		SHIFT POSITION (LINE,COLUMN)
MAXIMUM =	100	16.621	AT	(0, 0)
MINIMUM =	-13	-1.734		(2, 7)

SCALE CONVERSION = 1 UNIT NORMALIZED SCALE = 0.166 UNITS ACTUAL SCALE
0 0% NORMALIZED SCALE = 5 0% ACTUAL SCALE

Original Imagery

LARS Run #	Channel	Spectral Band	Area
73124700	20	0.8 - 1.1 μm	Line(55,165),Column(355,465)
73124700	8	0.8 - 1.1 μm	Line(55,165),Column(357,467)

Figure 5-10a. Difference image autocorrelation surface.

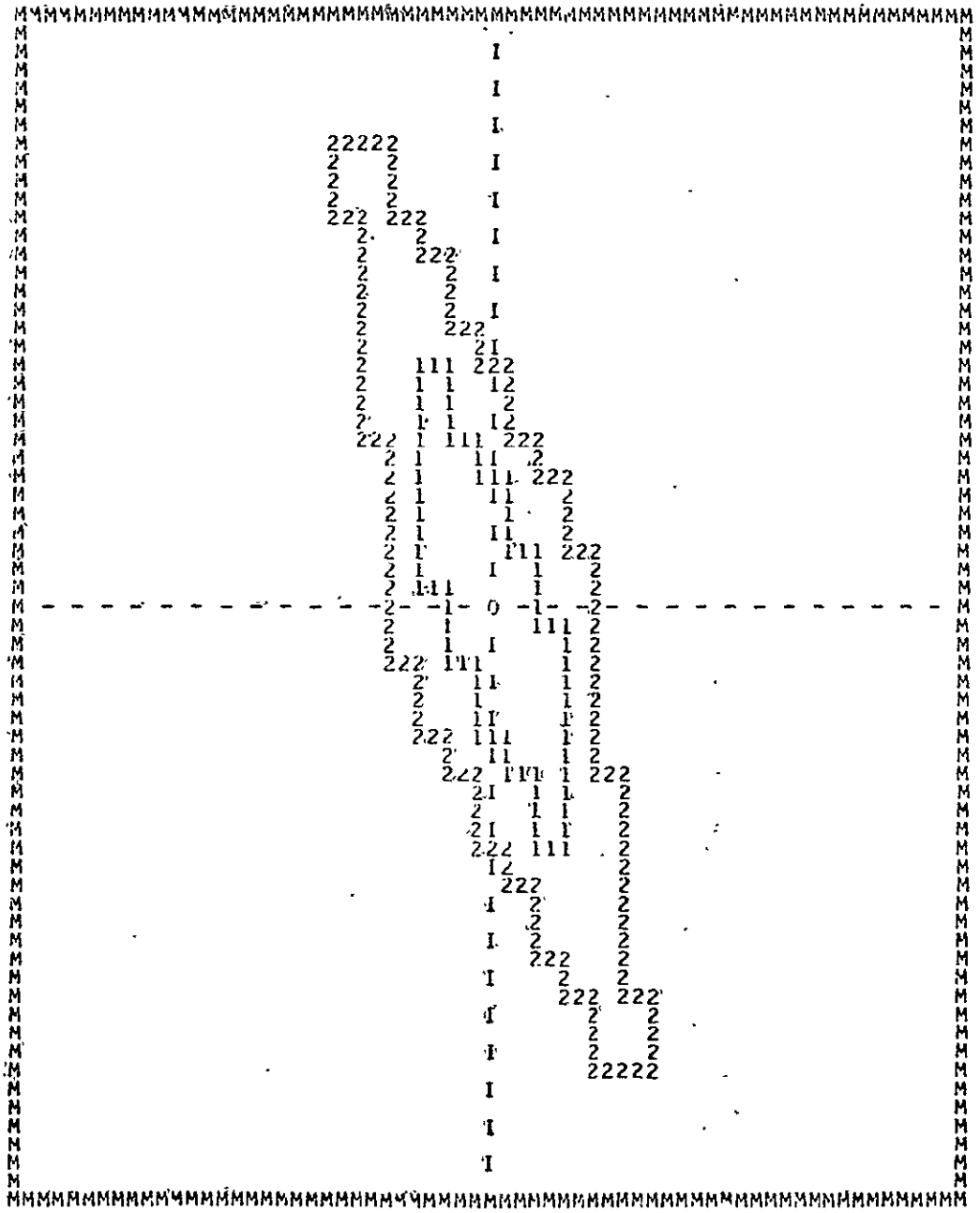

Figure 5-10b. Difference image autocorrelation surface contour.

```
-2 -2 -2 -1 -1 -1  0  0  0  0 -1 -1 -1 -1 -1 -3 -4 -5 -4 -5 -5 -5 -6 -7 -7 -7 -7 -6 -4 -3 -3 -3 -3
-2 -2 -2 -1 -1  0  0  0  0  0  0  0  0 -1 -2 -3 -4 -4 -4 -4 -4 -5 -6 -7 -7 -7 -6 -4 -3 -2 -2 -2
-2 -2 -1 -1  0  0 -1  0  0  0  0  0  0 -1 -2 -3 -4 -4 -4 -4 -4 -4 -5 -6 -6 -6 -5 -4 -2 -1 -1 -1
-1 -1 -1  0  0  0  0  0  0  1  1  2  1  0  0 -1 -2 -2 -2 -2 -3 -3 -4 -5 -6 -5 -6 -5 -3 -2 -1 -1
 0  0  1  2  2  3  2  1  1  2  2  3  4  3  3  2  1  0  0  0  0 -1 -2 -3 -4 -4 -3 -3 -4 -2  0  0  0
 0  0  1  2  2  2  2  2  2  2  3  3  4  4  4  3  3  1  0  0 -1 -1 -2 -3 -3 -3 -2 -2 -3 -2 -1 -1 -1
 0  1  2  3  3  3  3  4  4  4  4  4  5  5  5  4  3  2  0 -1 -2 -2 -3 -3 -4 -3 -3 -2 -2 -3 -2 -1  0
 0  1  3  3  4  3  3  3  3  3  4  5  5  6  6  4  3  2  1 -1 -2 -2 -2 -2 -3 -3 -2 -2 -2 -3 -3 -2 -2
 0  1  2  2  3  3  3  3  2  2  3  4  5  5  6  5  4  2  0 -1 -2 -2 -2 -2 -2 -3 -3 -3 -3 -3 -4 -3 -3
 0  1  2  3  3  3  3  2  2  2  3  4  5  7  7  6  4  3  1  0  0 -1 -1 -2 -3 -3 -4 -4 -4 -4 -4 -4 -4
 2  1  2  4  4  4  4  4  3  3  4  5  7  9 11  9  8  6  4  3  2  1  1  0  0  0 -1 -1 -1 -2 -3 -3 -3
 1  1  2  3  3  2  2  2  2  3  4  5  7  9 12 11 10  8  6  4  3  3  2  1  0  0 -1 -1 -2 -2 -2 -2 -1
 0  1  2  3  2  1  0  1  2  3  5  7  9 13 16 16 15 13 11  9  7  6  4  3  2  1  0  0 -1 -2 -1  0  0
 0  1  2  2  1  0  0  1  3  5  8 11 14 18 23 26 24 22 18 15 12 10  8  6  5  4  1  0  0 -1 -1  0  0
 0  0  2  2  2  1  1  2  4  7 10 14 19 25 32 40 41 35 28 24 20 17 13 11  9  7  4  2  0  0  0  0  0
 0  0  1  2  2  3  3  5  6 10 14 19 24 31 42 57 65 53 42 35 29 24 18 14 11  9  7  4  2  0  0  0  0
 1  2  2  2  4  5  7  8 13 14 18 24 31 41 54 78100 78 54 41 31 24 18 14 10  8  7  5  4  2  2  2  1
 0  0  0  0  2  4  7  9 11 14 18 24 29 35 42 53 63 57 42 31 24 18 14 10  6  5  3  3  2  2  1  0  0
 0  0  0  0  0  2  4  7  9 11 13 17 20 24 28 35 41 40 32 25 19 14 10  7  4  2  1  1  2  2  2  0  0
 0  0 -1 -1  0  0  1  4  5  6  8 10 12 15 18 22 26 26 23 18 14 11  8  5  3  1  0  0  1  2  2  1  0
 0  0 -1 -2 -1  0  0  1  2  3  4  6  7  9 11 13 15 16 16 13  9  7  5  3  2  1  0  1  2  3  2  1  0
-1 -2 -2 -2 -2 -1 -1  0  0  1  2  3  5  4  6  8 10 11 12  9  7  5  4  3  2  2  2  2  3  3  2  1  1
-3 -3 -3 -2 -1 -1 -1  0  0  0  1  1  2  3  4  6  8  9 11  9  7  5  4  3  3  4  4  4  4  4  2  1  2
-4 -4 -4 -4 -4 -4 -3 -3 -2 -1 -1  0  0  0  1  3  4  6  7  7  5  4  3  2  2  2  3  3  3  3  2  1  0
-3 -3 -4 -3 -3 -3 -3 -3 -2 -2 -2 -2 -2 -1  0  2  4  5  6  5  5  4  3  2  2  3  3  3  3  2  2  1  0
-2 -2 -3 -3 -2 -2 -2 -3 -3 -2 -2 -2 -2 -1  1  2  3  4  6  6  5  5  4  3  3  3  3  3  4  3  3  1  0
 0 -1 -2 -3 -2 -2 -3 -3 -4 -3 -3 -2 -2 -1  0  2  3  4  5  5  5  4  4  4  4  4  3  3  3  3  2  1  0
-1 -1 -1 -2 -3 -2 -2 -3 -3 -3 -2 -1 -1  0  0  1  3  3  4  4  4  3  3  2  2  2  2  2  2  2  1  0  0
 0  0  0 -2 -4 -3 -3 -4 -4 -3 -2 -1  0  0  0  0  1  2  3  3  4  3  2  2  1  1  2  3  2  2  1  0  0
-1 -1 -2 -3 -5 -6 -5 -6 -5 -4 -3 -3 -2 -2 -2 -2 -1  0  0  1  2  1  1  0  0  0  0  0  0 -1 -1 -1
-1 -1 -1 -2 -4 -5 -6 -6 -6 -5 -4 -4 -4 -4 -4 -4 -3 -2 -1  0  0  0  0  0  0  0 -1  0  0 -1 -1 -2 -2
-2 -2 -2 -3 -4 -6 -7 -7 -7 -5 -5 -4 -4 -4 -4 -4 -3 -2 -1  0  0  0  0  0  0  0  0  0 -1 -1 -2 -2 -2
-3 -3 -3 -3 -4 -6 -7 -7 -7 -7 -6 -5 -5 -5 -4 -5 -4 -3 -1 -1 -1 -1 -1  0  0  0  0 -1 -1 -1 -2 -2 -2
```

	NORMALIZED SCALE	ACTUAL VALUE		SHIFT POSITION (LINE,COLUMN)
MAXIMUM =	100	25.945	AT	(0, 0)
MINIMUM =	-7	-2.072		(15, -9)

SCALE CONVERSION - 1 UNIT NORMALIZED SCALE = 0.259 UNITS ACTUAL SCALE
0 ON NORMALIZED SCALE = 0 ON ACTUAL SCALE

Original Imagery

LARS Run #	Channel	Spectral Band	Area
72033804	4	0.8 - 1.1 μm	Line(745,855),Column(145,255)
72033804	12	0.8 - 1.1 μm	Line(745,855),Column(145,255)

Figure 5-11a. Difference image autocorrelation surface.

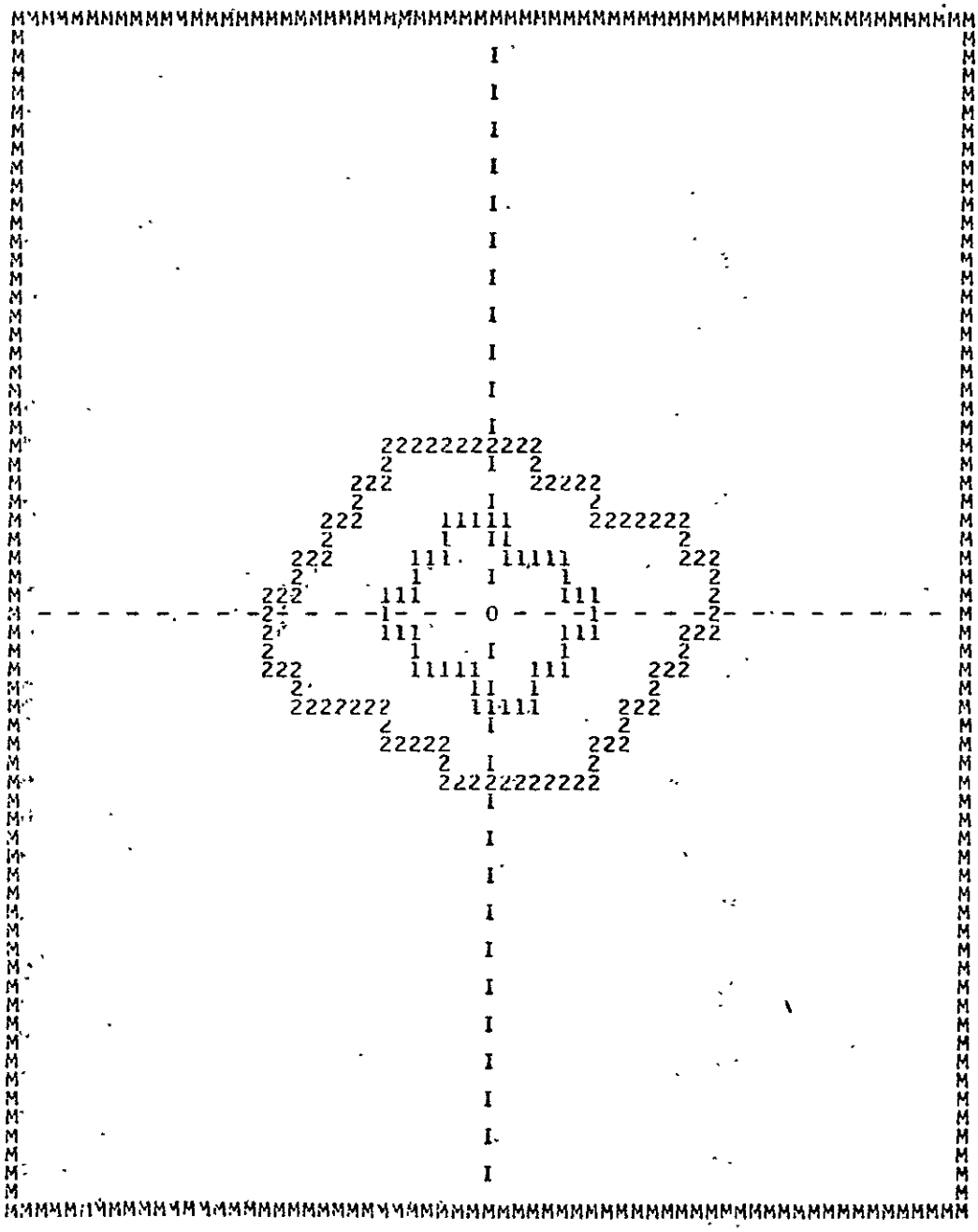

Figure 5-11b. Difference image autocorrelation surface contour.

One may now observe the characteristics of the surfaces. First note that the surfaces are smooth and nonincreasing for shifts around the central peak. A violation of this nonincreasing property occurs only for small values of $R_{\ell,k}$, and may be attributed to the property that the displayed surfaces are only estimates of the actual autocorrelation functions. Furthermore, by close examination, the surfaces appear to be exponential in nature. This last observation is best illustrated by plotting equiamplitude contours for each of the autocorrelation surface estimates. Figures 5-6b through 5-11b contain such equiamplitude contours for the corresponding surfaces, where the contour levels have been chosen at $R_{o,o}$, $R_{o,o}e^{-1}$, and $R_{o,o}e^{-2}$.

This particular choice of contours levels in terms of an exponentially decreasing function was prompted by the initial observation that the surfaces seemed to be exponential in form. Confirmation of this exponential property is achieved if the radial increment of the contours for each surface is a constant. From examination of these surface contours, it is seen that the radial increments are indeed approximately constant for each surface, so that the noise autocorrelation function is exponential in nature.

Now that one may reasonably model the autocorrelation surface of the temporal changes as exponential in form, one can use this model for the design of a registration processor. An example of an optimum processor based on an exponential autocorrelation function for the noise was given in Chapter 3. The reason for inclusion of this particular example in the previous chapter is now clear. It was in anticipation of the experimental observations that the example was chosen. It was presented in

the context of illustrating the method by which one solves for the processor based upon the noise autocorrelation characteristics. However, the example is directly applicable to the practical situation where an autocorrelation function of an exponential nature is actually observed.

Before applying the technique of the example to the experimentally determined autocorrelation surfaces, it is necessary to carry out an additional step. The example presumed the following functional form for the autocorrelation surface.

$$R(\tau_x,\tau_y) = A^2 e^{-\alpha|\tau_x| - \beta|\tau_y|} \qquad (5\text{-}10)$$

Note that this requires the major axes of the correlation surface to coincide with the x and y coordinate axes. Unfortunately, the experimentally observed surfaces do not comply with this assumption. However, this discrepancy is remedied quite easily by providing a linear spatial transformation to the correlation surface to adjust the major axes so that they are aligned with the x and y coordinate axes, solving for the filter function as is done in the example, and then applying the inverse of the linear spatial transformation to return to the original coordinate system. Again referring to the example solution (Equations 3-31 to 3-33), one finds that the prewhitening operation becomes a derivative type operator. This result suggests that the performance of the registration processor may be improved by first preprocessing the imagery via a derivative type operator followed by a crosscorrelation operation instead of just cross-correlating the imagery directly. The experimental study discussed in the next chapter supports this hypothesis, where it is found that preprocessing the imagery via a gradient type operator (which is a derivative operation) does increase the reliability of the registration processor.

CHAPTER 6

EXPERIMENTAL INVESTIGATION OF SIMILARITY MEASURES AND PREPROCESSING METHODS USED FOR IMAGE REGISTRATION

6.1. Introduction

The study described in this chapter is the experimental examination of several different processors designed to overlay digital imagery (a more detailed discussion of this study is presented in [35]). The impetus for such an investigation was provided by the development of several different registration algorithms that had evolved and been tested independently of one another [1, 2, 3, 8, 9, 11, 30], thus leaving the potential user at a loss to objectively compare the different methods. This study is designed to allay this problem of choice by an experimental comparison of the basic techniques used in each of these algorithms to spatially match two temporally differing images. The approach taken is to record the performance of each of the techniques over a series of selected test sites where multitemporal imagery was readily accessible. In this way a quantitative measure of the performance of the various algorithms on a comparative basis would be made available.

The images used in this investigation were taken by the LANDSAT I satellite multispectral scanner which operates in four spectral bands: 0.5-0.6 μm, 0.6-0.7 μm, 0.7-0.8 μm, and 0.8-1.1 μm. Orbiting at an altitute of about 600 miles, the recorded data samples have a resolution of approximately 50 meters along the scanner sweep by 80 meters along

the satellite's path, so that a full frame consisting of about 2340 lines by 3240 columns covers an area of about 100 by 100 miles. Multitemporal coverage of the same area is accomplished by the orbital path of the satellite which cyclically repeats itself about every 18 days.

Figures 6-1 through 6-4 contain several examples of multitemporal images over the same area. The images have been chosen from the general test site areas used in this investigation and are typical of those utilized for the experimental analysis. All of these pictures were taken by the LANDSAT I multispectral scanner and are in the 0.8-1.1 μm spectral band. Figure 6-1 shows two images over Tippecanoe County, Indiana, which were taken in September and November of 1972. A scene from Hill County, Montana over two times during the spring and summer seasons is pictured in Figure 6-2. An example of an area over a year's span is illustrated in Figure 6-3 where data over western Kansas is shown for July of 1973 and 1974. And two temporal differing data sets over Missouri are shown in Figure 6-4. Notice that in all of the examples the areas for each time pair are recognizable as the same, however, changes that have occurred are evident. Also observe that the spatial scale of both images in each time pair appears to be the same, with little relative distortion. This property of the images is derived from the stability of the satellite viewing platform which incurs minimal perturbations in its orbit. Such small fluctuations in scanner position over an area from one time to the next provides the approximate spatial congruence between the temporally differing images.

This investigative comparison experimentally explores the basic concepts which underlie these algorithms to provide an objective way of judging the performance of the different registration processors. All

9/30/72		11/29/72	
LARS Run #	Spectral Band	Lines	Columns
72053603	0.8 - 1.1 μm	(500,750)	(575,825)

Figure 6-1. LANDSAT I imagery over Tippecanoe County, Indiana.

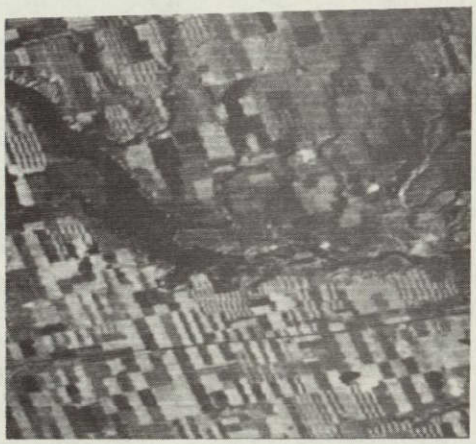

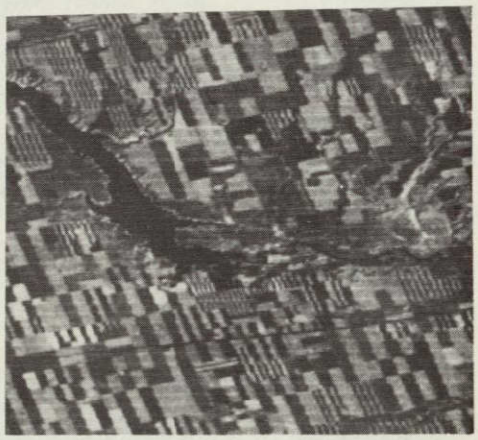

5/5/73		7/16/73	
LARS Run #	Spectral Band	Lines	Columns
73124700	0.8 - 1.1 μm	(110,360)	(110,360)

Figure 6-2. LANDSAT I imagery over Hill County, Montana.

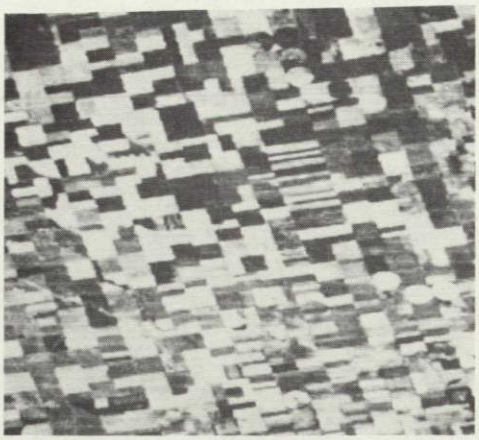

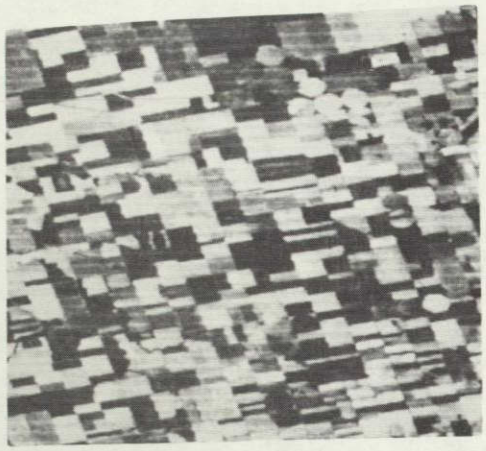

	7/6/73		7/1/74	
LARS Run #	Date Data Taken	Spectral Band	Lines	Columns
73046000	7/6/73	0.8 - 1.1 μm	(175,425)	(275,525)
74024200	7/1/74	0.8 - 1.1 μm	(275,525)	(175,425)

Figure 6-3. LANDSAT I imagery over Kansas.

	8/26/73		10/1/72
LARS Run #	Spectral Band	Lines	Columns
72033804	0.8 - 1.1 μm	(375,625)	(475,725)

Figure 6-4. LANDSAT I imagery over Missouri.

of the algorithms operate in the same fundamental manner. With the minimal relative spatial distortions between temporally differing LANDSAT I images, the first assumption made is that no relative spatial distortions exist for small images. Therefore, registration of these small images requires only an estimation of the relative translation between the images. Given the two images to be overlayed, a search procedure is performed to find this relative translation. One image is shifted about over a larger temporally differing image and a measure of the similarity is computed at each shift position. The translation at which this measure indicates the most similarity is designated as the registration position. This is the fundamental procedure utilized in each of the registration algorithms, however, the different methods depart from one another in the similarity measure employed and the type of images used.

The first part of the study examines the criteria used to measure the similarity between two images. This is an important part of the registration processor since the spatial matching of the imagery requires a quantitative measure of their similarity. Three different similarity measures, which are representative of those used in the algorithms of interest, are evaluated in this investigation. The first is the correlation coefficient which is the measure presently being used in the LARS registration system [1,5]. Second is the sum of the absolute values of differences, the measure utilized in an algorithm which comes under the heading of sequential similarity detection algorithms (SSDA's) [8,9]. Finally the correlation function, an unnormalized version of the correlation coefficient is compared. The expressions for each of these measures are contained in Table 6-1. Note the varying complexity of the computational requirements of each. The correlation coefficient requires

the operations multiplication, division, subtraction, and addition, while the correlation function uses multiplication and addition only. And the sum of the absolute differences requires only subtraction and addition. These computational requirements are reflected in the amount of operational time needed to evaluate each of the measures.

Secondly, preprocessing of the imagery prior to the actual registration and its effect on the overlay results is examined. Several incentives prompted this area of investigation. The first is that of improving the performance of the registration processor, and the second of reducing the operational time and storage allocation needed to implement the overlay algorithms.

Two approaches leading to the same type of preprocessing operation have been suggested for improving the performance of the registration processor over that when the original imagery is used. The first line of reasoning concerns the enhancement of the boundaries of an image. In many types of scenes the basic geometrical structure of the scene is contained in the boundaries (e.g., agricultural scenes or images containing roads). Since registration is a spatial matching of the images, it inherently uses the geometric structure of the scene. Therefore, processing the images via an algorithm which accentuates this geometrical structure prior to overlaying the images intuitively suggests that an improvement is possible. One such method of performing this boundary accentuation is by a gradient type operator. This was the method proposed in several registration algorithms implemented by previous investigators [11,30].

Another approach to the use of preprocessing for performance improvement is presented in Chapters 2, 3, 5 and Appendix A of this investigation.

In Chapter 2 and Appendix A an optimum registration processor is designed utilizing the statistical properties of the temporal changes, which are defined as additive noise in the context of parameter estimation theory. It is shown that use of a matched filter processor both maximizes the output signal-to-noise ratio and minimizes the variance of the registration error. A method for implementing this type of processor is given in Chapter 3 whereby a preprocessing operation (the prewhitening filter) is used. Therefore, this suggests using a preprocessing operation conforming to that which is part of the matched filter processor. From the temporal image statistical properties observed in Chapter 5 and the example given in Chapter 3, it is shown that this preprocessing operation utilizes a derivative type operator which may be approximated by the gradient operator suggested above.

The second type of preprocessing concerns reduction of operational time and storage allocation needed to register two sets of images. This may be achieved by converting the images to a binary format (having intensity level values of only zero or one). In this way a storage savings is realized since each data sample has been converted to one bit of information. Secondly, operational time may be reduced by using logical operations as opposed to arithmetical operations in the computer.

Three types of preprocessing were selected. The first is computing the magnitude of the gradient of the images (equation 6-1). From a visual standpoint this accentuates the boundaries within the images. Plus, it is a derivative type operator which is the optimum preprocessing operation derived in the example in Chapter 3 for temporal changes with an exponential autocorrelation function, the model observed for the temporal changes in Chapter 5. The second preprocessing operation is

thresholding the images at their medians (all values greater than or equal to the median are set equal to one, and all else set equal to zero). Finally, the magnitude of the gradient of the images is computed and then thresholded at an arbitrary level to be determined experimentally. Again this particular choice was made to approximate the preprocessing methods that had been proposed and implemented by other investigators.

6.2. Similarity Measures

An important decision that must be made in carrying out image registration is what criterion should be used to evaluate the similarity between two images. That is, what similarity measure should be selected. The similarity measures being considered can be divided into two general classes. The first class provides a measure on an absolute scale. An example of this is the correlation coefficient which is the similarity measure presently being used in the LARS registration system [1,5]. The values of the correlation coefficient range between plus and minus one. A value of one indicates that the two images are identical or differ by a positive constant factor about their means. A value of minus one indicates that the two images differ by a negative constant factor about their means. When using the correlation coefficient, the registration position is indicated by the maximum of its absolute value which is computed for each of the possible registration locations. It is necessary to consider the absolute value since it is possible that the temporal changes may cause a shift about the mean of the images which would result in a negative value for the correlation coefficient. Another feature of the correlation coefficient is that not only is its scale limited, but its value on that scale gives an indication of how good the images are

Table 6-1: Equations for the correlation coefficient, correlation function, and sum of absolute values of differences similarity measures.

A. Correlation Coefficient, $\rho_{\ell k}$:

$$\rho_{\ell k} = \frac{N^2 \overline{xy}_{\ell k} - \bar{x}\,\bar{y}_{\ell k}}{\{(N^2 \overline{x^2} - \bar{x}^2)(N^2 \overline{y^2}_{\ell k} - \bar{y}^2_{\ell k})\}^{1/2}}$$; correlation coefficient at shift (ℓ,k)

where,

$$\overline{xy}_{\ell k} = \sum_{i=1}^{N} \sum_{j=1}^{N} x_{ij}\, y_{i+\ell,\, j+k}$$

$$\bar{x} = \sum_{i=1}^{N} \sum_{j=1}^{N} x_{ij}$$

$$\bar{y}_{\ell k} = \sum_{i=1}^{N} \sum_{j=1}^{N} y_{i+\ell,\, j+k}$$

$$\overline{x^2} = \sum_{i=1}^{N} \sum_{j=1}^{N} x^2_{ij}$$

$$\overline{y^2}_{\ell k} = \sum_{i=1}^{N} \sum_{j=1}^{N} y^2_{i+\ell,\, j+k}$$

B. Correlation Function, $r_{\ell k}$:

$$r_{\ell k} = \overline{xy}_{\ell k} = \sum_{i=1}^{N} \sum_{j=1}^{N} x_{ij}\, y_{i+\ell,\, j+k}$$; correlation function at shift (ℓ,k)

C. Sum of Absolute Values of Differences, $a_{\ell k}$:

$$a_{\ell k} = \sum_{i=1}^{N} \sum_{j=1}^{N} |x_{ij} - y_{i+\ell,\, j+k}|$$; sum of absolute values of differences at shift (ℓ,k)

linearly related. The expression for the correlation coefficient is given in Table 6-1.

The second class indicates the registration position by a maximum or minimum value at the registration location. Two examples of this are the correlation function, which is an unnormalized version of the correlation coefficient, and the sum of the absolute values of the differences between the two images, the similarity measure used in a registration algorithm which comes under the heading of sequential similarity detection algorithms (SSDA's) [8,9]. The expressions for these similarity measures are listed in Table 6-1. For the correlation function, the registration position is indicated by a maximum or minimum value which is computed for each of the possible overlay locations. For the sum of the absolute differences measure the registration position is indicated by a minimum value. In these examples there is no absolute scale, so that the value of this maximum or minimum by itself will not give a good indication of how closely the two images match. The exception to this occurs in the absolute value of the differences case when the two images match perfectly. However, if the difference between the two images is modeled as additive noise, a confidence interval can be established in the absolute value of the difference case by using the resulting minimum value in conjunction with the probability distribution of the noise [9].

The choice that must be made with regard to the similarity measures is influenced by considerations such as the following. (1) How well do the different methods perform? Is there a way to theoretically predict this performance, and if so, what are the results? Also included in this question is whether there exists some sort of confidence measure so that the results may be evaluted quantitatively. (2) What operations are

involved for each of the methods, and what are the comparative times needed? (3) If it has been determined that several methods of registration yield reasonable results with respect to the ability to find the correct registration position, then what are the tradeoffs between the accuracy and the time and number of operations involved? For example, if one method yields the correct registration position in 95% of the attempts but requires twice the operational time as a method which is able to find the correct location 75% of the time, which method should be used? One criterion that is essential for this decision is whether the occurrence of a false indicated registration position is known to be false when it appears.

For the experimental analysis, test sites were chosen from LANDSAT I imagery over Missouri and Kansas. Tables 6-2 and 6-3 contain listings of the dates the data were taken and the approximate location of the LANDSAT I frame centers for the data. A complete tabulation of these sites is given in [35]. The spectral bands chosen for this analysis were 0.8-1.1 μm for the Missouri data and 0.6-0.7 μm for the Kansas images. The subimages used to evaluate the registration algorithms were 51 lines by 51 columns in size. Typical pictures of these general areas are shown in Figures 6-3 and 6-4.

Evaluation of the results is in terms of the percentage of acceptable registrations out of a given number of attempts. The nonacceptable attempts are those where the indicated registration location was known to be false. Such a criterion clearly requires some a priori knowledge of the relative translation between the images in question. For the Missouri imagery three temporally differing sets of data had been previously registered to within a few pixels via the LARS registration system [35].

Table 6-2. Test site area in Missouri.

Approximate location of frame center: Latitude: 37°24'N
Longitude: 88°45'W

LARS Run Number: 72033804

Date Data Taken	Corresponding Channels in Run 72033804
9/13/72	1-4
8/26/72	5-8
10/1/72	9-12

Table 6-3. Test site area in Kansas.

Approximate location of frame center: Latitude: 37°28'N
Longitude: 100°31'W

LARS Run #	Date Data Taken
73046000	7/6/73
73064000	8/29/73
74024100	5/26/74
74024200	7/1/74

Therefore, any substantial deviation from this was taken as an unacceptable attempt. For the Kansas data this a priori information was supplied by careful visual checking of the imagery.

The overall acceptability comparisons are listed in Table 6-4. The results are tabulated for both the original and preprocessed imagery so that a particular similarity measure may be crossreferenced among the different types of images registered. For example, with the correlation coefficient there is a 90% acceptability using the original images, 100% for the magnitude of the gradient of the images, 65% for the images thresholded at their median, and 90% with the magnitude of the gradient of the images thresholded at an appropriate level.

Between the three similarity measures examined, the correlation coefficient consistently yielded the highest percentage of acceptable registrations. This is evidenced by the range of percent acceptabilities within each column. For example, when the magnitude of the gradient of the images were registered, there was a 100% acceptability for the correlation coefficient measure, 74% with the correlation function, and 92% acceptability with the sum of the absolute values of the differences measure. Therefore, on a performance-wise basis, these results indicate that the correlation coefficient should be chosen as the similarity measure.

However, the question of the tradeoff between operational time required and performance must still be examined. Is there a measure which reduced the reliability only slightly while accompanied by a large time savings? Refer to the percentage acceptable registrations in Table 6-4 for the magnitude of the gradient of the imagery. Note that while there was 100% acceptability using the correlation coefficient, there also was

Table 6-4. Percent (Number) of Acceptable Registration Attempts

Similarity Measure	Total Number of Attempts	Original Imagery	Magnitude of the Gradient	Thresholding at the Median	Thresholding the Magnitude of the Gradient
		90	66	66	30
Correlation Coefficient		90% (81)	100% (66)	65% (43)	90% (27)
Correlation Function		38% (34)	74% (49)	55% (36)	87% (26)
Sum of Absolute Values of Differences		69% (62)	92% (61)	62% (41)	87% (26)

a 92% performance with the sum of the absolute difference measure. This result in conjunction with the reduction in the number of computations and thus, time savings achieved, by using this latter measure (Table 6-1), indicates that in a time-performance evaluation, it might be more advantageous to use the sum of the absolute difference measure as opposed to the correlation coefficient.

Overall, the best performance was achieved by the correlation coefficient using the magnitude of the gradient of the imagery. Therefore, if percent acceptability is of prime importance, this preliminary comparison indicates that preprocessing the imagery via a gradient type processor enhances the ability to find an acceptable registration position. The next section concerning the effects of preprocessing prior to registration pursues this observation in more depth.

6.3. Preprocessing Methods

In the search for an optimum processor for image registration it has been proposed that preprocessing of the data prior to the actual overlaying procedure may be a step towards the solution of this problem. There are several underlying reasons for this suggestion. First, preprocessing may yield a greater reliability of the system's registration performance. This is supported by the analyses in Chapters 2, 3, 5, and Appendix A. In Chapter 2 and Appendix A it is shown that the optimum processor utilizes the statistical properties of the temporal changes. In particular, the optimum processor is a matched filter which requires knowledge of the spectral density function or autocorrelation function of the temporal changes. Chapter 3 presents a method of implementing the optimum processor using a preprocessing operation which is analogous to the

experimental investigation in this section. Therefore, once a model of the autocorrelation function of the temporal changes is determined, the preprocessing operation corresponding to that for the optimum processor may be found. In the experimental investigation discussed in Chapter 5, the results indicated that an exponentially decaying autocorrelation function is a reasonable model for the autocorrelation function of the temporal changes. When this model is used it is found in the example of Chapter 3 that a derivative type preprocessing operation will yield the optimum processor. Thus, implementation of a preprocessing operation of this form should improve the registration performance.

Secondly, the time and operations required may be substantially reduced. An example of this is conversion of the original image into a binary image (data values of only 0 or 1) so that logical operations may be employed in the computer instead of arithmetical operations.

The study undertaken here is an experimental examination of several preprocessing techniques and their effects on image registration. Three basic methods were chosen. The first method utilizes the magnitude of the gradient of the imagery given by,

$$|\text{Gradient of } X_{i,j}| = \{(X_{i+1,j} - X_{i-1,j})^2 + (X_{i,j+1} - X_{i,j-1})^2\}^{1/2} \qquad (6\text{-}1)$$

where $X_{i,j}$ is the image intensity at coordinate (i,j). Since the gradient operation is a derivative type operation, this method of preprocessing conforms to the optimum approach derived using the observed autocorrelation function of the temporal changes of Chapter 5 in the example of Chapter 3. Therefore, based on this analysis, use of the gradient preprocessing operation should improve the registration processor performance.

The second method consists of thresholding the imagery at its median (all values greater than or equal to the median are set equal to one, and all else set equal to zero). And the third method computes the magnitude of the gradient of the imagery and then thresholds it at an appropriate level.

Typical images resulting from carrying out these preprocessing operations are shown in Figure 6-5. Figure 6-5a is the original image taken by the LANDSAT multispectral scanner over Hill County, Montana. Thresholding the original image at its median results in Figure 6-5b. Note that although the thresholded image contains only two levels (0 and 1), it represents the field structure of the scene quite well.

The magnitude of the gradient of the image is illustrated in Figure 6-5c. Note that boundaries between the fields have been accentuated by the gradient operation. This is the expected result. The gradient is a derivative type operator, so its magnitude at a point increases with the slope at that point. Since the boundaries of the scene indicate an increase in slope, the magnitude of the gradient at the boundaries is large.

Figure 6-5d shows the resultant image after the magnitude of the gradient has been computed for the original image and then thresholded at an appropriate level. This is a binary image containing value of only zero and one. Again the basic field structure is represented quite well.

LANDSAT imagery over Hill County, Montana, Tippecanoe County, Indiana, and Kansas were used for the analysis. The ready availability of multitemporal data prompted these particular choices. A listing of the dates the data were taken and the approximate location of the LANDSAT

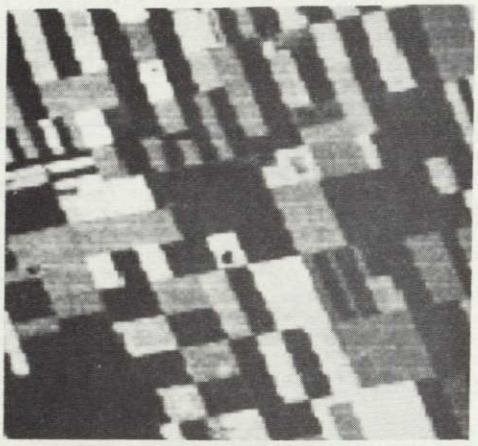

a. Original LANDSAT I image over Hill County, Montana.

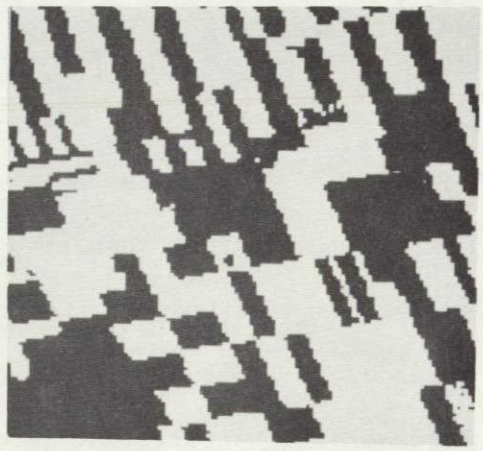

b. Original image thresholded at its median.

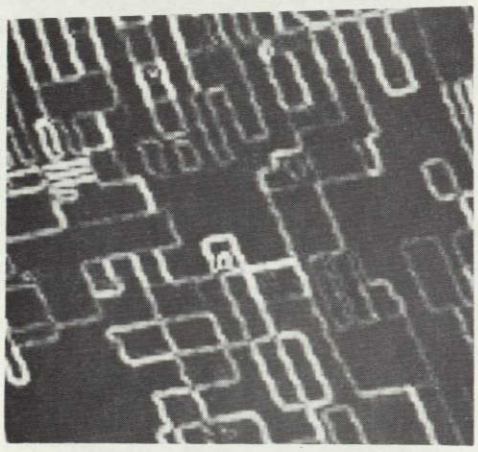

c. Magnitude of the gradient of the original image.

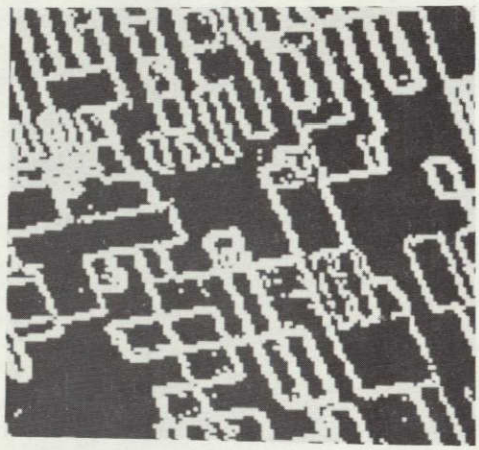

d. Magnitude of the gradient that has been thresholded at an appropriate level.

Original Image

LARS Run #	Date Data Taken	Spectral Band	Lines	Columns
73124700	5/5/73	0.8 - 1.1 μm	(329,451)	(80,206)

Figure 6-5. Examples of images resulting from different preprocessing techniques.

I frame centers are shown in Tables 6-2, 6-3, 6-5 and 6-6. For a complete tabulation of the test sites refer to [35]. The actual subimage sizes that were to be registered for these comparisons were 51 lines by 51 columns.

Again, evaluation of the performance is in terms of the percent of acceptable registration attempts. Like the similarity measure comparisons, visual examination or previous registration to within a few pixels provided the a priori information for determining the acceptability of an indicated registration position. Also, in order to provide a common basis for comparison, the correlation coefficient was chosen as the similarity measure for all of the attempted registrations.

The acceptable-unacceptable attempts are tabulated in Table 6-7. Note that the results have been divided into three sections: (1) the cases where the magnitude of the correlation coefficient ($|\rho|$) for the original imagery is greater than or equal to 0.5, (2) the $|\rho|$ for the original imagery is less than 0.5, and (3) the overall results. The underlying reason for this partition is to examine the relative performance for the high correlation cases ($|\rho| \geq 0.5$) and the low correlation cases ($|\rho| < 0.5$) separately, as well as for the overall results.

First consider the overall results. Preprocessing the imagery via the magnitude of the gradient yielded the highest percent acceptability with 100%. Also, thresholding the magnitude of the gradient performed very well (97%). The important point to note, aside from the best performance, is that on an overall basis preprocessing of the imagery with a gradient type transformation boosted the performance over that utilizing the original imagery. This result supports the analysis of Chapters 2, 3, 5, and Appendix A where the optimum processor in the presence of

Table 6-5. Test site area in Indiana.

Approximate location of frame center: Latitude 40°20'N
Longitude 86°21'W

LARS Run Number: 72053603

Date Data Taken	Corresponding Channels in Run 72053603
9/30/72	1-4
10/19/72	5-8
11/29/72	9-12

Table 6-6. Test site area in Hill County, Montana.

LARS Run Number: 73124700

Date Data Taken	Corresponding Channels in Run 73124700
5/5/73	1-4
5/23/73	21-24
6/10/73	17-20
7/16/73	9-12
8/3/73	5-8

Table 6-7. Percent (Number) of Acceptable Registration Attempts

	Original Imagery		Magnitude of the Gradient		Thresholding at the Median		Thresholding the Magnitude of the Gradient	
	Acceptable Attempts	Total # Attempts	Acceptable Attempts	Total # Attempts	Acceptable Attempts	Total # Attempts	Acceptable Attempts	Total # Attempts
$\|\rho\| \geq 0.5$ for Original Imagery	100% (75)	75	100% (75)	75	96% (72)	75	100% (64)	64
$\|\rho\| < 0.5$ for Original Imagery	65% (37)	57	100% (57)	57	61% (35)	57	89% (25)	28
Overall	85% (112)	132	100% (132)	132	81% (107)	132	97% (89)	92

exponentially autocorrelated temporal changes utilizes a derivative type operator in the preprocessing stage. The analysis is also corroborated for the other similarity measures in Table 6-4. Comparison of the percentage of acceptable registrations for the gradient type preprocessors shows a substantial improvement in performance over both the original imagery, and the images thresholded at their median for each of the similarity measures. This indicates that choice of a preprocessing operation conforming to that derived via the matched filter (Chapter 3) may indeed provide a more reliable registration processor.

Several questions may be asked about this observation. Is there any trend to this increased reliability? Are there any image characteristics which seem to contribute to these observations? One answer to these questions is embodied in the partitioning of the overall results into the high and low correlation cases.

Examination of the high correlation instances ($|\rho| \geq 0.5$ for the original data) shows that all of the preprocessing methods performed exceedingly well with 96% acceptability for thresholding the data at its median and 100% for the rest. This indicates that when the original imagery is highly correlated, any of the preprocessing methods works equally well. In this case no advantage is gained performance-wise by preprocessing the imagery prior to registration.

The most striking result came with the low correlation cases ($|\rho| < 0.5$ for the original data). For these cases a marked advantage over using the original imagery was obtained by preprocessing the data via a gradient type processor. Use of the magnitude of the gradient of the imagery provided a 100% acceptability compared with the 65% performance for the original data. Thresholding the magnitude of the gradient also

indicated a distinct increase in reliability. These results suggest that a substantial increase in the reliability of the registration processor may be achieved when the original imagery is not highly correlated by preprocessing the imagery prior to registration via an operation conforming with the preprocessing operation derived from the matched filter configuration of the registration processor (Chapter 3).

Earlier, it was mentioned that a priori information was used to determine the acceptability of indicated registration positions. For imagery that had not been previously registered this took the form of visual examination for an individual test site. Such a procedure is quite time consuming and does not lend itself readily to an automatic mode of operation. However, while attempting the registrations at the selected test sites it was found that relative spatial information could be used for several test sites located in the same general area, or the same test site for over several different times. For example, if several different test sites indicated the same relative translation for registration, while the registration position of another test site within the same general area indicated a substantially different translation, then this latter registration attempt would be unacceptable. Similar reasoning follows for several time pair registration attempts for a single test site.

Another observation which may be made directly from Table 6-2 also suggests a way by which a partial acceptability decision might be made automatically. This approach is in terms of an absolute scale confidence measure. Since the value of the correlation coefficient (ρ) indicates the linearity of the relationship between two images, possibly a range of values for ρ exists which could be used to determine acceptability.

This is suggested in the first line of Table 6-7 where the results when the magnitude of the correlation coefficient is greater than or equal to 0.5 for the original imagery are listed. For the original data there is a 100% acceptability for this range of ρ. This suggests that the value of the correlation coefficient may be used to help in the determination of the acceptability of an indicated registration position.

6.4. Performance of an Operational Algorithm Which Utilizes Gradient-Type Preprocessing

The observation made in sections 6-2 and 6-3 suggested that an improvement in the performance of the registration processor could be realized by first preprocessing the images via a gradient type processor and then registering these gradient images. It was also found that use of the correlation coefficient as the similarity measure yielded the highest percentage acceptability of the three measures compared. Independent of this experimental study, but at approximately the same time, an algorithm designed to register LANDSAT I images was developed at Computer Sciences Corporation [30], which utilizes both a gradient type preprocessing of the images and a similarity measure closely approximating the correlation coefficient. The availability of this algorithm made it possible to experimentally observe the extension of the results obtained in the similarity measure and preprocessing comparisons to an algorithm designed for operational image registration.

The fundamental operation of this algorithm is the same as that for the other registration processors compared in this chapter. The images are assumed to be spatially congruent thereby reducing the registration operation to that of finding the relative translation between the images. The translation is found by shifting one image (the overlay image) over

a larger temporally differing second image (the reference image) computing a value of the similarity measure at each shift position. The shift position at which the similarity measure indicates the best spatial match is taken as the registration position. In this case the images used for registration are the original images from two spectral bands that have been passed through a gradient type processor, thresholded at an appropriate level, and then combined to form a composite image. The similarity measure used is an approximation to the correlation coefficient designed specifically to operate with binary images.

The gradient type preprocessing operation is expressed as follows,

$$X_{ij} = |I_{i+1,j} - I_{i-1,j}| + |I_{i,j+1} - I_{i,j-1}| + |I_{i+1,j-1} - I_{i-1,j+1}| + |I_{i+1,j+1} - I_{i-1,j-1}| \quad (6\text{-}2)$$

where,

$I_{i,j}$ = original image intensity value at coordinate (i,j)

$X_{i,j}$ = intensity value of image sample at position (i,j) after preprocessing

After an image has been passed through this gradient type operation it is thresholded at the level which is exceeded by only fifteen percent of the data values. In this way the original image is converted to a binary image having values of only zero and one, with a prescribed percentage of points having the value one.

These gradient and threshold operations are applied to two spectral bands of each image set. The two binary images from each spectral band then are combined via a logical 'or' operation to produce a single image to be used for the registration, the resulting image containing between 15% and 30% values of one. In this fashion it is possible to use

information from more than one spectral band simultaneously for the overlay processor.

The similarity measure used to determine the relative translation between these preprocessed images is defined as the ratio of number of coincident points between the overlay and reference image having the value of 1 divided by the total number of points having value 1 in that portion of the reference image being tested as the registration location.

$$P_{N_{\ell,k}} = \frac{\sum_{i=1}^{N}\sum_{j=1}^{N} X_{i,j}\, Y_{i+\ell,j+k}}{\sum_{i=1}^{N} Y_{i+\ell,j+k}}$$

Where,

$P_{N_{\ell;k}}$ = value of the similarity measure at shift (ℓ,k)

$X_{i;j}$ = value (either 0 or 1) of the overlay image at coordinate (i,j)

$Y_{i+\ell,j+k}$ = value (either 0 or 1) of the reference image at coordinate $(i+\ell,j+k)$

N = number of lines and columns in the overlay image

Once the preprocessing has been completed, two methods of operation may be employed. The first approach is to compute fully the value of the similarity measure at all of the shift positions. The second method involves partial computation of p_N; the value of p_N is fully computed only if its estimated magnitude exceeds a certain level. For a complete discussion of this latter approach refer to Nack [30] where the algorithm is discussed. Use of this latter method finds its advantage in terms of the time savings achieved by estimating p_N rather than computing it fully at all shift positions.

This investigation entailed implementation of this algorithm over the same test sites used for the similarity measure and preprocessing

analysis. Since the primary objective of this section is to relate the overall performance of this registration processor to the results obtained in the previous two sections, the performance of the processor when p_N is fully calculated at all shift positions is discussed here. For a discussion of the results when the estimation procedure was also utilized refer to [35].

For a meaningful comparison the size of the test sites and the acceptability-unacceptability criteria remained the same. The test sites chosen covered all of those used for the similarity measure and preprocessing method comparisons. These were from Kansas, Missouri, Indiana, and Montana. The general areas are listed in Tables 6-2, 6-3, 6-5, and 6-6, while a complete tabulation of all of the test sites is given in [35].

Since a single method of registering the images was tested, the performance results may be summed up in terms of the percent acceptable registrations out of the total number attempted. The overall tabulation showed that 190 out of 192 registration attempts were successful, which is a 99% success rate. This result is in close agreement with the previous findings of sections 6.2 and 6.3, where preprocessing via a gradient operator followed by use of the correlation coefficient yielded the highest performance (Table 6-4). This high performance rate also corroborates the analysis presented in Chapters 2, 3, 5 and Appendix A, where it is shown that preprocessing via a derivative type operator yields an optimum registration processor.

BIBLIOGRAPHY

BIBLIOGRAPHY

1. Anuta, P.E., "Computer-Aided Analysis Techniques for Remote Sensing Data Interpretation," LARS Info. Note 100675, LARS, Purdue University, 1975.

2. Anuta, P.E., Guide to Use of the Fast Fourier Transform Algorithm for Two Dimensional Imagery Correlation, LARS Info. Note 121069, LARS, Purdue University, December 1969.

3. Anuta, P.E., "Spatial Registration of Multispectral and Multitemporal Digital Imagery Using Fast Fourier Transform Techniques," IEEE Trans. Geoscience Electronics, October 1970, p. 353-368.

4. Anuta, P.E., "Spline Function Approximation Techniques for Image Geometric Distortion Representation," LARS Info. Note 103174, LARS, Purdue University, 1974.

5. Anuta, P., Bauer, M., "An Analysis of Temporal Data for Crop Species Classification and Urban Change Detection," LARS Info. Note 110873, LARS, Purdue University, 1973.

6. Arcese, A., Mengert, P.H., Trombini, E.W., "Image Detection Through Bipolar Correlation," IEEE Trans. Info. Th., September 1970, p. 534-541.

7. Atkinson, R.J., Hodges, B.C., Thomas, D.T., Bond, A.D., Ramapriyan, H.K., "Image Analysis Techniques Associated with Automatic Data Base Generation," AIAA Paper No. 73-430, AIAA Computer Network Systems Conference, Huntsville, Alabama, April 16-18, 1973.

8. Barnea, D.I., Silverman, H.F., "A Class of Algorithms for Fast Digital Registration," IEEE Trans. on Computers, February 1972, p. 179-186.

9. Barnea, D.I., Silverman, H.F., "The Class of Sequential Similarity Detection Algorithms (SSDA's) for Fast Digital Image Registration," IBM Research Paper, May 10, 1971. Copies may be requested from IBM Thomas J. Watson Research Center, P.O. Box 218, Yorktown Heights, New York, 10598.

10. Bauer, M.E., Cary, T.K., Davis, B.J., Swain, P.H., "Crop Identification Technology Assessment for Remote Sensing (CITARS)," LARS Info. Note 072175, LARS, Purdue University, 1975.

11. Beaudet, P.R., "Rapid Alignment Algorithms for Successive ERTS Images," Computer Sciences Corp., 8728 Colesville Road, Silver Spring, Maryland. This was a presentation.

12. Bonrud, L.O., Henrikson, R.J., "Correlation and Registration of ERTS Multispectral Imagery, NASA-CR-134294 Report No., Control Data Corp., Minneapolis, Minnesota, April 1974.

13. Delashmit, W.H., Webber, R.F., "Analytical and Experimental Results for Maximizing the Pull-In Range of Product Correlators," IEEE Trans. on Aerospace and Electronic Systems, March 1974, p. 216-222.

14. Delashmit, W.H., Webber, R.F., "Product Correlator Performance for Gaussian Random Scenes," IEEE Trans. on Aerospace and Electronics Systems, July 1974, p. 516-520.

15. DiFranco, J.V., Rubin, W.L., Radar Detection, Prentice-Hall, Inc., New Jersey, 1963.

16. Emmert, R.A., McGillem, C.D., Conjugate Point Determination for Multitemporal Data Overlay, LARS Info. Note 111872, LARS, Purdue University, November 1972.

17. Emmert, R.A., McGillem, C.D., "Multitemporal Geometric Distortion Correction Utilizing the Affine Transformation," Proceedings of the Conference on Machine Processing of Remotely Sensed Data, Purdue University, October 16-18, 1973, p. 1B-24 to 1B-32, IEEE Catalog No. 73 CHO 834-2 GE.

18. Franks, L.E., Signal Theory, Prentice-Hall, Inc., Englewood Cliffs, New Jersey, 1969, p. 135-148.

19. Hall, F.G., Bauer, M.E., Malila, W.A., "First Results From Crop Identification Technology Assessment for Remote Sensing (CITARS)," LARS Info. Note 041874, LARS, Purdue University, 1974.

20. Henrikson, P., "Techniques and Applications of Digital Change Detection," Computer Image Processing and Recognition Symposium, University-Columbia, Columbia, Missouri, August 24-26, 1972.

21. Hogg, R.V., Craig, A.T., Introduction to Mathematical Statistics, The Macmillan Company, Collier-Macmillan Limited, London, 1970, p. 274-276.

22. Lam, Maj. C.F., Hoyt, R.R., "High Speed Image Correlation for Change Detection," National Aeronautics and Electronics Conference, (NAECON), Dayton, Ohio, May 15-17, 1972.

23. Lee, G.M., McCormack, D.S., Popp, D.J., "Digital Image Registration by Correlation Techniques," IEEE 1972 National Telecommunications Conference, p. 24D-1 to 24D-5.

24. Lehmann, E.L., Testing Statistical Hypotheses, New York, John Wiley & Sons, Inc., 1959, p. 63-67.

25. Lillestrand, R.L., "Image Processing of Remote Sensor Data," Presented before the Committee on Science and Astronautics, U.S. House of Representatives, 13th meeting with the panel on Science and Technology, January 27, 1972.

26. Lillestrand, R.L., "Techniques for Change Detection," IEEE Trans. on Computers, July 1972, p. 654-659.

27. McGillem, C.D., Svedlow, M., Image Registration Error Variance as a Measure of Overlay Quality, LARS Info. Note 090274, LARS, Purdue University.

28. McGillem, C.D., Svedlow, M., "Image Registration Error Variance as a Measure of Overlay Quality," Proceedings of Symposium on Machine Processing of Remotely Sensed Data, June 3-5, 1975, Purdue University, p. 3A-30 to 3A-37, IEEE Catalog No. 75CH 1009-0-C.

29. McGillem, C.D., Thurman, L.A., "Radar Resolution Enhancement and Target Surface Reconstruction," TR-EE 73-14, April 1973, Purdue University.

30. Nack, M.L., "Temporal Registration of Multispectral Digital Satellite Images Using Their Edge Images," AAS/AIAA Astrodynamics Specialist Conference, Nassau, Bahamas, July 28-30, 1975, Paper #AAS75-104.

31. Nilsson, N.J., "On the Optimum Range Resolution of Radar Signals in Noise," IEEE Trans. on Info. Th., October 1961, p. 245-253.

32. Pratt, W.K., "Correlation Techniques of Image Registration," IEEE Trans. on Aerospace and Electronic Systems, May 1974, p. 353-358.

33. "Proceedings Before the Committee on Science and Astronautics," House of Representatives, 92nd Congress, 2nd Session, January 25-27, 1972, Panel on Science and Technology, 13th meeting.

34. Slepian, D., "Estimation of Signal Parameters in the Presence of Noise," IEEE Trans. on Info. Th., March 1954, p. 68-69.

35. Svedlow, M., McGillem, C.D., Anuta, P.E., "Experimental Examination of Similarity Measures and Preprocessing Methods Used for Image Registration," LARS Info. Note 052175, LARS, Purdue University, 1975.

36. Swain, P.H., "Data Processing I: Advancements in Machine Analysis of Multispectral Data," LARS Info. Note 012472, LARS, Purdue University, 1972.

37. Swain, P.H., "Pattern Recognition: A Basis for Remote Sensing Data Analysis," LARS Info. Note 111572, LARS, Purdue University, 1972.

38. Swerling, P., "First Order Error Propagation in a Stagewise Smoothing Procedure for Satellite Observations," The Journal of the Astronautical Sciences, Autumn 1959, Volume 6, p. 46-52.

39. Swerling, P., "Parameter Estimation Accuracy Formulas," IEEE Trans. on Info. Th., October 1964, p. 302-314.

40. Thomas, G.B., Jr., Calculus and Analytic Geometry, Fourth Edition, Addition-Wesley Publishing Company, Reading, Massachusetts, 1968, pp. 308-310.

41. Thomas, J.B., Williams, T.R., Wolff, S.S., "The Polarity-Coincidence Correlator: A Nonparametric Detection Device," IRE Trans. on Info. Th. January 1962, p. 5-9.

42. Ulstad, M.S., "An Algorithm for Estimating Small Scale Differences Between Two Digital Images," Pattern Recognition, Received October 31, 1972.

43. Van Trees, H.L., Detection, Estimation, and Modulation Theory, Part I, John Wiley and Sons, Inc., New York, 1968, p. 66-84.

44. Wainstein, L.A., Zubakov, V.D., Extraction of Signals From Noise, Prentice-Hall, Inc., New Jersey 1962.

45. Webber, W.F., "Techniques for Image Registration," Proceedings of the Conference of Machine Processing of Remotely Sensed Data, Purdue University, October 16-18, 1973, p. 1B-1 to 1B-7, IEEE Catalog No. 73 CHO 834-2 GE.

46. Yao, S.S., "A Method for Digital Image Registration Using a Mathematical Programming Technique," Proceedings of the Conference on Machine Processing of Remotely Sensed Data, Purdue University, October 16-18, 1973, p. 1B-8 to 1B-23, IEEE Catalog No. 73 CHO 834-2 GE.

APPENDIX

APPENDIX A

PROOF THAT THE MATCHED FILTER MINIMIZES THE REGISTRATION ERROR VARIANCE

In section 2.3 an expression for the variance of the registration error is derived. The basic design criterion for this method of approach is that the second image (misregistered image plus noise) be passed through a filter whose output is a maximum at the correct registration position in the absence of noise. General relations for the variance are given by equations (2-27) and (2-28) where the variance may be evaluated by inserting a particular filter function. At that point the matched filter was used to evaluate these expressions, which leads to compact formulas for the variance of the registration error along the x and y coordinate axes. In this appendix it is shown that not only does the matched filter provide the maximum output signal-to-noise ratio at the correct registration location and compact expressions for the variance, but it is the optimum filter in the sense that it minimizes the variance of the error.

To begin the proof one starts with the general expressions for the variance of the registration error along the coordinate axes, equations (2-27) and (2-28), which are repeated here.

$$\overline{(\hat{x}-\tilde{x})^2} = \frac{g_{xy}^2\,\overline{n_y^2} - 2g_{xy}g_{yy}\,\overline{n_y n_x} + g_{yy}^2\,\overline{n_x^2}}{[g_{xx}g_{yy} - g_{xy}^2]^2} \qquad \text{(A-1)}$$

$$\overline{(\hat{y}-\tilde{y})^2} = \frac{g_{xy}^2\,\overline{n_x^2} - 2g_{xy}g_{xx}\overline{n_y n_x} + g_{xx}^2\,\overline{n_y^2}}{[g_{xx}g_{yy} - g_{xy}^2]^2} \tag{A-2}$$

Note that these relations are greatly simplified when the term g_{xy} equals zero. In this situation the variance expressions become,

$$\overline{(\hat{x}-\tilde{x})^2} = \frac{\overline{n_x^2}}{g_{xx}^2} \tag{A-3}$$

$$\overline{(\hat{y}-\tilde{y})^2} = \frac{\overline{n_y^2}}{g_{yy}^2} \tag{A-4}$$

It is convenient to determine the conditions under which the term $g_{xy}(\tilde{x},\tilde{y})$ does equal zero. Since $g(x,y)$ is modeled as a second order polynomial in x and y about the true registration location, and is a maximum at this position, one may apply a linear spatial transformation to the (x,y) coordinate system so that in the new coordinate system, say (x_1,y_1), the term $g_{x_1y_1}(\tilde{x},\tilde{y})$ will equal zero. One may then solve for the filter which minimizes the registration error variance in this new coordinate system. Once this filter is found, the inverse linear spatial transformation may be applied to return to the original coordinate system. Therefore, no generality is lost by assuming $g_{xy}(\tilde{x},\tilde{y})$ equals zero, so that one may begin with expressions (A-3) and (A-4).

The equations for the variance may be expressed in their equivalent integral form (equations (2-29), (2-31), (2-32), and (2-33)),

$$\overline{(\hat{x}-\tilde{x})^2} = \frac{\iiiint h(\alpha,\beta)h(\gamma,\xi)R_{xx}(\alpha-\gamma,\beta-\xi)\,d\alpha d\beta d\gamma d\xi}{\left[\iint h(\alpha,\beta)\,F_{xx}(\tilde{x}-\alpha,\tilde{y}-\beta)\,d\alpha d\beta\right]^2} \tag{A-5}$$

$$\overline{(\hat{y}-\tilde{y})^2} = \frac{\iiiint h(\alpha,\beta)h(\gamma,\xi)R_{yy}(\alpha-\gamma,\beta-\xi)\,d\alpha d\beta d\gamma d\xi}{\left[\iint h(\alpha,\beta)\ f_{yy}(\tilde{x}-\alpha,\tilde{y}-\beta)\,d\alpha d\beta\right]^2} \tag{A-6}$$

where R(x,y) is the autocorrelation function of the input noise, f(x,y) is the known signal (first image), and subscripts again denote the partial derivatives with respect to the corresponding variables.

Given these expressions for the variance, one would like to find the filter h(x,y) which minimizes $\overline{(\hat{x}-\tilde{x})^2}$ and $\overline{(\hat{y}-\tilde{y})^2}$. For this derivation the problem will be broken down into two parts, first the minimization of $\overline{(\hat{x}-\tilde{x})^2}$, then of $\overline{(\hat{y}-\tilde{y})^2}$.

To begin, first restate the problem in an equivalent form. Minimization of $\overline{(\hat{x}-\tilde{x})^2}$ may be stated in the following equivalent form.

Minimize

$$I(\underline{h}) = \iiiint h(\alpha,\beta)h(\gamma,\xi)R_{xx}(\alpha-\gamma,\beta-\xi)\,d\alpha d\beta d\gamma d\xi \tag{A-7}$$

Subject to

$$J(\underline{h}) = \left[\iint h(\alpha,\beta)\ f_{xx}(\tilde{x}-\alpha,\tilde{y}-\beta)\,d\alpha d\beta\right]^2 = K_1^2 \tag{A-8}$$

where K_1 is a constant and I(h) and J(h) are functionals of the filter h(x,y).

The method of solution employed will follow that presented by Franks [18]. However, before solving the problem several notational conventions that are used must be defined. The first is that of an inner product and the second that of an operator. Given two functions, g(x,y) and h(x,y), the inner product, $\langle \underline{g},\underline{h}\rangle$, is defined by,

$$\langle \underline{g},\underline{h}\rangle = \iint g(x,y)\ h(x,y)\ dxdy \tag{A-9}$$

and an operator, A(x,y), on a function h(x,y) is defined as,

$$\underline{A}\ \underline{h} = \iint A(x-\alpha,y-\beta)h(\alpha,\beta)\,d\alpha d\beta \tag{A-10}$$

Note that $\underline{A}\,\underline{h}$ is a function of the variables x and y.

With these integral representations, $I(\underline{h})$ and $J(\underline{h})$ may be expressed in terms of operations in Hilbert space as

$$I(\underline{h}) = \langle \underline{R}_{xx}\underline{h}, \underline{h}\rangle \tag{A-11}$$

$$J(\underline{h}) = \langle \underline{h}, \underline{s}\rangle^2 \tag{A-12}$$

where,

$$\underline{s} = s(x,y) = f_{xx}(\tilde{x}-x, \tilde{y}-y) \tag{A-13}$$

Since each of the functions, $R_{xx}(x,y)$, $h(x,y)$, and $f(x,y)$ are real, and $I(\underline{h})$ and $J(\underline{h})$ are quadratic functionals, it is shown in Franks [18] that the filter which minimizes $I(\underline{h})$ subject to $J(\underline{h}) = K_1^2$ is the solution to,

$$\underline{\nabla I} - \lambda_1 \underline{\nabla J} = \underline{0} \tag{A-14}$$

where λ_1 is a Lagrange multiplier and $\underline{\nabla I}$ and $\underline{\nabla J}$ are the gradient vectors corresponding to $I(\underline{h})$ and $J(\underline{h})$. These gradient vectors may be found from evaluating the directional derivatives of $I(\underline{h})$ and $J(\underline{h})$ which are defined as follows,

$$D_{\underline{u}} I(\underline{h}) = \lim_{\varepsilon \to 0} \frac{I(\underline{h} + \varepsilon \underline{u}) - I(\underline{h})}{\varepsilon} = \langle \underline{\nabla I}, \underline{u}\rangle \tag{A-15}$$

$$D_{\underline{u}} J(\underline{h}) = \lim_{\varepsilon \to 0} \frac{J(\underline{h} + \varepsilon \underline{u}) - J(\underline{h})}{\varepsilon} = \langle \underline{\nabla J}, \underline{u}\rangle \tag{A-16}$$

where,

$D_{\underline{u}} I(\underline{h})$ = directional derivative of $I(\underline{h})$ with respect to $\underline{u}$

$D_{\underline{u}} J(\underline{h})$ = directional derivative of $J(\underline{h})$ with respect to $\underline{u}$

and $\underline{u}$ is an arbitrary function with the property that,

$$\langle \underline{u}, \underline{u}\rangle = \iint u^2(x,y)\,dx\,dy = 1 \tag{A-17}$$

Substitution of equations (A-11) and (A-12) into (A-15) and (A-16), and

using the inner product properties for real functions $g(x,y)$, $h(x,y)$ and $A(x,y)$, with $A(x,y)$ an even function,

$$\langle g,\underline{h}\rangle = \langle \underline{h},g\rangle \tag{A-18}$$

$$\langle \underline{A}\ g,\underline{h}\rangle = \langle \underline{A}\ \underline{h},g\rangle \tag{A-19}$$

yields,

$$\langle \underline{\nabla I},\ \underline{u}\rangle = \langle 2\ \underline{R_{xx}}\underline{h},\ \underline{u}\rangle \tag{A-20}$$

$$\langle \underline{\nabla J},\ \underline{u}\rangle = \langle 2\ \langle \underline{h},\underline{s}\rangle \underline{s},\ \underline{u}\rangle \tag{A-21}$$

or equivalently,

$$\langle \underline{\nabla I},\ \underline{u}\rangle = (2\ \underline{R_{xx}}\underline{h},\ \underline{u}) \tag{A-22}$$

$$\langle \underline{\nabla J},\ \underline{u}\rangle = (2K_1\ \underline{s},\ \underline{u}) \tag{A-23}$$

since $\langle \underline{h},\underline{s}\rangle = K_1$.

From these expressions one obtains the gradient vectors,

$$\underline{\nabla I} = 2\ \underline{R_{xx}}\underline{h} \tag{A-24}$$

$$\underline{\nabla J} = 2\ K_1\ \underline{s} \tag{A-25}$$

Then from equation (A-14), one must solve,

$$2\ \underline{R_{xx}}\underline{h} - \lambda_1 2K_1\ \underline{s} = \underline{0} \tag{A-26}$$

Rewriting this in integral form,

$$2 \iint R_{xx}(x-\alpha,y-\beta)h(\alpha,\beta)d\alpha d\beta - 2\lambda_1 K_1\ f_{xx}(\tilde{x}-x,\tilde{y}-y) = 0 \tag{A-27}$$

so that,

$$\iint R_{xx}(x-\alpha,y-\beta)h(\alpha,\beta)d\alpha d\beta = \lambda_1 K_1\ f_{xx}(\tilde{x}-x,\tilde{y}-y)$$

The solution to this equation is found by taking the Fourier transform of both sides.

$$\iiiint R_{xx}(x-\alpha,y-\beta)h(\alpha,\beta)e^{-j2\pi(ux+vy)}d\alpha d\beta dxdy$$

$$= \lambda_1 K_1 \iint f_{xx}(\tilde{x}-x,\tilde{y}-y)e^{-j2\pi(ux+vy)}dxdy \qquad \text{(A-28)}$$

Which becomes,

$$-4\pi^2u^2 S_m(u,v) H(u,v) = -4\pi^2u^2\lambda_1 K_1 F^*(u,v)e^{-j2\pi(\tilde{x}u+\tilde{y}v)} \qquad \text{(A-29)}$$

where,

$S_m(u,v)$ = Fourier transform of $R(x,y)$

$H(u,v)$ = Fourier transform of $h(x,y)$

$F(u,v)$ = Fourier transform of $f(x,y)$

Rearranging this expression in terms of the filter, $H(u,v)$, one obtains,

$$H(u,v) = \lambda_1 K_1 \frac{F^*(u,v)e^{-j2\pi(\tilde{x}u+\tilde{y}v)}}{S_m(u,v)} \qquad \text{(A-30)}$$

which is the definition of the matched filter multiplied by an arbitrary constant factor, $\lambda_1 K_1$. Thus, the filter which minimizes the variance along the x-axis is the matched filter.

Alternatively, minimization of $\overline{(\hat{y}-\tilde{y})^2}$ may be done in the same manner where the problem is equivalently stated as,

Minimize

$$\overline{n_y^2} = \iiiint h(\alpha,\beta)h(\gamma,\xi)R_{yy}(\alpha-\gamma,\beta-\xi)d\alpha d\beta d\gamma d\xi \qquad \text{(A-31)}$$

Subject to

$$g_{yy}^2 = \left[\iint h(\alpha,\beta)f_{yy}(\tilde{x}-\alpha,\tilde{y}-\beta)d\alpha d\beta\right]^2 = K_2^2, \text{ a constant} \qquad \text{(A-32)}$$

Since the problem is now in terms analogous to the minimization of $\overline{(\hat{x}-\tilde{x})^2}$, one may follow the same steps which result in the following solution for $H(u,v)$.

$$H(u,v) = \lambda_2 K_2 \frac{F^*(u,v)e^{-j2\pi(\tilde{x}u+\tilde{y}v)}}{S_m(u,v)} \tag{A-33}$$

where λ_2 is the corresponding Lagrange multiplier. Therefore, the filter which minimizes $\overline{(\hat{y}-\tilde{y})^2}$ is the matched filter.

Since the constants K_1 and K_2 are arbitrary, one may choose K_1 and K_2 such that $\lambda_1 K_1 = 1 = \lambda_2 K_2$. Thus $\overline{(\hat{x}-\tilde{x})^2}$ and $\overline{(\hat{y}-\tilde{y})^2}$ are minimized simultaneously by using,

$$H(u,v) = \frac{F^*(u,v)e^{-j2\pi(\tilde{x}u+\tilde{y}v)}}{S_m(u,v)} \tag{A-34}$$

which is the matched filter. Therefore, use of the matched filter not only maximizes the output signal-to-noise ratio at the correct registration location and yields compact expressions for the variance, but it also minimizes the variance of the registration error.